UNIVERSITY OF CALIFORNIA,
IRVINE

Regulation of Macrophage Function by the Adhesive Microenvironment

DISSERTATION

submitted in partial satisfaction of the requirements
for the degree of

DOCTOR OF PHILOSOPHY

in Pharmacological Sciences

by

Thuy U. Luu

Dissertation Committee:
Professor Wendy F. Liu, Advisor
Professor Andrej Luptak, Chair
Professor Weian Zhao

2018

TABLE OF CONTENTS

LIST OF FIGURES

LIST OF TABLES

Page

ACKNOWLEDGEMENTS

I would like to express my debt of gratitude to my advisor, Professor Wendy Liu, for all her guidance and support for many years of my graduate training. I still remember five years ago, when I did not know whether I would be able to continue my Ph.D., and with her kindness, Dr. Liu gave me a chance to do a rotation, and later accepted me to her laboratory as a graduate student. With her kindness and optimistic perspectives on our research, I was able to keep pursuing projects that I wanted to do. She is one of my role models and inspired me to work hard. I also would like to thank my committee chair, Professor Andrej Luptak, who I came to ask for advice when I was in a difficult situation and did not know how to make a decision. I also would like to thank my committee member, Professor Weian Zhao, who provided me with fresh perspectives and insights into my project.

I would like to thank all members of the Liu laboratory, with whom I shared great times and engaging scientific discussions. Special thanks to Dr. Yoon Kim for her thoughtful advice, Esther Chen for our great friendship and her beautiful illustrations for my project, Dr. Vijaykumar Meli for working with me on fibrin project, L. McCarthy for technical assistance in the laboratory, Adeela Syed for technical assistance in the Optical Biology Center, and the Lodoen laboratory for guidance with cell isolation and culture.

No words can describe my deepest gratitude to my parents who always believe in me and support me in everything. I also thank my sister and her family, who have been always there to support me. Without my parents, my sister, my brother-in-law, my niece and my nephew, I would not be who I am today.

CURRICULUM VITAE

Thuy U. Luu

2018	**Ph.D.** in Pharmacological Sciences
	University of California, Irvine, CA
2010	**B.S.** in Biochemistry, Honor College
	University of California, Los Angeles, CA

Publications

1. F.Y. McWhorter, T.D. Smith, **T.U. Luu**, M.K. Rahim, J.B. Haun, W.F. Liu, Macrophage secretion heterogeneity in engineered microenvironments revealed using a microwell platform, Integr. Biol., 2016. doi: 10.1039/c6ib00053c
2. T. Wang, **T.U. Luu**, A. Chen, M. Khine, W.F. Liu, Topographical modulation of macrophage phenotype by shrink-film multi-scale wrinkles, Biomater. Sci., 2016. doi: 10.1039/c6bm00224b
3. A. Alfonso-García, T.D. Smith, R. Datta, **T.U. Luu**, E. Gratton, E. Potma, W.F. Liu, Label-free identification of macrophage phenotype by fluorescence lifetime imaging microscopy, J. Biomed. Optics, 2016, 21, 046005. doi: 10.1117/1.jbo.21.4.046005
4. **T.U. Luu**, S. C. Gott, B. W. K. Woo, M. P. Rao, W. F. Liu, Micro- and nanopatterned topographical cues for regulating macrophage cell shape and phenotypes, ACS Appl. Mater. Interfaces, 2015, 7, 28665-28672. doi: 10.1021/acsami.5b10589

ABSTRACT

Regulation of Macrophage Function by the Adhesive Microenvironment

By

Thuy U. Luu

Doctor of Philosophy in Pharmacological Sciences

University of California, Irvine, 2018

Professor Wendy F. Liu, Advisor

Professor Andrej Luptak, Chair

Professor Weian Zhao, Committee member

Macrophages are plastic innate immune cells, involved in both inflammation and tissue repair processes. In the presence of danger signals, macrophages adopt a pro-inflammatory phenotype and secrete cytokines and reactive species to defeat infection. On the other hand, for wound healing, macrophages polarize towards a pro-healing phenotype and secrete anti-inflammatory cytokines. Modulation of macrophage behavior has emerged as a promising strategy in the design of materials used in medicine, given their prominent role in inflammation and wound healing. Although there is substantial evidence demonstrating how soluble factors such as cytokines and chemokines influence immune cell function, little is known about how physical and adhesive cues regulate macrophage behavior. While it has long been thought that biomaterial surface chemistry regulates the

immune response, recent studies have suggested that material geometry may also contribute to this regulation. Our previous work demonstrated that elongation of macrophages induced their polarization towards a pro-healing phenotype. Using micropatterning technique, we demonstrated the effect of cell shape on macrophage polarization towards pro-inflammatory or pro-healing states. Macrophages forced to elongate on line substrates expressed biomarkers of pro-healing phenotype without the addition of exogenous cytokines. In this work, we examined how adhesive properties of the cellular microenvironment regulate the function of macrophages. To achieve this goal, we have demonstrated how micro- and nano-scale topographical features as well as the composition and architecture of the extracellular matrix influences macrophage adhesion and function. We found that promoting cellular elongation through surface grooves and extracellular matrix-based hydrogels enhanced pro-healing activation and inhibited the inflammatory activation of macrophages. In addition, we have demonstrated a potential underlying molecular mechanism of regulating macrophage function by adhesive microenvironment. These findings provide insight to the design of new materials to harness macrophage-mediated wound healing.

CHAPTER 1- Macrophage Biology in Diseases and Tissue Engineering

1.1 Macrophage Plasticity and Phenotype Polarization

Macrophages are immune effector cells, essential for innate and adaptive functions of the immune system. Macrophages are found in every type of tissue, where they can assume many different phenotypes and diverse functions in host defense, wound healing and immune regulation. In response to injury and infection, monocytes are recruited into injured sites or tissues where they can differentiate into either macrophages or dendritic cells depending on endogenous stimuli [1] produced by other immune cells or damaged cells. These stimuli not only influence the physiology of macrophages but also enhance their immune functions [2]. Therefore, it is important to understanding how microenvironment cues affect macrophage phenotypes for therapeutic purposes.

Macrophages are remarkably plastic cells that alter their phenotype based on microenvironmental cues. Although macrophages are capable of acquiring many different functions, they are often classified into two main categories that refer to their inflammatory states: a classically activated macrophage or an alternatively activated macrophage (Figure 1). In response to the non-self pathogens and danger signals in microenvironment, macrophages acquire classically activated phenotype and secret pro-inflammatory cytokines to fight infection [3]. Alternatively, in the presence of wound healing signals, macrophages assume alternatively activated phenotype and express anti-inflammatory cytokines to facilitate tissue repair [3]. To control murine macrophage polarization *in vitro*, interferon- γ (IFN-γ) and lipopolysaccharide (LPS), and interleukin-4 (IL-4) and interleukin-13 (IL-13) are commonly used to simulate macrophages to adopt pro-

inflammatory and anti-inflammatory phenotypes respectively (Figure 1). In addition to those stimuli, many other factors in microenvironment can lead to macrophage activation.

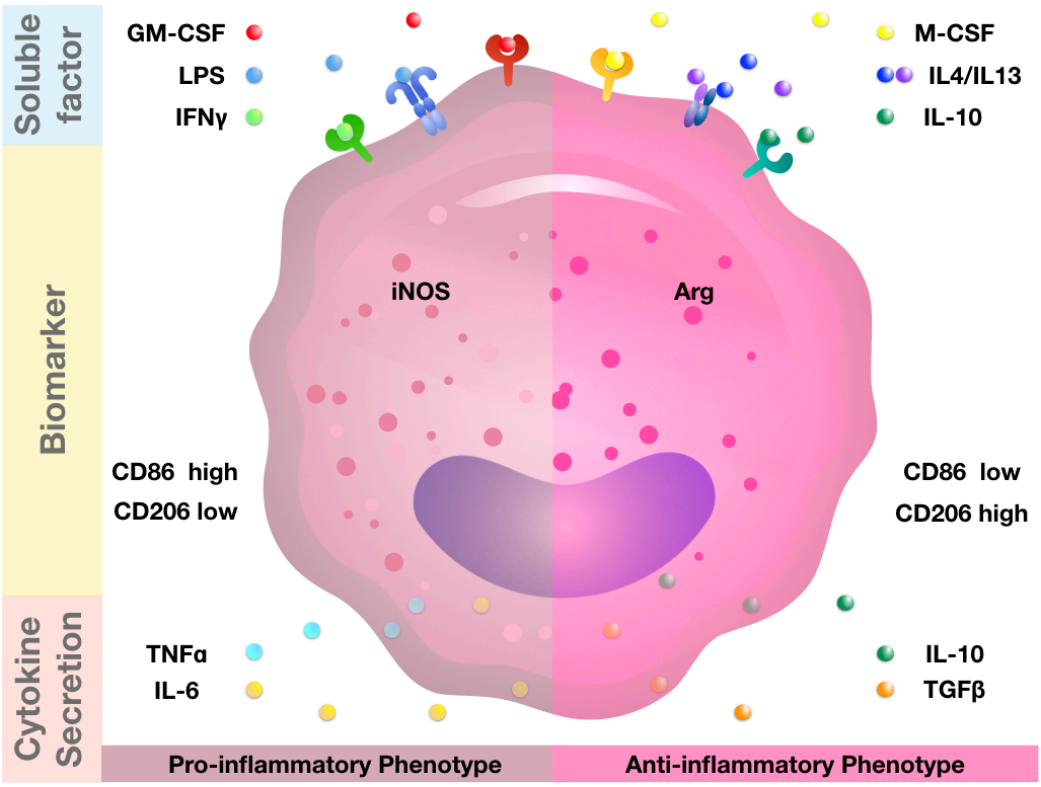

Figure 1. Macrophage polarization. Figure courtesy of Esther Y. Chen.

During cell-mediated immune responses, mononuclear phagocytes are activated to function as pro-inflammatory macrophages by IFN-γ or the combination of two signals: IFN-γ and microbial products such as LPS. During infection and inflammation, innate and adaptive immune cells such as natural killer cells and T helper 1 cells can produce IFN-γ to activate macrophages [3]. Activated macrophages in turn secrete pro-inflammatory cytokines such as interleukin-6 (IL-6), interleukin-12 (IL-12) and tumor-necrosis factor-alpha (TNF-α) that give rise to microbicidal or tumoricidal capacity of macrophages (Figure 1). In addition, classically activated macrophages generate pro-inflammatory mediators such as

inducible nitric oxide synthase (iNOS) that catalyzes the reaction of L-arginine and nicotinamide adenine dinucleotide phosphate to produce nitric oxide and reactive oxygen intermediates to enhance phagocytic ability of macrophages [1]. While classically activated macrophages suppress anti-inflammatory cytokines, alternatively activated macrophages that are stimulated by IL-4 and IL-13 inhibit pro-inflammatory cytokines via STAT-3 dependent signaling pathways by interleukin-10 (IL-10). In addition, murine anti-inflammatory macrophages promote the synthesis of arginase that catalyzes the production of ornithine and urea from L-arginine to enhance polyamine synthesis and wound healing [4]. Promoting ornithine synthesis up-regulates the production of proline, a precursor in collagen synthesis. In mice, because both iNOS and arginase act on L-arginine to produce mediators for killing intracellular pathogens or facilitating tissue repair, they are considered as appropriate markers to identify pro-inflammatory and anti-inflammatory macrophages respectively. Moreover, upon stimulation with IL-4, anti-inflammatory macrophages enhance the expression of mannose receptors such as CD206 that is required for microbicidal activity of macrophages and the formation of foreign body giant cells during foreign body reaction to biomaterials [5]. Together, macrophages are able to adapt different phenotypes because of cues in their microenvironment.

1.2 The Role of Macrophages in Tissue Remodeling and Diseases

1.2.1 Host Foreign Body Response to Implantation of Biomaterials

In recent years, implantation of medical devices such as prostheses and biomaterials has been commonly used as a therapeutic approach in medicine [5]. Although the technology

to develop medical devices has improved tremendously, the last phase of inflammation and wound healing responses occurring after the implantation of the devices, namely the foreign body reaction to biomaterials, still inhibits the duration and functionality of the devices [5]. Because macrophages are thought to be the most critical effector cells in foreign body reaction, a better understanding of the interaction between macrophages and biomaterials could improve development of biomaterials that regulates immune response and promotes the wound healing process.

The host response is a complex cascade of events that takes place after the implantation of biomaterials. The response is initiated with injury at the site of implantation followed by the interaction between blood and the implanted biomaterial. The interaction is marked with the protein adsorption to the surface of the biomaterial. The type and conformation of plasma proteins adsorbed to the biomaterial depend on biomaterial surface properties, which determine cell adhesion and viability. Based on the Vroman Effect, many of the adsorbed proteins are released rapidly from the biomaterial and then the fibrin-rich provisional matrix is developed on and around the biomaterials [5]. The provisional matrix formation leads to acute and chronic inflammation, together with the infiltration of inflammatory cells such as neutrophils, monocyte-derived macrophages and lymphocytes to the implant site [6]. During acute inflammation, mast cells release IL-4 and IL-13 in a degranulation process that mediates monocyte adhesion to the biomaterial surface [5]. Moreover, phagocytes including macrophages are recruited to the biomaterial by mast cell degranulation and histamine [7]. At the site of the implanted biomaterial, macrophages release more chemokines, such as platelet-derived growth factor (PDGF), TNF-α and IL-6 to attract more macrophage migration to the biomaterial [8]. In *in vitro*

culture system, it is shown that the expression of monocyte chemotactic proteins such as CCL4, CCL2 and CCL13 recruit additional macrophages to the implanted biomaterial's interface [5]. At the interface, macrophages can adhere, differentiate, generate signal transduction and be activated to express distinct phenotypes. Meanwhile, lymphocytes, in particular, T helper 2 cells produce IL-4 and IL-13 to regulate macrophage differentiation and up-regulate macrophage mannose receptors. In addition, the formation of granulation tissue is determined by the presence of macrophages and fibroblasts. While macrophage activation and phagocytosis lead to macrophage fusion, which is a foreign body giant cell formation, the infiltration of fibroblasts directs fibrous capsule formation on and around the biomaterial. As a result, a collagen-rich fibrous capsule covers the biomaterial that inhibits the longevity and functionality of the device [6]. Because macrophages influence not only the early stage but also the late stage of the host response to implants, we believe that their modulation can control the host foreign body response and minimize scar formation.

1.2.2 Wound Healing

Extracellular matrix (ECM), an architectural support for the tissues, is dynamic in wound healing and the composition of ECM influences macrophage behavior. In wound healing, the re-epithelialization and matrix remodeling influence on immune cells and keratinocytes' filtration, migration, proliferation, and functions [9,10]. Upon injury, the wound healing process is initiated by the formation of the fibrin-rich provisional matrix followed by epidermal cell migration and inflammation [11-13]. At the later stage, the matrix is replaced by a collagen-rich matrix, which is regulated in part by the presence of TGFβ, and cell adhesion by providing integrin binding sites and a matrix upon which cells can contract

[14,15]. In addition, macrophages play a critical role in wound healing, both at the early stage and the later stage of the process. At the early stage, monocytes are recruited by neutrophils, and then differentiated to monocyte-derived macrophages. Macrophages are activated from pro-inflammatory phenotypes to anti-inflammatory phenotypes by soluble cues in the wound environment [16]. Macrophage polarization facilitates wound healing process, and then recruits fibroblasts that later remodels wound tissues and triggers scar formation. Because of different ECM composition and the function of macrophages during wound healing process, understanding the effect of ECM ligands on macrophages' function will contribute to control the scar formation.

1.2.3. Cancer

In cancer, malignant growth of tissues is associated with changes in the ECM structure and composition. Earlier work has shown a major contribution of substrate stiffness in cancer progression [17]. Culturing MCF10a cells on stiff polyacrylamide gels (> 5 kPa) and soft gels (< 400 Pa), Mouw *et al*. demonstrated that cells on stiff gels enhanced FAK phosphorylation and inhibited the expression of PTEN, the tumor suppressor [18]. Moreover, stiff ECM stimulated tumor metastasis by enhancing TGF-β induced epithelial-mesenchymal transition while suppressing collagen crosslinking and softening matrix prevent tumor metastasis [19]. In addition, macrophages are thought to contribute to tumor progression. At the tumor initiation stage, macrophages have been shown to secrete high concentration of inflammatory cytokines such as TNF-α and IL-6 in response to chronic infections [3]. However, at the later stage, tumor-associated macrophages (TAMs), a major immune cell type in tumor environment, express high level of anti-inflammatory

biomarkers and low level of pro-inflammatory chemokines receptors, similar to alternatively activated macrophages [16]. TAMs are thought to orchestrate many activities that promote tumor progression such as angiogenesis, metastasis, and immune suppression via upregulation of pathways including NF-κB, STAT3, and CTL proliferation [16,20]. Thus, targeting tumor-associated macrophages is a potential therapeutic approach to treat cancer.

1.2.4 Atherosclerosis

Macrophages influence the development of atherosclerosis, an inflammatory disease of the cardiovascular system. In atherosclerosis, plaques are slowly built up on the artery walls. Plaques are composed of a lipid-laden core containing many immune cells including macrophages, within an ECM capsule, which can vary in architecture and composition. Using collagen type-specific antibodies, Katsuda *et al.* demonstrated that 70% collagen in human atherosclerotic plaques was collagen type I [21]. Moreover, compared to the early stage, the content of collagen is more concentrated at the later stage of atherosclerosis [22]. High concentration of collagen type I promotes macrophage differentiation and regulates macrophage functions, and matrix metalloproteinase (MMP)-9 production [23]. In atherosclerosis, using macrophage scavenger receptors, inflammatory macrophages uptake phospholipids and cholesterol derivatives, and secrete inflammatory cytokines such as TNF-α that leads to increased lesion size and induces apoptosis of other cells such as endothelial cells and smooth muscle cells [24,25]. Moreover, macrophages contribute to the progression of atherosclerosis via foam cell formation, which is found in the lipid core [26]. In

summary, the effect of inflammatory and anti-inflammatory macrophages on the development of atherosclerosis is still not well defined and understood.

1.3 The Effect of Physical and Adhesive Cues on Macrophage Morphology and Function

1.3.1 Topography

Cells respond to myriad cues from their microenvironment that control both their morphology as well as their function. In recent years, it has become widely appreciated that similar to biochemical cues, physical cues presented by the microenvironment can also regulate behaviors including cell morphology [27,28], proliferation [29,30], migration [31,32] and differentiation [33-36]. It is thought that the ECM provides resident cells topographic stimuli with micro- and sub-microscale structures of fibrous proteins as instructive cues to control cell morphology and behavior. Because of the effect of ECM physical cues on cell shape and function, biomaterial surface topography has been explored as a way to regulate cellular activities. Several studies have indicated that because of the physical properties of a biomaterial surface, the topographical structures can remarkably govern cell responses [27].

Micro- and nano-patterned topography regulates cell alignment, migration and behavior. Many studies investigating the effect of micro-patterned topography have found that parallel micro groove patterns direct cell alignment along the grooves and in turn influence cellular activities [37-39]. Using micropatterned perfluoropolyether (PFPE) substrates, Bartneck *et al.* demonstrated that human macrophages cultured on 10 μm-patterned substrates assumed pro-inflammatory phenotype, but anti-inflammatory

phenotype when cells were cultured on 20 μm-cylindrical post substrates [40]. Using nano-imprinting lithography and hybrid technique to imprint parallel gratings on poly(ε-caprolactone), poly(lactic acid) and poly(dimethyl siloxane), Chen *et al.* demonstrated that macrophages elongated maximally on 500 nm grating substrates, compared to flat substrates [41]. Moreover, TNF-α and vascular endothelial growth factor (VEGF) secretion levels by macrophages were regulated by topographical cues [41]. In addition, micro-grating patterns with different line width stimulated cell elongation and the cell shape might modulate cell activation. McWhorter *et al.* reported that on 20 μm wide lines that were created by micropatterning lines of fibronectin on PDMS coated glass, macrophages elongated more than on 50 μm lines. When macrophages are forcibly elongated on the engineered substrates, they were activated and produced cytokines associated with alternatively activated phenotypes [2]. Taken together, these studies suggest that micro and nano-patterned topographies modulate macrophage morphology and function. However, the mechanism underlying topography-induced changes in macrophage function are not well understood.

1.3.2 2D versus 3D Microenvironment

Cell-matrix adhesion has been extensively studied *in vitro*, 2D and 3D cultures, as well as the role of matrix on cell function in many adhesive cell types [42,43]. A study by Yamada group on fibroblast demonstrated that cell-derived 3D matrix mediated cell adhesion with the triple colocalization of paxillin, α5 integrin, and fibronectin, and the distribution of tyrosine phosphorylation FAK, which were different from 2D substrates. In addition, fibroblasts cultured on the 3D culture adopted higher migration rate than on 2D

culture [44]. Moreover, Li *et al.* showed that compared to fibroblasts on 2D substrates, cells on fibrin-based 3D culture expressed higher level of MMPs and increased the reprogramming to cardiomyocytes [45]. Moreover, using 2D substrates and 3D organoid stem cell systems, Otani *et al.* demonstrated that the development of cortical neurogenesis was not dependent on 3D structures, but on species-specific program [46]. Although there is much evidence demonstrating the different effect of 2D and 3D microenvironments on cell adhesion, differentiation, and migration, less is understood how 3D microenvironment influences macrophage morphology and function. Using a 3D *in vitro* model, co-culture system of macrophages and human squamous cell carcinoma in collagen hydrogels, to study tumor-associated macrophages, Linde *et al.* showed that in organotypic co-cultures, macrophages were viable, polarized by soluble factor stimulations, and regulated tumor progression [47]. Moreover, while monocytes used the amoeboid mode to migrate in 3D cultures, anti-inflammatory macrophages formed podosome rosettes and used mesenchymal mode to migrate through the matrices [48,49]. Compared to 2D collagen type I coated substrates, human macrophages differentiated on 3D collagen type I substrates exhibited higher expression of CD71, MMP-2, and MMP-9 [50]. Together, compared to 2D culture, 3D culture is much closer to *in vivo* environment and it is important to understand the effect of 3D matrices on macrophage polarization in order to design new biomaterial scaffolds for tissue engineering.

1.3.3 Stiffness

Stiffness of tissue and matrix appears important in regulating the morphology and function of many adhesive cells such as fibroblast, endothelial cells, and stem cells. Because

of tissue stiffness, cells adopt different types of adhesion, cytoskeletal structures, differentiation [51]. Examining the response of fibroblasts and endothelial cells to the stiffness of culture substrates, Pelham *et al.* demonstrated that cells on soft 1 kPa matrices assumed diffuse and dynamic structures while cells on stiff matrices, 30 to 100 kPa, expressed stable localization of vinculin [52]. Fibroblasts cultured on stiff polyacrylamide gels, 16 kPa, expressed stress fibers or high level of actin but no actin was detected when cells were grown on softer gels [53]. Mesenchymal stem cells (MSCs) cultured on soft materials, 0.1 to 1 kPa, expressed high neurogenic biomarkers, cells cultured on medium stiff materials, 8 to 17 kPa, expressed high level of myogenic markers, but on the most stiff materials, cells were differentiated to osteogenic phenotypes [54]. The effects of stiffness on macrophage phenotypes have recently been explored. Using polyacrylamide and PEG to create interpenetrating polymer networks with varying moduli, Irwin *et al.* reported that stiffer substrates, 348 kPa, enhanced human macrophages attachment than softer substrates, 1 to 10 kPa [55]. Moreover, the concentration of TNF-α was secreted higher by THP-1 cells attached on softer substrates (1.4 kPa, 6.0 kPa), compared to stiffer substrates [55]. Similarly, Blakney *et al.* also showed that compared to soft substrates, stiffer substrates enhanced macrophage spreading and reduced inflammatory response *in vitro* and *in vivo* [56]. Moreover, macrophages cultured on stiffer substrates such as 240 kPa and 840 kPa, were more spread, compared to softer substrates, 130 kPa. Without LPS stimulation, gene expression of inflammatory cytokines such as TNF-α, IL-1β, and IL-6 was reduced in macrophages while the stiffness of hydrogels was increased [56]. In a separate study, Previtera *et al.* demonstrated that when the stiffness of substrates was increased from 0.1, 1, 10, 100 to 1000 kPa, the expression of pro-inflammatory markers was increased in

macrophages [57]. Moreover, Adlerz *et al.* also reported that substrate stiffness regulated the response of human monocyte-derived macrophages to polyacrylamide gels, including cell adhesion, morphology, proliferation, and migration [58]. In conclusion, these studies suggest that the stiffness of cell culture substrates regulate macrophage adhesion and activation.

1.4 Overview of Dissertation Research

Macrophages, which are found in every type of tissue, play a critical role in innate and adaptive immune system. They evolve in host defense and maintenance of tissue homoeostasis with distinct functions depending on polarization state [59]. To display anatomical and functional diversity, macrophages assume a spectrum of activation for which the mechanism has not been fully elucidated.

Macrophages are highly plastic cells that alter their phenotype in response to cues in the microenvironment. Although many studies have elucidated about how soluble cues influence macrophage phenotype, relatively few are focused on how physical cues in the microenvironment regulate their behavior and alter their signaling processes. In our previous work, we demonstrated that cell shape or the geometry of adhesion influences macrophage phenotype. More specifically, we found that forcing cells to elongate led to an increase in the expression of biomarkers associated with the alternatively activated pro-healing phenotype [2]. We confirmed that extracellular matrices' physical properties instructively regulated cell behaviors. Moreover, many recent studies have indicated that surface topography structure of materials also influence morphology and behavior of many other cell types [54,60,61]. In this project, we explore how insoluble cues including surface topology and 2D versus 3D microenvironment might be leveraged to alter macrophage cell

shape and phenotype and the signaling downstream of regulating macrophage function by 2D and 3D cultures. **The goal of the dissertation** is to elucidate how the adhesive microenvironment contributes to macrophage morphology and function. This work is focused on three specific aims:

Specific Aim 1: Characterize macrophage function on surfaces with micro- and nano-scale topographical features *in vitro* and *in vivo*. We used techniques to create micro- and nano-pattern topographical cues, and examined their effects on macrophage cell shape and phenotype. Titanium substrates with multiple groove sizes and wrinkled substrates with multi-scale grooves were used, and topographical modulation of macrophage function was examined *in vitro* and *in vivo*.

Specific Aim 2: Examine the effect of ECM ligands on macrophage function in 2D and 3D microenvironment. The effect of ECM ligands on macrophage cell shape and function was examined in both in 2D and 3D cultures. We examined the effects of adhesion to different matrix ligands on macrophage response to cytokine stimulation.

Specific Aim 3: Understand signaling pathways downstream of adhesion in regulating macrophage inflammatory responses. We examined the effect of adhesion on the expression of integrin CD11b, TLR4 by macrophages in response to LPS stimulation. The effect of adhesion on MAPK and NF-κB signaling pathways was investigated in both 2D and 3D cultures.

CHAPTER 2- Investigation of Macrophage Function on Surfaces with Micro- And Nano-Scale Topographical Features *In Vitro* and *In Vivo*

2.1 Micro- and Nanopatterned Topographical Cues for Regulating Macrophage Cell Shape and Phenotype [62]

2.1.1 Introduction

Implantation of a biomaterial-containing device is an essential component of many therapies used in modern medicine [63], and although medical devices have significantly advanced in complexity and functionality, the host response to the biomaterial itself is still a major concern for the longevity of most devices. This foreign body response begins with injury to the tissue caused by surgical implantation, and is followed by inflammatory cell infiltration and activation, and finally the formation of a fibrous capsule to isolate the implant. It is thought that macrophages, immune cells that regulate inflammatory and wound healing processes, are a key determinant of the overall response to the foreign material [5]. Macrophages are highly plastic cells that are involved in host defense, wound healing, and immune regulation. To perform these diverse functions, they polarize towards different phenotypes in response to cues in their microenvironment. For example, in response to inflammatory or danger signals including lipopolysaccharide or interferon-γ (IFN-γ) macrophages secrete pro-inflammatory cytokines, such as tumor necrosis factor-α (TNF-α) and express inducible nitric oxide synthase (iNOS) to fight infection. In contrast,

in a wound healing environment, they produce anti-inflammatory mediators, such as interleukin 10 (IL-10) and arginase-1 (Arg1) to facilitate tissue repair [3,64]. Understanding how biomaterials regulate the phenotypic polarization of macrophages will likely aid the design of biomaterials for medical devices.

It has conventionally been thought that the chemistry of biomaterials dictates the behavior of infiltrating immune cells by altering cell adhesive interactions. However, recent evidence suggests that material geometry, or size and shape, may in fact dominate the overall response [28,65,66]. Biomaterial surface micro-topography has also been explored as physical cue to control the host response, and offers the advantage of long-term stability and cost-effective fabrication methods. Studies have generally suggested that surfaces that contain micro-scale features appeared to enhance the adhesion of macrophages and their secretion of inflammatory cytokines including IL-1β, IL-6, and nitric oxide when compared to macrophages on smooth surfaces [35,67-69]. More recently, it has been suggested that the degree of roughness is important, since TiO_2 surfaces that were moderately roughened induced polarization towards a pro-healing phenotype, whereas greater roughness led to inflammatory activation [65]. Precisely engineered microfabricated substrates have further helped to elucidate the effects of topography on macrophage behavior and the host response. Lithographically generated gratings as well as different post geometries have also been shown to modulate macrophage TNF-α and vascular endothelial growth factor (VEGF) secretion [40,41]. Finally, using electrospinning to create three-dimensional micro- or nano-scale fibers, it has been observed that nanofibers elicit significantly less macrophage adhesion and inflammatory activation, and minimize the host response, when compared to microfibers [70-72]. Taken together, these studies suggest that micro and nano-patterned

topographies modulate macrophage behavior *in vitro* as well as the host response *in vivo*. However, the mechanism underlying topography-induced changes in macrophage function is still not well understood.

We recently demonstrated that cell shape is involved in regulating macrophage polarization state[2]. Specifically macrophages forced to elongate on fibronectin micropatterned lines exhibited an increase in expression of M2 polarization markers. Cell elongation influences the behavior of many cell types, particularly myocytes, which rely on their shape for directional force generation [73-75]. While the function of macrophages in the body is quite different, these cells have been shown to exhibit different shapes *in vivo*, where M2 polarized cells are more elongated and often found within fibrous tissue architectures [31,76,77]. Immune cells may in fact share similar mechanisms with other cell types for sensing their extracellular environment. Elongated cells generally exhibit focal adhesions that are aligned along the direction of elongation and a more organized cytoskeletal components [78-81]. While macrophages do not form extensive focal adhesions, phalloidin staining of the actin cytoskeleton of M2 polarized or micropatterned macrophages is indeed brighter [2]. Furthermore, a growing body of evidence in the stem cell field suggest that physical features on the culture substrate regulate differentiation through changes adhesion signaling and cytoskeletal organization [82-84]. As such, it is possible that changes in macrophage behavior from surface topographies may also depend on a mechanism involving changes in cell shape and adhesion.

In this study, we hypothesized that surface topography alters macrophage function through control of cell shape. To test this, we examined the effect of surface grooves on macrophage cell elongation and polarization. Using deep-etch techniques, we fabricated

titanium surfaces containing micro and nano-patterned grooves, which have been previously shown to promote bone marrow stromal and endothelial cells to elongate and regulate cell function [61,85]. We characterized the degree of macrophage elongation resulting from adhesion to a range of groove widths and examined the expression of phenotypic markers, as well as secretion of cytokines. The results demonstrate that elongation and degree of M2 polarization are correlated, and suggest a promising approach for modulating macrophage function in response to biomaterial implants by using structured immunomodulatory surfaces.

2.1.2 Materials and Methods

Patterned Ti substrate design and fabrication

Titanium substrates were fabricated as previously described [85]. Briefly, polished Grade 1 Ti substrates were cleaned thoroughly by sequential sonication in acetone and isopropanol, followed by rinsing in deionized water, and drying with N_2 gas. A SiO_2 etch mask was deposited using plasma-enhanced chemical vapor deposition (VLR, Unaxis), followed by thermoplastic resist spin-coating. Patterns were transferred from a silicon nanoimprint master to the resist using thermal nanoimprint lithography (NX2000, Nanonex). The patterns were transferred into the SiO_2 mask layer by plasma-etching, and then the underlying Ti substrate by titanium deep reactive ion etching (Ti DRIE) (E620 R&D, Panasonic Factory Solutions) [86,87]. Subsequent removal of the remaining SiO_2 from the patterned surface by plasma etching revealed the bare patterned Ti. Each 22 mm x 22 mm substrate contained sixteen discrete 25 mm^2 patterned regions, including a unpatterned region (i.e., Blank) that served as a control. The pattern groove width (D) was varied from

0.15 mm to 50 mm and the pitch (P) was twice the groove width (Figure 2A). The groove depth ranged between 0.8 μm to 1.3 μm. While multiplexed Ti substrates containing all groove dimensions were used for most *in vitro* experiments, a separate set of 22 mm x 22 mm substrates was fabricated with a single groove width patterned across the entirety of the surface (i.e., 200 nm, 450 nm, 5 μm, 50 μm, or unpatterned), for use in the BMDM cytokine secretion experiments. Prior to all *in vitro* experiments, Ti substrates were sterilized by incubating in 70% ethanol for 30 min, sonicating for 5 min, and then washing thoroughly with sterile PBS.

Cell isolation and culture

Bone marrow cells were isolated from femurs of C57BL/6 mice (Jackson Laboratories). Cells were treated with ACK lysis buffer (Invitrogen) to remove red blood cells, centrifuged, and then resuspended and cultured in D10 media consisting of high glucose DMEM supplemented with 10% heat-inactivated FBS, 2 mM L-glutamine, 100 units/mL, 100 μg/mL streptomycin (all from Invitrogen), and 10% conditioned media containing macrophage colony stimulating factor (M-CSF) produced by CMG 12-14 cells [88] to induce differentiation to bone marrow derived macrophages (BMDMs). BMDMs were maintained at 37°C in a humidified 5% CO_2 incubator. On day 7 of culture, BMDMs were dissociated using Cell Dissociation Buffer (Invitrogen) and on average, 20 million BMDMs were obtained per femur. Day 7 BMDMs were seeded on Ti substrates, which were not pre-treated before seeding. After 4 h of culture to allow adhesion of cells, the Ti substrates were transferred to a new culture well with fresh D10 media and then cultured for an additional 24 h or 36 h. Substrates were washed thoroughly with sterile PBS to remove non-adherent

cells prior to all assays. All protocols involving animals were approved by the Institutional Animal Care and Use Committee at the University of California Irvine prior to initiation of the study.

Scanning electron microscopy

Dissociated day 7 BMDMs were seeded at a density of 70,000 cells/cm^2 on Ti substrates. After 36 h of culture, samples were fixed with 2.5% glutaraldehyde (Electron Microscopy Sciences) for 1 h and washed thoroughly with PBS, followed by a graded series of ethanol for dehydration. Samples were chemically dried by submerging in a bath of hexamethyldisilazane (Sigma-Aldrich) for 5 min. Dried samples were sputter-coated with iridium (South Bay Technology Ion Beam Sputtering System) prior to imaging by scanning electron microscopy (FEI Quanta 3D FEG Dual Beam). All images were taken at 15 kV accelerating voltage, high vacuum with 30 μm aperture.

Cell shape and morphological analysis

Dissociated day 7 BMDMs were seeded at a density of 100,000 cells/cm^2 on Ti substrates. To assess cell shape and morphology, cells were incubated with 10 μM CellTracker Green CMFDA (5-Chloromethylfluorescein Diacetate) (Invitrogen) in serum-free DMEM at 37 °C in a humidified 5% CO_2 incubator for 45 min, and then transferred to fresh D10 media. After 30 min, the samples were washed thoroughly with sterile PBS before imaging. For analysis of cell morphology, cells were visualized using an Olympus inverted microscope with a 20x objective. The long axis and short axis of each cell were manually traced and measured using ImageJ software (National Institutes of Health). The

long axis was determined as the longest length of the cells and the short axis was defined as the length across the nucleus, perpendicular to the long axis. Elongation factor was calculated as the ratio of the long axis to the short axis. A hundred cells per condition across three separate biological experiments were examined.

Fluorescence staining and imaging

Dissociated day 7 BMDMs were seeded on Ti substrates at a density of 100,000 cells/cm^2 for Arg1 and iNOS staining and 30,000 cells/cm^2 for vinculin staining. Samples were fixed with 4% paraformaldehyde (Electron Microscopy Sciences) for 5 min, and washed thoroughly with PBS containing 0.05% Tween-20 (Sigma-Aldrich). To permeabilize cells, the samples were treated with 0.1% Triton X-100 (Sigma-Aldrich) in PBS for 5 min, washed, and then blocked with 5% normal goat or donkey serum (Jackson ImmunoResearch) in PBS overnight at 4^{o}C. Cells stained with Arg1 were fixed with 100% cold methanol on ice for 15 min. Cells were then incubated with primary antibodies including goat anti-arginase-1 (Santa Cruz Biotechnology Inc.), rabbit anti-NOS2 (Santa Cruz Biotechnology Inc.), or mouse monoclonal hVIN-1 anti-vinculin antibody (Sigma Aldrich) for 1 h, washed thoroughly with 1% BSA, and then incubated with Alexa Fluor-594 donkey anti-goat, Alexa Fluor-488 goat anti-rabbit or Alexa Fluor-594 goat anti-mouse fluorescent secondary antibodies (Jackson ImmunoResearch) for 1 h. For analysis of actin, samples were incubated with Alexa Fluor-488 conjugated phalloidin (Invitrogen). All cells were counterstained with Hoechst 33342 dye (Invitrogen), washed thoroughly, and then imaged using an Olympus inverted microscope (for Arg1 and iNOS) or a Zeiss LSM780 confocal microscope with 63x oil objective (for actin and vinculin). For fluorescence

intensity analysis, sets of nuclear and Arg1 fluorescence images or nuclear and iNOS fluorescence images were taken of each sample and the integrated fluorescence intensity was quantified using CellProfiler software (MIT Broad Institute). Cells were determined to be positive for Arg1 or iNOS staining if integrated fluorescence for each cell exceeded a threshold value chosen such that more than 95% of non-stimulated cells on glass substrates were negative. At least three hundred cells per condition were examined across three separate biological experiments.

Cytokine secretion

BMDMs were cultured on Ti substrates as described above. In addition, cells were cultured on glass substrates and stimulated with a combination of E.coli LPS (Sigma-Aldrich), recombinant murine IFN-γ (R&D systems, Minneapolis, MN), IL-4 (Invitrogen) and IL13 (Invitrogen) with concentrations as described in the figure legends. Dissociated day 7 BMDMs were seeded at a density of 100,000 cells/cm^2 on Ti and glass substrates. After an additional 36 h, supernatants were collected and analyzed for TNF-α and IL-10 by ELISA (enzyme-linked immunosorbent assay) following the manufacturer's instructions (BioLegend, San Diego, CA). Three separate biological experiments were performed.

Statistical analyses

Statistical analysis was performed using ordinary one-way ANOVA with Dunnett's post hoc test and uncorrected Fisher's LDS (multiple comparisons test). $p<0.05$ was considered statistically significant.

2.1.3 Results

Micro and nano-patterned grooves regulate macrophage elongation

Titanium (Ti) substrates were fabricated with highly defined and uniform patterned surface topographies, as demonstrated by scanning electron microscopy (SEM) (Figure 2B). Measurements of grooves using SEM micrographs confirmed that the groove width and pitch, or distance between grooves, were achieved as designed. Macrophages seeded on Ti materials adhered and spread to a flat, pancake shape on unpatterned surfaces after 36 h of culture (Figure 2B). Consistent with previous observations in other cell types as well as macrophage cell lines [36,41,80], bone marrow derived macrophages aligned along the grooved surface topographies, generally in the direction parallel to the grooves (Figure 2B). We observed that compared to cells on the unpatterned surfaces, many cells on the patterned surfaces appeared to be less flattened, which was accentuated on surfaces with grooves smaller than 5 mm wide (Figure 2B). Cell elongation appeared to be most dramatic on substrates with 450 nm wide groves (Figure 2B).

In order to more quantitatively assess cell shape and allow better detection of the cell borders, we used Cell Tracker Green (CMFDA) to fluorescently label cells, and examined their shape by fluorescent light microscopy (Figure 3A). Macrophages were seeded on titanium surfaces with groove widths ranging from 150 nm to 50 mm. Similar to the images taken by SEM, fluorescent images of macrophages also showed alignment along the length of the grooves, with cells exhibiting the highest degree of elongation along the 400-500 nm grooves. The degree of elongation was determined by measuring the length of the longest axis and dividing by the width across the cell nucleus, and revealed a biphasic dependence of elongation on groove width. Compared to blank Ti substrate, widths, that

were in a range between 200 nm and 10 μm, led to higher cell alignment and significant higher elongation factor (Figure 3B). The highest degree of elongation was observed on surfaces with grooves of approximately 450-500 nm wide (Figure 3B). The degree of cell spreading was similar and averaged approximately 550-750 mm^2 across all groove widths (Figure 3C). Together, these data suggested that surface grooves on titanium surfaces influence macrophage elongation without altering spread cell area.

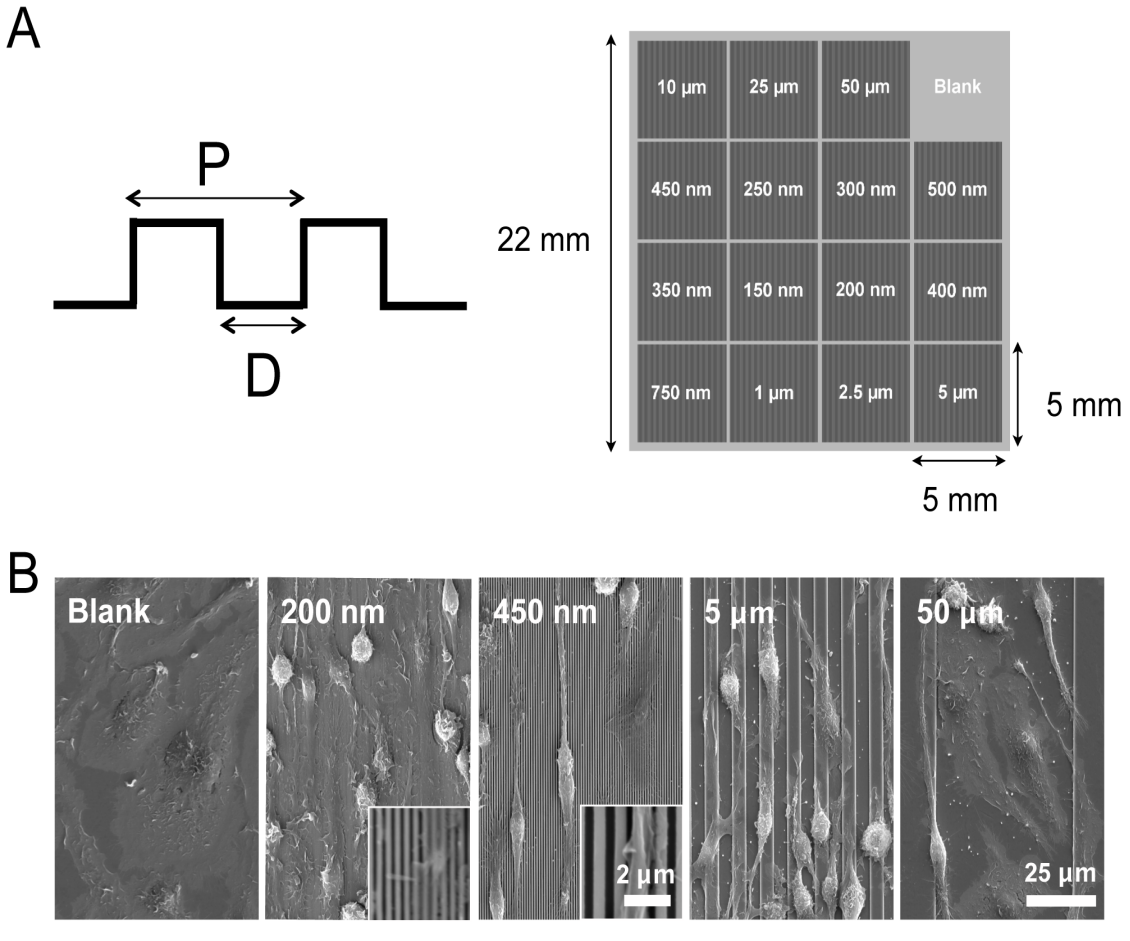

Figure 2. Deep-etched titanium surfaces with varied groove dimensions. (A) Schematic of the Ti substrate with micro- and nano-patterned surface topographies used in this study. D denotes groove width; P denotes pitch, which is twice the groove width. Groove depth is approximately 0.8 μm to 1.3 μm for all widths. **(B)** Scanning electron

microscopy micrographs of BMDM after 36 h culture on Ti substrate with 200 nm, 450 nm, 5 μm, and 50 μm grating patterns and non-patterned control. [62]

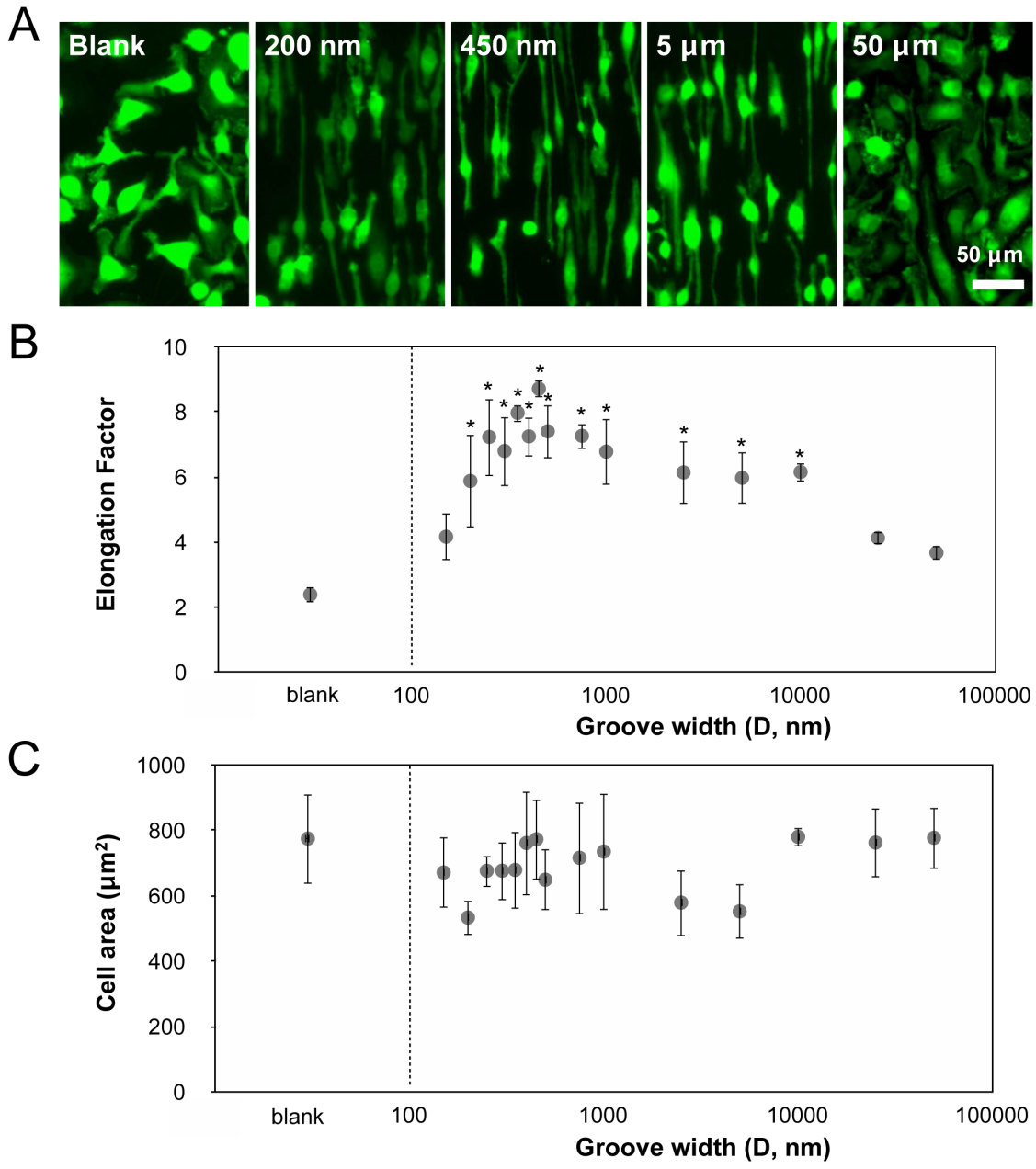

Figure 3. Grooved surfaces regulate macrophage elongation. (A) Fluorescence micrographs of BMDM after 24 h culture on bulk Ti substrate with 200 nm, 450 nm, 5 μm, and 50 μm grating patterns and non-patterned control. Cells were stained using CellTracker

Green CMFDA dye for monitoring cell shape. Scale bar = 50 μm. **(B)** Quantification of BMDM elongation factor on Ti surfaces of varied groove widths. Mean ± SEM (*p < 0.05; ordinary one-way ANOVA with Dunnett's post test, in comparison to blank Ti substrate, *n* = 3). (**C**) Quantification of BMDM cell area on Ti surfaces of varied groove widths. Mean ± SEM, *n* = 3.
62

Surface grooves alter adhesive and cytoskeletal structure

To more closely examine the interactions between macrophages and grooved Ti substrates, we evaluated adhesive structures and actin filaments using fluorescent microscopy. Macrophages were cultured on 200 nm, 450 nm, 5 μm, 50 μm patterned surfaces and non-patterned surfaces and analyzed for vinculin by immunostaining and actin by phalloidin binding (Figure 4). Consistent with what we and others have previously observed, macrophages do not exhibit organized stress fibers. Instead, the cells exhibited diffuse actin staining with some clustering particularly at the tips of elongated cells on 450 nm and 5 μm grooves. Well spread cells also showed actin clusters within lamellepodia. Vinculin staining revealed similarly diffuse structures with few focal adhesions. Interestingly, cells cultured on 200 nm grooved surfaces exhibited few structures containing actin clusters and less overall vinculin staining, suggesting that 200 nm grooves may in fact depress adhesive interactions. Together, these data demonstrate that although adhesive and cytoskeletal structures in macrophages are relatively disorganized compared to other adhesive cell types including fibroblasts and endothelial cells, surface grooves do alter these structures.

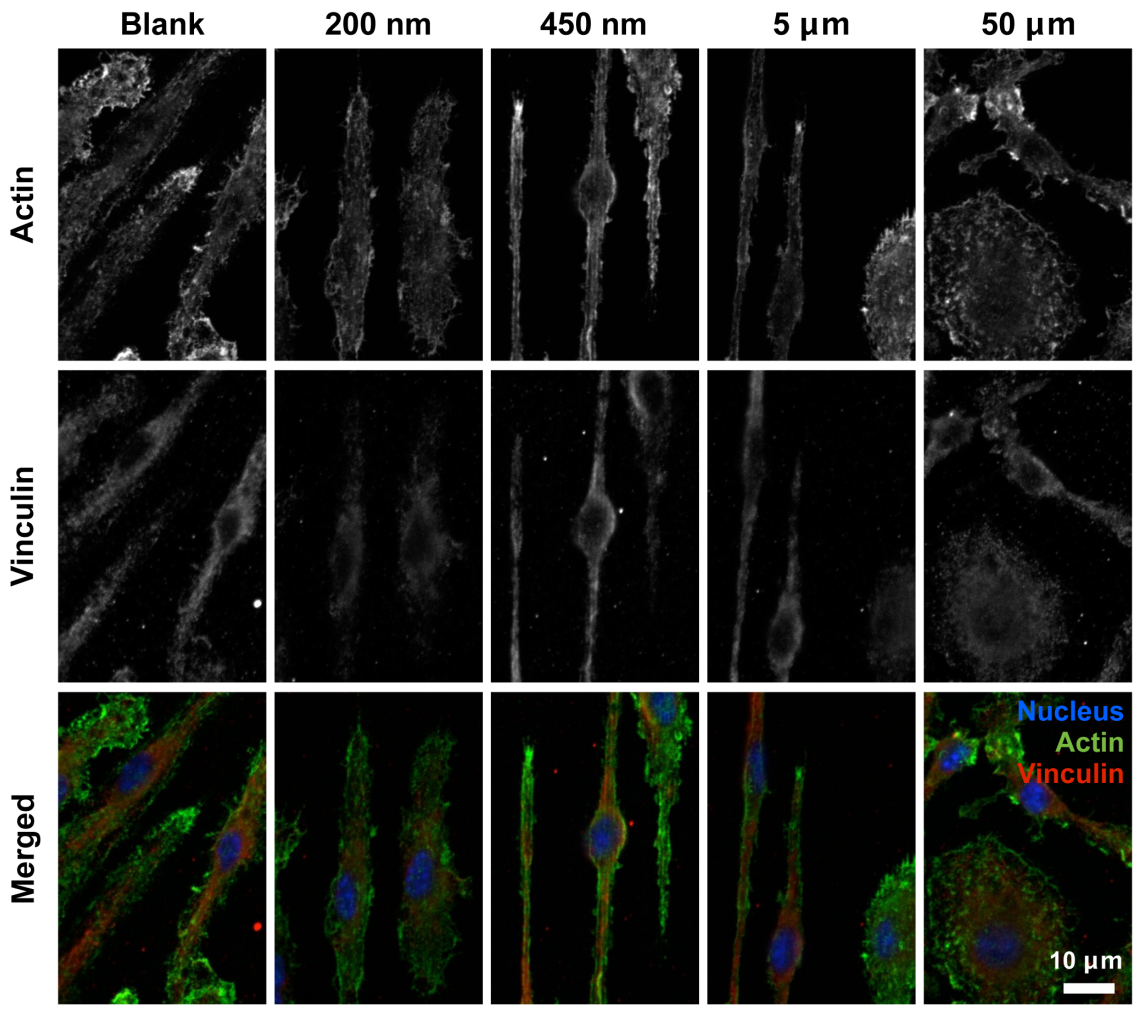

Figure 4. Adhesive and cytoskeletal structures of macrophages on grooved surfaces. Fluorescent images of vinculin (red; immunostaining) and actin filaments (green; phalloidin staining) in BMDMs cultured on various groove sizes. [62]

Surface grooves modulate macrophage phenotype

We previously reported that BMDM cell shape influences their phenotype, and specifically that cells forced to elongate on micropatterned lines increased expression of phenotypic markers associated with the alternatively activated, M2 phenotype. We anticipated that since surface grooves alter macrophage cell shape, they might also be

leveraged to modulate phenotype. To investigate this, we examined arginase-1 (Arg1, anti-inflammatory marker) and inducible nitric oxide synthase (iNOS, inflammatory marker) expression by immunofluorescence microscopy. Expression levels were compared against control cells polarized by cytokine treatment. We found that in comparison to IL-4/IL-13 treatment, the expression of Arg1 on titanium surfaces was lower, but varied and dependent on groove dimensions (Figure 5B). At very small groove widths, expression of Arg1 was low, and increasing the groove width led to an increase in Arg1 expression peaking broadly on substrates containing 400 nm - 5 mm grooves (Figure 5B). Arg1 expression in cells on 300 nm, 500 nm, 1 mm, 2.5 mm, 5 mm, and 10 mm grooves was significantly different from expression in cells on 150 nm grooves. The expression of Arg1 was generally correlated with the degree of elongation, although at wider groove dimensions (25 – 50 mm) and flat titanium surfaces where elongation was generally lower, the Arg1 expression remained relatively high. The expression of iNOS remained similarly low across all groove widths (Figure 5D) and much less than macrophages stimulated towards an M1 phenotype by treatment with 10 ng/mL LPS and 10 ng/mL IFN-γ. Thus, these data suggested that surface grooves on Ti do not affect inflammatory activation, but drive macrophages to polarize towards an anti-inflammatory, pro-healing phenotype.

To further investigate whether grooves altered the secretion of cytokines associated with phenotypic polarization, we examined levels of IL-10 and TNF-α, representative anti- and pro- inflammatory cytokines respectively in the media after macrophages were cultured on Ti substrates containing single grooved patterns including 200 nm, 450 nm, 5 mm or 50 mm grooves, as well as an unpatterned control Ti surface. We found macrophages cultured on 5 mm surfaces exhibited significantly higher secretion of the anti-

inflammatory cytokine, IL-10, when compared to cells on other Ti surfaces (Figure 6A). In comparison, secretion of TNF-α remained low in macrophages across all conditions (Figure 6B). Together, these data show that for Ti substrates, grooved surfaces can indeed modulate the function of macrophages, promoting an anti-inflammatory phenotype.

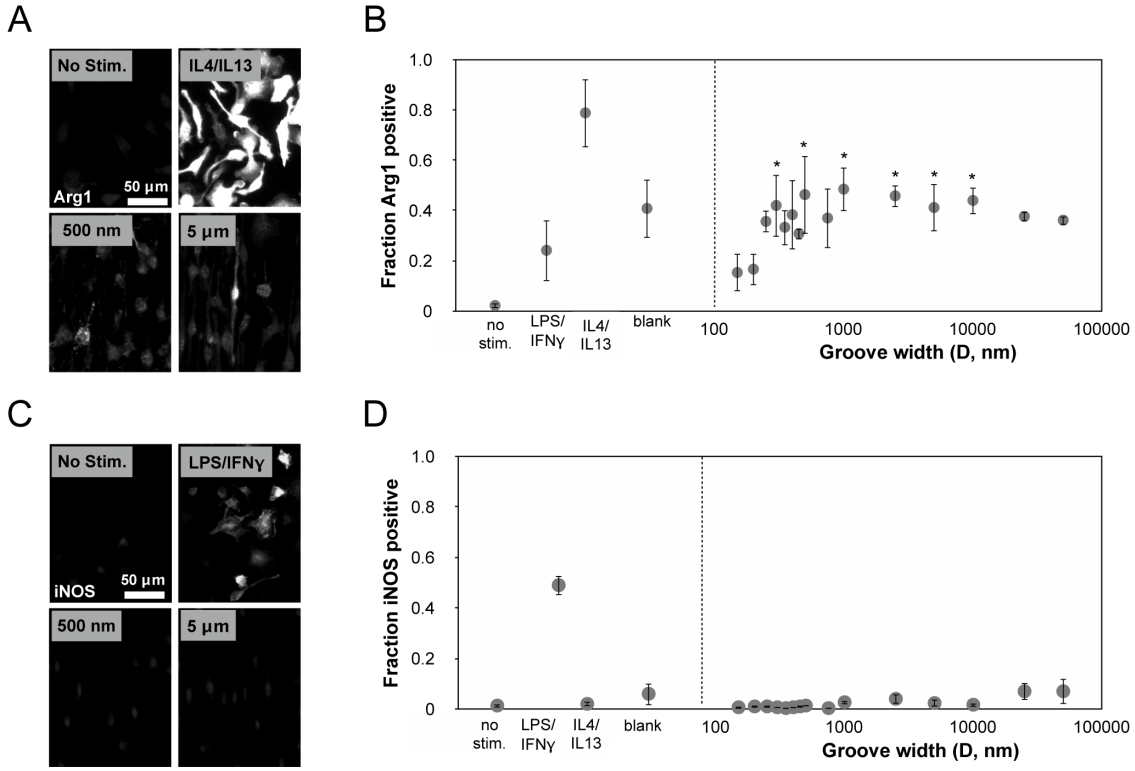

Figure 5. Expression of macrophage polarization markers on grooved surfaces. (**A**) Representative Arg1 immunofluorescent images of BMDMs on control and grooved substrates. Scale bar = 50 µm **(B)** Quantification of Arg1 expression corresponding to the groove width. Mean ± SEM (*$p < 0.05$; ordinary one-way ANOVA with uncorrected Fisher's LDS, blank and grooved surface topography substrates compared to 150 nm grooved substrate, $n = 3$). (**C**) Representative iNOS immunofluorescent images of BMDMs on control and grooved substrates. Scale bar = 50 µm. **(D)** Quantification of iNOS expression corresponding to the groove width. Mean ± SEM, $n = 3$. No stim. denotes unstimulated, LPS/IFN-γ was stimulated with 10 ng/mL LPS and 10 ng/mL IFN-γ, LPS/IL4/IL13 was stimulated with 20 ng/mL IL4 and 20 ng/mL IL13, Blank denotes unstimulated cells on a flat Ti substrate. [62]

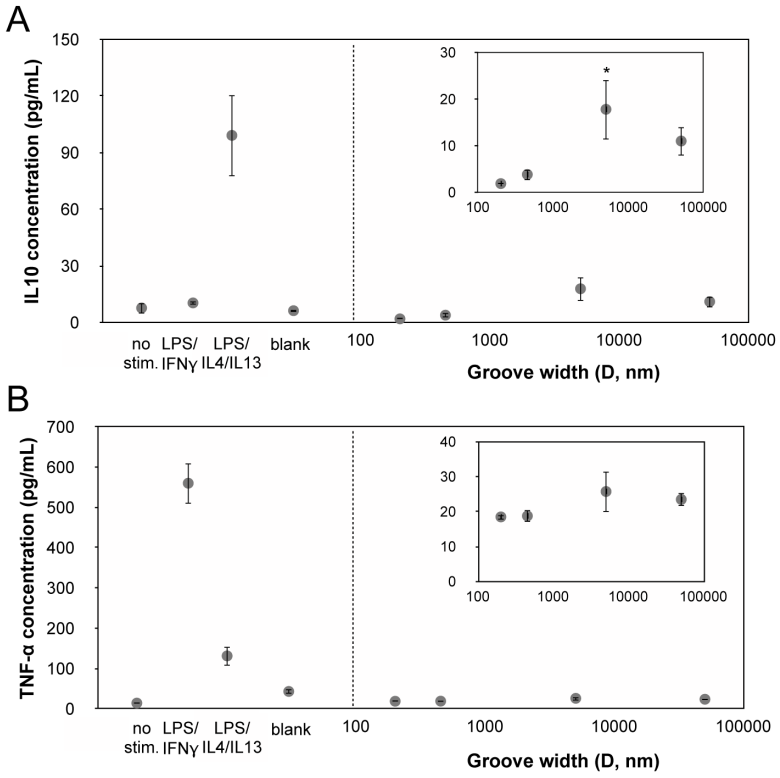

Figure 6. Cytokine secretion from macrophages on grooved surfaces. (A) Quantified IL10 secretion from macrophages cultured on different groove widths. Mean ± SEM (*p < 0.05; ordinary one-way ANOVA with Dunnett's post test, in comparison to 200 nm grooved substrate, *n* = 3). **(B)** Quantified TNF-α secretion from macrophages cultured on different groove widths. Mean ± SEM, *n* = 3. No stim. denotes unstimulated, LPS/IFN-γ was stimulated with 0.5 ng/mL LPS and 10 ng/mL IFN-γ, LPS/IL4/IL13 was stimulated with 0.5 ng/mL LPS, 20 ng/mL IL4 and 20 ng/mL IL13, Blank denotes unstimulated cells on a flat Ti substrate. [62]

2.1.4 Discussion

We demonstrate the effect of grooved topographies on bone marrow derived macrophage shape, phenotypic markers, and cytokine secretion. Our results show that for Ti substrates, micro and nano-grooved topographies caused macrophages to elongate along the direction of the grooves, consistent with previous studies with other cell types on

similar substrates [85]. Interestingly, the degree of cell elongation level was biphasic and decreased when cells were cultured on grooves less than 200 nm or greater than 10 mm. When the grooves were too narrow, cells did not elongate likely because adhesions could not form. When the grooves were too wide grooves, most cells also did not elongate as they tended to spread in the flat regions, but a few elongated cells were observed along the edge of the grooves. These data suggest that for Ti substrates, there is a minimum groove width that is necessary for cells to elongate, and that wider grooves lead cells to spread in all directions on the flat regions with minimal elongation. The total extent of cell spreading, as measured by the spread cell area, was consistent across substrates with different groove sizes, suggesting that changes in elongation were not caused by an inhibition or enhancement of overall cell spreading.

We found that Ti surface topography regulates polarization-associated macrophage markers, and moderately but significantly affect their release of cytokines. In our previous work, we demonstrated that geometry of cell adhesion influences macrophage phenotype [2]. The results from the current study corroborate with our previous work and show that macrophage Arg1 expression and IL-10 secretion was modulated by cell elongation, and depended on groove size. Our study did not distinguish between specific alternative activation phenotypes (M2a, M2b, and M2c), which is an important area of future investigation. Moreover, these results were obtained in calcium-containing DMEM media, and further studies using alternative media may help to elucidate a potential role for calcium, which has previously been shown to impact macrophage inflammatory activation [89]. Interestingly, the degree of Arg1 expression was somewhat elevated on substrates with wider groove sizes, even though the average cell elongation was not elevated relative to

unpatterned blank surfaces. It is possible that cells that elongate along the 1 mm high edge of the grooves promote an overall alternatively-activated polarization response through paracrine effects. In particular, few elongated cells polarized towards an anti-inflammatory phenotype could in turn influence the behavior of neighboring non-elongated cells [64]. Moreover, surface topography did not affect on the expression of iNOS and TNF-α, markers of macrophage inflammatory M1 polarization. Together, these data demonstrated that for Ti substrates, surface grooves help polarize macrophages toward an anti-inflammatory, pro-healing phenotype independent of exogenous cytokine stimulation.

Grooved surfaces have been shown to modulate adhesion, adhesion signaling, and cytoskeletal organization of many cell types including fibroblasts, myocytes, epithelial cells, and mesenchymal stem cells. The size of focal adhesions in epithelial cells, as detected by immunostaining of vinculin, is often directly correlated with groove width, and increased from 400 nm to 1500 nm as grooves on Si substrates were increased from 330 nm to 2100 nm and were 600 nm deep [79]. Grooved substrates also lead to changes in integrin expression and focal adhesion kinase (FAK) phosphorylation [82]. While vinculin staining in macrophages is not as intense, as shown by our own work and others [32,90,91], our data show that on very narrow 200 nm wide grooves where macrophages were not elongated, adhesion size appeared to be diminished relative to cells on other groove sizes and flat substrates. In addition, our results show that macrophage elongation influences the organization of actin cytoskeletal components, since the intensity of phalloidin staining was higher in elongated cells. These data show that while macrophages do not appear to exhibit highly organized cytoskeletal and adhesive structures when compared to other groove-sensitive cell types, topographical substrates are capable of modulating these cellular

components, and may indeed play an important role in regulating macrophage polarization.

Understanding how physical cues presented by biomaterial surfaces regulates macrophage adhesion and polarization will have important implications for medical device design. While biomaterial chemistry has long been thought to regulate macrophage response, to date less is known about how physical cues might regulate macrophage function. Our data suggest that surface topographies that modulate macrophage cell shape, for example micro-scale grooves, may be used to regulate macrophage behavior and specifically their activation towards a pro-healing alternatively activated M2 phenotype. Given the important role of macrophages in wound healing and tissue repair, this may provide a simple method for regulating the host response to biomaterial implants. While the current work has been focused on two-dimensional biomaterial surfaces, it is likely that three-dimensional scaffolds that present topographical cues including fibrous tissue architectures may similarly alter macrophage function and the wound healing response. Moreover, further studies using human cells will be necessary to unveil the true translational potential of topography-mediated macrophage polarization and wound healing. Ultimately, controlling the immune response to 3D biomaterial architecture may be useful for leveraging immune-mediated healing in tissue engineering and regenerative medicine [92].

In conclusion, we demonstrate that micro and nano-patterned surface groove cues regulate macrophage elongation and phenotype polarization. Using deep-etched titanium surfaces with a wide range of groove sizes (150 nm to 50 μm), we found that BMDM elongation and expression of phenotypic markers associated with a pro-healing M2

phenotype was highest on intermediate groove sizes ranging from 400 nm to 5 μm in width. Collectively, these results highlight the potential utility of grooved materials to promote wound healing in response to biomaterial implants.

2.2 Topographical Modulation of Macrophage Phenotype by Shrink-Film Multi-Scale Wrinkles [93]

(Wang, T., Luu, T. U., Chen, A., Khine, M. & Liu, W. F. Topographical modulation of macrophage phenotype by shrink-film multi-scale wrinkles. *Biomater Sci* **4**, 948-952, (2016) – Reproduced by permission of The Royal Society of Chemistry)

2.2.1 Introduction

The host response to biomaterials remains a major challenge for implanted medical devices [5]. Chronic inflammatory activation caused by the presence of a foreign body often leads to the formation of a thick fibrous capsule, which ultimately prevents the function of the device. Recently, approaches to actively modulate the immune system have emerged as a promising strategy to minimize inflammation and achieve appropriate wound healing response in response to biomaterial implants. Towards this goal, macrophages have been an attractive target for immunomodulation given their role in inflammation and wound healing [94-96]. These cells are capable of polarizing towards a pro-inflammatory (classically activated) or anti-inflammatory (alternatively activated) phenotype depending on their microenvironment [97,98]. In an inflammatory environment containing damage or pathogen associated molecular patterns including LPS and IFN-g, macrophages polarize towards an inflammatory phenotype, and release cytokines and reactive species to promote inflammation. However, during wound healing and in the presence of Th2 cytokines including IL-4 and IL-13, the same cells acquire an anti-inflammatory phenotype and

express IL-10 and Arg1 (in mice), which are involved in dampening inflammation and mediating tissue regeneration. While the molecular mediators of macrophage phenotype polarization have been well-documented, less is known about how physical properties presented by a biomaterial surface might modulate their behavior.

Recent studies suggest that biomaterial size and shape, rather than surface chemistry, play a dominant role in the host response [66,99]. At the surface scale, it is thought that roughness or topographical features modulate macrophage behavior [35,65,72], with surface features generally eliciting lower levels of inflammation when compared to flat surfaces of the same chemistry. However, the mechanism underlying topography-induced modulation of macrophage phenotype remains unclear, and precise design criteria to leverage topography-mediated changes in the immune response have not been established. In addition, methods that specifically promote an anti-inflammatory phenotype have remained elusive. Our laboratory has demonstrated that macrophage elongation induced by surface adhesive micropatterns leads to an increase in expression of markers associated with an alternatively activated phenotype [2]. Since surface grooves have been shown to elicit cell elongation in macrophages as well as many other cell types [41,82,100], we postulated that topological features could be leveraged to control macrophage shape and polarization, and therefore the foreign body response to an implanted material. We recently showed using deep etched titanium surfaces that 0.5-1 mm grooves optimally induced macrophage elongation and alternative activation [62]. This work suggested that topography may be used to modulate macrophage phenotype, and surface features may be designed to mitigate the foreign body response to implanted materials.

2.2.2 Materials and Methods

Material fabrication

The flat, 1D and 2D wrinkled substrates were fabricated from polyethylene (PE) films (Cryovac D-film, LD935, Sealed Air Corporation). Both 1D and 2D wrinkled substrates were treated with oxygen plasma (Plasma Prep II, SPI Supplies) for 5 minutes. The treated PE films were constrained on two opposite sides, and were thermally-shrunk at 150°C for 3 minutes to creating 1D wrinkles. To create the 2D wrinkles, the treated films were shrunk on all sides without any constrain.

Characterization of wrinkles

Both SEM and AFM were performed to characterize the wavelengths and depths, respectively, of the wrinkles. To characterize the wavelengths, the wrinkled substrates were coated with 4 nm gold/palladium (Polaron SC7620), and SEM images were obtained at various magnifications (1,000x to 20,000x) (FEI Quanta 3D FEG). The wavelengths of the wrinkles were calculated by using an in-house developed MATLAB (MathWorks Inc., Natick, MA, USA) code based on fast Fourier transformation. To characterize the depths, AFM was conducted on the wrinkled substrates in tapping mode using silicon tip with a resonant frequency of about 75 kHz and force constant of 3 N/m on a MFP-3D inverted optical microscope (Asylum Research, Santa Barbara, CA). The software used for data acquisition and analysis was IGOR Pro 6.0 (Wavemetrics, Portland, OR).

Cell isolation and culture

All protocols involving animals were approved by the Institutional Animal Care and Use Committee at the University of California Irvine prior to initiation of the study. Bone marrow cells were isolated from femurs of C57BL/6 mice (Jackson Laboratories) as previously described. Cells were treated with ACK lysis buffer (Invitrogen) to remove red blood cells, centrifuged, and then resuspended and cultured in D10 media composed of high glucose DMEM supplemented with 10% heat-inactivated FBS, 2 mM L-glutamine, 100 units/mL, 100 μg/mL streptomycin (all from Invitrogen), and 10% conditioned media containing macrophage colony stimulating factor (M-CSF) produced by CMG 12-14 cells to induce differentiation to BMDMs. BMDMs were maintained at 37°C in a humidified 5% CO_2 incubator. After 7 days of culture, cells were dissociated using Cell Dissociation Buffer (Invitrogen) and seeded on wrinkled substrates. After 4 h of culture to allow adhesion of cells, substrates were transferred to a new culture well with fresh media and then cultured for an additional 24 h.

Cell shape and morphological analysis

Cells were incubated with 10 μM CellTracker Red CMTPX (Invitrogen) in serum-free DMEM at 37 °C in a humidified 5% CO_2 incubator for 45 min, and then transferred to fresh D10 media. After 30 min, the samples were rinsed with sterile PBS before imaging. For analysis of cell morphology, cells were visualized using an Olympus inverted microscope with a 20x or 40x objective. The long axis, or longest length of the cell, and short axis, or the length across the nucleus, of each cell were manually traced and measured using ImageJ software (National Institutes of Health). Elongation factor was calculated as the ratio of the long axis to the short axis.

Immunofluorescence staining and Western blotting

Cells were fixed with 100% cold methanol on ice for 15 min, washed thoroughly with PBS, and then blocked with 5% normal donkey serum (Jackson ImmunoResearch) in PBS overnight at 4°C. Cells were then incubated with goat anti-arginase-1 (Santa Cruz Biotechnology Inc.), washed thoroughly with 1% BSA, incubated with Alexa Fluor-594 donkey anti-goat fluorescent secondary antibodies (Jackson ImmunoResearch) for 1 h, and then counterstained with Hoechst 3342 dye (Invitrogen). Samples were imaged using an Olympus inverted microscope. For Western blot, cells were rinsed in PBS and lysed in RIPA buffer supplemented with 1% protease inhibitor cocktail (both from Sigma Aldrich). Cells were scraped and agitated at 4C for 20 minutes and centrifuged to pellet cellular components. The supernatant was collected and total protein content was measured by BCA protein assay (Thermo Fisher). Samples were then denatured in a Laemmli sample buffer (Biorad) at 95°C, and separated by standard SDS-PAGE using 7.5% polyacrylamide gels. Proteins were transferred to nitrocellulose membranes and then detected using goat anti-arginase-1, rabbit anti-iNOS (both from Santa Cruz) or mouse anti-tubulin (Sigma) antibodies, followed by HRP-conjugated secondary antibodies (Santa Cruz). HRP substrate solution (Millipore) was applied to the membrane and imaged using a ChemiDoc XRS System (Biorad).

Cytokine secretion

BMDMs were cultured on substrates as described above for 24 h, after which supernatants were collected and analyzed for TNF-α and IL-10 by enzyme-linked

immunosorbent assay (ELISA) following the manufacturer's instructions (BioLegend, San Diego, CA).

Material implantation and Immunohistochemistry

All protocols involving animals were approved by the Institutional Animal Care and Use Committee at the University of California Irvine prior to initiation of the study. 6-week-old female C57BL/6J mice (Jackson Laboratories) were first anesthetized by 2% isoflurane inhalation, and placed in prone position on a sterilized heat pack. The hair of the mid-dorsal skin was shaved, cleaned with ethanol and betadine. Following sterilization, a 1.5 cm incision through the skin was made using a sterile disposable blade. Sterile blunt forceps were used to separate the skin and then create subcutaneous pockets on both sides of the incision. Sterilized wrinkle and flat control materials were placed into each subcutaneous pocket and on top of the subcutaneous musculature. Skin staples with autoclips were used to close the incision. The mouse was place in a clean cage with heat pack. Recovery and health of mice were monitored daily for 7 days after surgery. At 7 days after implantation, mice were euthanized by carbon dioxide and cervical dislocation, then skin tissue containing materials were collected and fixed in 10% formalin solution for 24 h at 4^{o}C. Fixed tissues were embedded in paraffin blocks, sectioned and stained with hematoxylin and eosin (H&E) and Masson's trichrome by AML laboratories (Baltimore, MD). For immunohistochemistry, sections were heated to 60^{o}C for 50 min, then deparraffinized and rehydrated using Histo-Clear II (National Diagnostics) and an ethanol gradient before staining. After incubating in target retrieval solution (Dako), dual endogenous enzyme-blocking reagent (Dako), and washing with TBS-A (Tris-buffered saline with 0.1% Triton X-

100), the sections were blocked with TBS-B (TBS-A with 2% BSA and 1.5% donkey serum), then incubated with goat anti-arginase-1, rabbit anti-iNOS, or rabbit anti-F4/80 antibodies (all from Santa Cruz Biotechnology Inc.) for 16 h at 4^{o}C, followed by HRP conjugated donkey anti-goat, or goat anti-rabbit IgG antibodies (both from Santa Cruz Biotechnology Inc.) for 1 hour. Following secondary antibody incubation and washes, avidin-peroxidase reaction was developed using DAB (diaminobenzidine) and DAB plus Chromogen solution (Dako). The sections were counterstained with hematoxylin (Vector Laboratories) for nuclei as needed. Sections were imaged using Nikon Eclipse 80i with 20x objective (for Hematoxylin and DAB stained sections) and with 40x objective (for DAB stained sections). Unless otherwise noted, at least 3 implants in separate animals were collected per substrate and representative images are shown.

Quantification method for DAB staining

DAB stained sections imaged using Nikon Eclipse with 40x objective were used for DAB quantification. Colorimetric DAB images were converted to grayscale images using CellProfiler software (MIT Broad Institute). 0 – 50 mm and 50 – 150 mm distance from implant regions were manually measured and traced using ImageJ software. To define positive stained areas, a threshold value was applied to the grayscale images. Representative images are shown in figure 9. Percent positive stained area was calculated as the number of positive pixels in the thresholded image divided by the total area within the indicated region, multiplied by 100. At least 2 sections for each implant were used for DAB quantification.

Statistical analyses

Statistical analysis was performed using Student's t-test or one-way ANOVA with Sidak's post hoc test (multiple comparisons test). $p<0.05$ was considered statistically significant.

2.2.3 Results and Discussion

In this study, we sought to determine (1) whether multi-scale wrinkled surfaces on a polymeric material produced by shrink film methods could also induce cell shape and phenotypic changes in macrophages, and (2) whether changes in macrophage behavior *in vitro* correlated with a change in the *in vivo* foreign body response. Self-assembled wrinkles by shape memory polymers has been shown to create biomimetic wrinkles [100,101]. This facile fabrication technique leveraging shrink film offers a low-cost, high throughput approach to create micro- to nano-scale topological features on biomaterials. This general technique can be applied to thermally-induced shape-memory polymers, and can further be molded using thermoset polymers including poly(dimethyl siloxane) (PDMS). Materials were fabricated using methods as previously described [100] and further elaborated in Supplemental Information. One-dimensional (1D) wrinkles were generated by creating a stiff layer via plasma treating, and then confining the material along one direction upon heat induced shrinkage in order to constrain shrinkage of the material in the perpendicular direction, whereas two-dimensional (2D) wrinkles were generated by shrinking under unconfined conditions. The wrinkled surfaces were imaged by scanning electron microscopy (SEM, Figure 7A) and confirmed to have dimensions of approximately 1 nm – 5 mm by atomic force microscopy (summarized in Figure 7B).

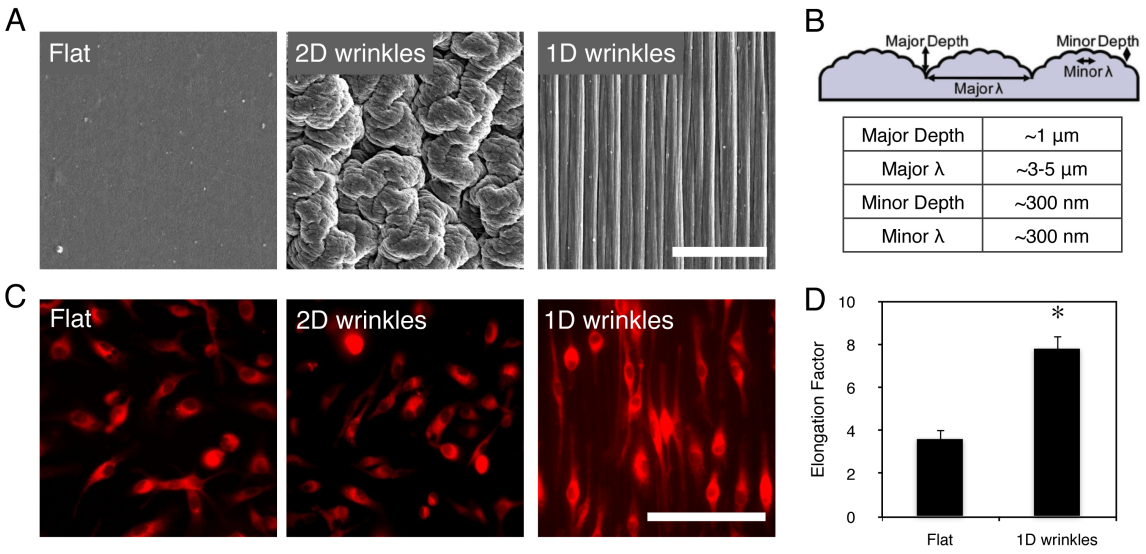

Figure 7. Macrophages elongate on shrink-induced multi-scale wrinkles. (A) Scanning electron microscopy micrographs of flat surface, 2D wrinkles, and 1D wrinkles. **(B)** Schematic of depth and width of 1D wrinkle surfaces as measured by atomic force microscopy. **(C)** Fluorescent micrographs of BMDM on flat, 2D wrinkle, and 1D wrinkle surfaces. Cells were stained using CellTracker Red CMTPX dye for monitoring cell shape. **(D)** Quantification of cell elongation on flat, 2D wrinkle, and 1D wrinkle surfaces. Mean ± SEM, * $p < 0.05$ compared to Flat surfaces by paired Student's t-test, *n = 3*. Scale bar = 50 µm. [93]

Murine bone marrow derived macrophages were seeded onto 1D wrinkles, 2D wrinkles, and flat materials for 24 hours and stained with Cell Tracker Red for visualization by fluorescence microscopy. Macrophages seeded on 1D wrinkled materials elongated and oriented along the direction of the groove, whereas macrophages on 2D wrinkles were not elongated and similar in morphology to cells on flat surfaces (Figure 7C). We quantified the degree of elongation by measuring the long axis of the cell and dividing by the width across the nucleus, and found that this ratio or "elongation factor" was approximately 8, which is similar to the level of elongation that we have previously observed in IL-4/IL-13 treated

alternatively activated macrophages, as well as macrophages seeded on lined micropatterns [2]. Cells seeded on flat surfaces were on average less elongated with a ratio of approximately 3-4 (Figure 7D). On 2D wrinkled surfaces, the periphery of the cells were difficult to ascertain by fluorescence microscopy because of the undulating nonplanar features, and therefore elongation was not quantified. These data suggest that wrinkled surfaces lead to adhesive changes in macrophages that result in cell elongation.

To determine whether adhesion to surfaces of varied topologies altered the polarization state of macrophages, cells were seeded on 1D wrinkles, 2D wrinkles, and flat surfaces for 24 hours and assayed for markers of Arg1 and iNOS, markers of alternative and classical activation, respectively. We found that several cells on 1D wrinkles exhibited strikingly high Arg1 staining intensity, which was not observed on flat or 2D wrinkles (Figure 8A). The shape of the high expressing cells as visualized by fluorescence microscopy was elongated. This was further confirmed and quantified by Western blot, where Arg1 levels were significantly higher in macrophages cultured on 1D wrinkles when compared to cells cultured on flat surfaces or 2D wrinkles (Figure 8B). In contrast, levels of iNOS, a marker of inflammatory polarization was undetectable in cells cultured on all three types of substrates; a-tubulin was used as a loading control and was not statistically different across the three culture conditions. The Arg1 levels in macrophages cultured on wrinkled surfaces were similar in magnitude to the levels observed in elongated cells cultured on micropatterned adhesive lanes, which was more moderate than that caused by stimulation of Th2 cytokines IL-4 and IL-13 [2].

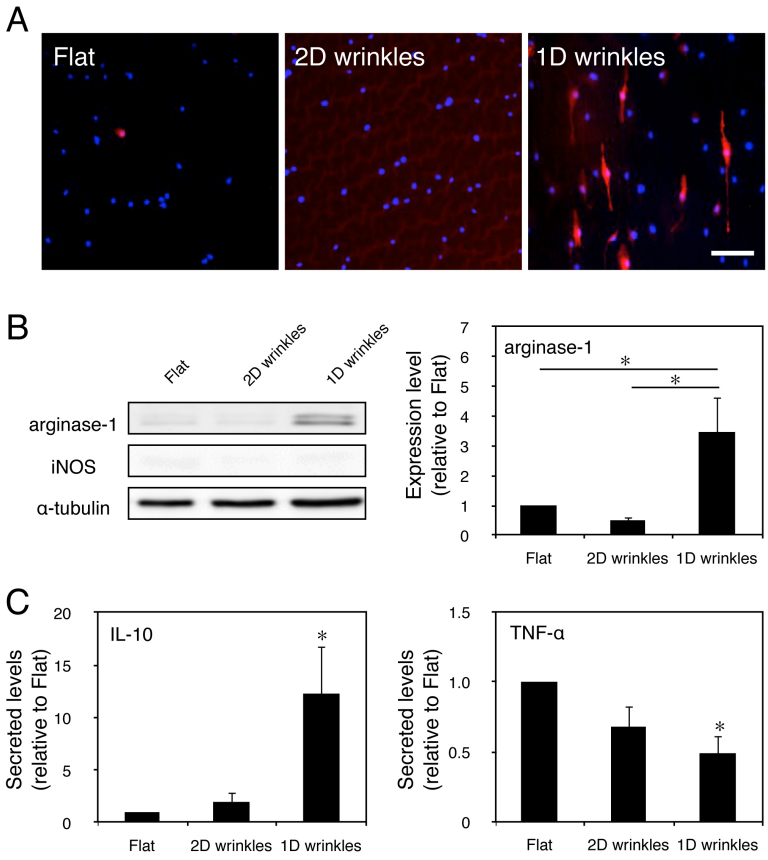

Figure 8. Surface topology regulates macrophage phenotype and cytokine secretion. **(A)** Immunofluorescence images of Arg1 on flat, 2D wrinkle, and 1D wrinkle surfaces. Scale bar = 50 μm. **(B)** Representative Western blot of Arg1, iNOS, and a-tubulin on flat, 2D wrinkle, and 1D wrinkle surfaces (left) and quantification of Arg1 expression of flat, 2D wrinkle, and 1D wrinkle surfaces (right). Mean ± SEM, *p < 0.05; one-way ANOVA with Tukey's posthoc test, *n = 3*. **(C)** Secretion of IL-10 (left) and TNF- α (right) by BMDM cultured on flat, 2D wrinkle, and 1D wrinkle surfaces for 24 hours. Mean ± SEM, * p < 0.05 compared to flat surfaces; one-way ANOVA with Sidak's posthoc test, *n = 3*. [93]

To further examine whether surface topography altered macrophage function, we examined the presence of an anti-inflammatory cytokine, IL-10 and a pro-inflammatory cytokine, TNF-α, in the supernatants of macrophages after culture on substrates for 24 hours (Figure 8C). We found that secretion of IL-10 was significantly greater and TNF-α

level was significantly lower from macrophages on 1D wrinkles when compared to macrophages on flat surfaces. Together with immunostaining of Arg1, these data suggest that 1D wrinkled surface topology induce murine macrophages towards an alternatively activated, anti-inflammatory phenotype. These changes were not attributed to changes in surface composition associated with material shrinkage, since 2D wrinkles that also undergo a shrink procedure did not elicit Arg1 expression or IL-10 secretion. Interestingly, while 1D wrinkled surfaces did not alter iNOS expression, the levels of TNF-α were moderately less compared to flat surfaces. These data suggest that while surface topological features such as those present on 2D wrinkles might inhibit inflammatory activation, grooved surfaces created on 1D wrinkles most significantly depress inflammatory activation.

To demonstrate whether surface topography influences the host tissue response to a biomaterial *in vivo*, we surgically implanted wrinkled and flat materials in the subcutaneous space of C576BL/6J mice. Tissue surrounding the material was excised one week after material implantation, and evaluated by histology and immunohistochemistry (Figure 10). It appeared that the extent of inflammatory infiltration was similar in the tissue surrounding the flat material compared to the tissue surrounding the wrinkled material, as indicated by H&E staining (Figure 10A). However, Masson's trichrome staining revealed the highest extent of fibrillar collagen deposition in the tissue directly adjacent to the flat material (Figure 10B). Tissue surrounding the wrinkled material also exhibited some fibrillar collagen but the density was not as high or localized. Higher magnification images also show changes in collagen fibril structure, although the heterogeneity of fibril deposition particularly in the wrinkled material condition made it difficult to quantify.

Many newly formed blood vessels were found in the tissue directly around both implants materials. The most striking difference was observed in immunohistochemistry for Arg1, which showed higher percentage of positively stained Arg1 area in the inflammatory tissue around wrinkled materials compared to flat materials, confirming the results from *in vitro* macrophage experiments (Figure 10C and 10D). Interestingly, the positive staining of Arg1 was observed not only in the tissue directly adjacent to the material, but also 50 – 150 mm away from the implant surface, suggesting that paracrine effects from cells adhering to the material may potentiate the response. In addition, Arg1 expression appeared to be co-localized with collagen deposition in both implant conditions. Expression of F4/80 also appeared to be higher in the tissue surrounding the wrinkled implants when compared to flat implants, but expression of the inflammatory marker iNOS was reduced (Figure 11). Together, these data demonstrate that surface topography modulates the recruitment and activity of local macrophages. It is likely that these cells work in concert with other cell types including fibroblasts to alter tissue remodeling response *in vivo* [78,102].

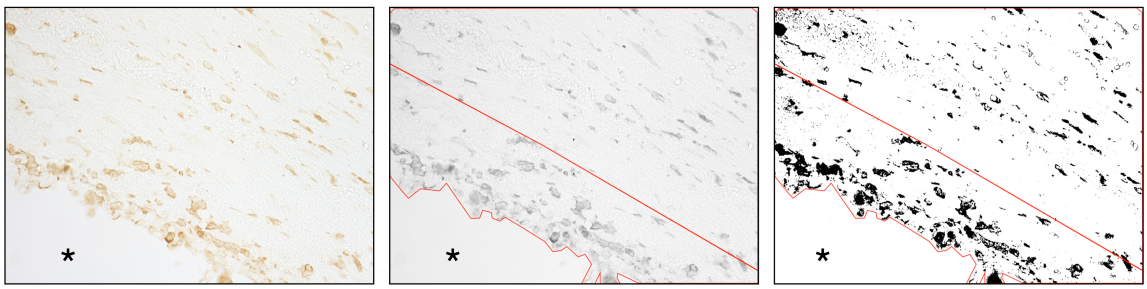

Figure 9. Method for quantification of DAB-stained sections. Original image (left), grayscale image (middle) and thresholded image (right) with 0 – 50 mm and 50 – 150 mm distance from implant regions indicated with red outline. Percent positive area was calculated by the number of positive pixels in the thresholded image divided by the total area within the indicated region, multiplied by 100. [93]

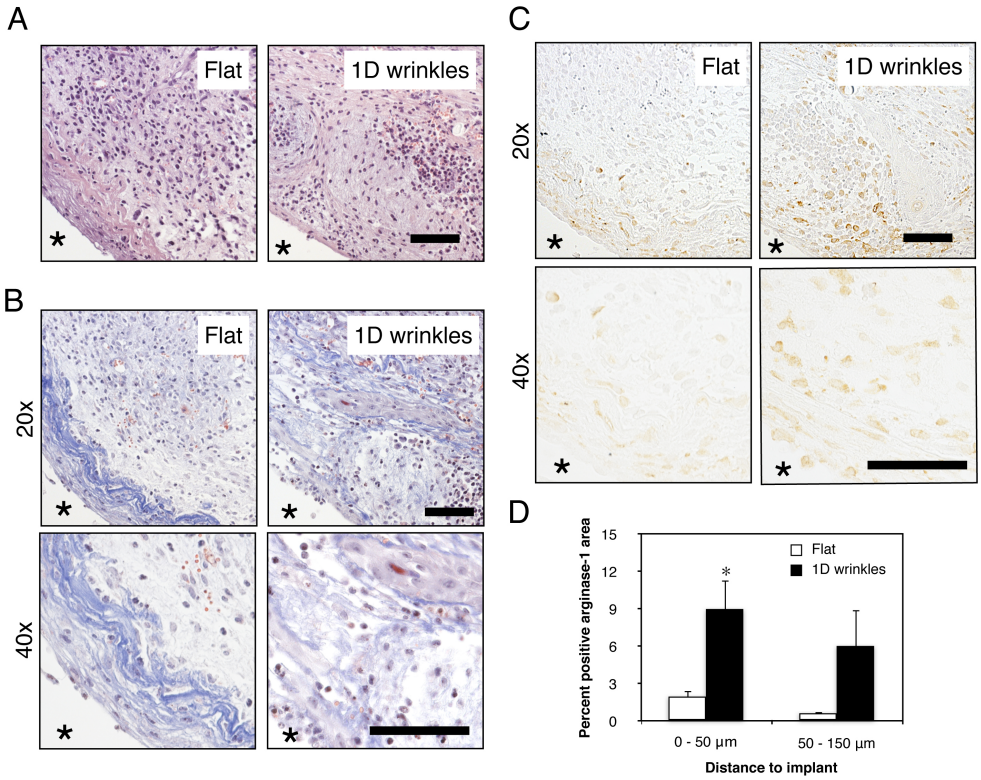

Figure 10. Surface wrinkles modulate arginase-1 expression *in vivo*. Representative **(A)** H&E stained and **(B)** Masson's Trichrome, and **(C)** Arg1 stained images of flat and 1D wrinkle surface implants at 7 days after subcutaneous implantation in C57BL/6J mice. Astericks denotes location of material. **(D)** Quantification of percent positive Arg1 area at indicated distances from the implant. Mean ± SEM, * $p < 0.05$ compared to control flat surfaces; unpaired Student's t-test, *n = 3*. Scale bar = 50 µm. [93]

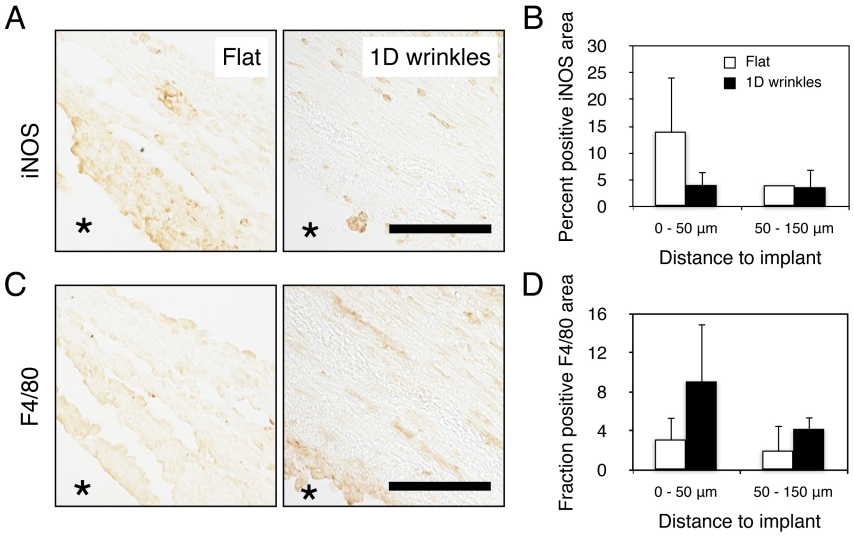

Figure 11. Surface wrinkles modulate iNOS and F/480 expression. Representative iNOS **(A)** and F4/80 **(C)** stained images of flat and 1D wrinkle surface implants at 7 days after subcutaneous implantation in C57BL/6J mice. Astericks denotes location of material. Quantification of percent positive iNOS **(B)** and F4/80 **(D)** area at indicated distances from the implant. Mean ± SD, *n = 2*. Scale bar = 50 μm. [93]

In this study, we demonstrate that wrinkled surfaces modulate murine macrophage cell shape phenotype, specifically promoting their elongation and alternative activation. Wrinkles fabricated from shrink films offers a low cost and high throughput method of generating topologies containing micro- and nano-scale features. 1D wrinkled materials that contain grooves led to higher macrophage expression of Arg1 both *in vitro* and *in vivo*. In addition, macrophages secreted higher levels of IL-10 and lower levels of TNF-α on 1D wrinkles when compared to 2D wrinkles or flat surfaces *in vitro*, and also promoted blood vessel formation *in vivo*. Together these data suggest that surface wrinkles promote alternative activation of macrophages and may be used to modulate the foreign body response to implants. However, it is still not clear whether wrinkled surface-induced changes in macrophage function will lead improved wound healing, as it has recently been shown that heightened alternative activation may in fact lead to fibrosis [103,104]. Nevertheless, topological features have long been clinically used as a strategy to mitigate the foreign body response to biomaterial implants [28,105], and this study may provide a cellular and molecular mechanism underlying improved response to roughened surfaces. Our work suggests that topological features including wrinkled surfaces promote changes in macrophage cell shape, which in turn modulate their phenotypic activation state [35,41,70]. Further work examining additional markers and using human cell systems will be needed

to elucidate the translational potential of topological regulation of the foreign body response.

In conclusion, we demonstrate that shrink-film multi-scale wrinkled materials modulate the shape and function of macrophages. Wrinkled materials induced macrophage elongation along the direction of 1D wrinkles, and led to increases in Arg1 expression and IL-10 secretion. Furthermore, implanted 1D wrinkled materials increased Arg1 and reduced iNOS expression in tissue around the material. Together these results suggest the potential use of material topography to control the macrophage response to biomaterial implants. Further studies will be necessary to determine the long-term fibrotic response to materials of varied topographies.

CHAPTER 3- The Effect of 2D and 3D Microenvironment on Macrophage Function

3.1 Introduction

The extracellular matrix serves not only as an architectural support for cells within tissues, but also as an important signaling role through interactions with adhesion receptors, growth factors, and among other molecules [10,11,15,19,106,107]. The extracellular matrix is dynamically remodeled during wound healing, as well as in diseases such as cancer and atherosclerosis. Upon injury, the wound healing process is initiated by the formation of the provisional matrix, composed of mainly fibrin, fibronectin (Fn), and vitronectin (Vn), which is followed by epidermal cell migration and inflammation [11-13]. At the later stage, the provisional matrix is remodeled and replaced by a collagen rich matrix, which directly facilitates cell adhesion and also alters cellular function through interactions with growth factors [14,15]. Changes in ECM architecture, including excess accumulation and crosslinking of collagen, are often considered as one of the hallmarks of cancers [108-110] and fibrosis [111,112]. Additionally, in atherosclerosis, intimal layer where endothelial cells are resided is rich in laminin (Ln), Fn, and collagen type IV (CIV) while medial layer is made of smooth muscle cells, collagen type I, III, V, and VIII, Fn, and proteoglycans [113]. Compared to the early stage of atherosclerosis, the content of collagen is more concentrated at the late stage [22]. Higher collagen type I (CI) concentration promotes macrophage differentiation and regulates macrophage functions, matrix metalloproteinase (MMP)-9 production [23]. How the composition and structure of the ECM feed backs to regulate macrophages, one of

the major cellular components in wound healing, cancer, and atherosclerosis, still remain relatively unknown.

Studies from the early 1990s showed that ECM proteins could influence macrophage spread morphology and their differentiation from bone marrow cells [114]. ECM proteins including Fn, Ln, CI, and CIV were pre-coated on tissue culture plates before seeded with bone marrow cells. On day 6 of differentiation, we observed that macrophages adhered but remained rounded on CIV, and Ln coated substrates while they were well-spread on CI, Fn coated substrates, and uncoated substrates. However, macrophages treated with IFN-γ and LPS assumed a circular, spread morphology regardless of the ECM proteins. Their study also found that the concentration of IL-6 secreted by macrophages was similar in all ECM conditions, but TNF-α was not able to detect in any condition. More recently, Zaveri *et al.* demonstrated that adhesion to ECM proteins regulated macrophage phagocytosis but not inflammatory response to LPS [115]. Polystyrene micro-particles (MPs) were pre-coated with Fn, Vn and fibrinogen (Fg), adsorbed with LPS, and then added to macrophages. At early time points, uptake of Fn coated MPs were significantly higher than MPs coated with other ECMs. Similar to the earlier study, levels of IL-6 and TNF-α secreted by macrophages were similar in all ECM coated MP exposure conditions. Together, these two studies suggested that while ECM composition may alter macrophage morphology and particle uptake, there were minimal effects on their inflammatory activation.

Additionally, substantial evidence has demonstrated that 2D and 3D microenvironments influence cell adhesion and behavior, but little is understood the effect of 3D culture on macrophage function, compared to 2D culture. In addition to studies of migratory behavior, 3D culture systems have also been used to investigate macrophage

function (see Chapter 1.3.2 for more details). Macrophages were co-cultured with carcinoma in collagen hydrogels as a 3D *in vitro* model to study adhesion and function of tumor associated macrophages (TAM) [47]. 2D and 3D microenvironment directed macrophage migration differently in matrices [48,49]. Compared to 2D microenvironment, macrophages differentiated in 3D microenvironment expressed higher concentration of CD71, MMP-2, and MMP-9 suppressing tumor invasion and metastasis [50,116].

We recently demonstrated that cell shape regulates macrophage polarization. Specifically, macrophages enhanced expression of markers associated with anti-inflammatory phenotype when forced to elongate on micropatterned lines of fibronectin [2]. In addition, macrophages aligned along grooves on titanium or polymeric substrates, and increase their expression of anti-inflammatory markers both *in vitro* and after implantation *in vivo* [93]. Furthermore, our previous work on the effect of fibri(ogen) on BMDMs indicated that soluble fibrinogen triggered inflammatory response of macrophages cultured on polystyrene, however fibrin inhibited the fibrinogen-triggered inflammatory response when cells were cultured on fibrin gels [117]. In this study, we hypothesized that ECM composition and geometry of adhesion could independently influence macrophage cell shape and function. To systematically test this, we first examined the effect of an array of ECM proteins on cell morphology and response to prototypical inflammatory (IFN-γ and LPS) and wound healing (IL-4 and IL-13) stimuli. Second, we examined how hydrogels including fibrin, collagen I gels, and matrigels modulated inflammatory response of human macrophages to LPS, with and without soluble fibrinogen. We found that despite differences in morphology on selective ECMs, the cytokine secretion response to stimulation was largely similar across all matrix proteins tested. Interestingly, when we

examined arginase-1 expression of cells cultured on different ECMs, we found significant differences, and patterning ECM in lines elicited an increase in the expression of Arg1, as we had previously observed on fibronectin. In addition, we also found that compared to polystyrene 2D substrates, human macrophages on hydrogels inhibited TNF-α secretion in response to TLR ligands. Comprehensively, our results demonstrate that (1) cytokine secretion from macrophages is independent of ECM ligands, (2) expression of Arg1 was indeed dependent on ECM, and (3) 3D hydrogels inhibited inflammatory effect on human macrophages, compared to polystyrene surfaces as 2D microenvironment.

3.2 Materials and Methods

Cell isolation and culture

All protocols involving animals were approved by University of California Irvine's Institutional Animal Care and Use Committee, which is accredited by the Association for the Assessment and Accreditation of Laboratory Animal Care International (AAALACi). Bone marrow derived monocytes were isolated and cultured as previously described [62]. Briefly, bone marrow was isolated from femurs of 6-12 week old C57BL/6 mice (Jackson Laboratories) and cells were collected, treated with ACK lysis buffer (Invitrogen) and resuspended and cultured in D10 media composed of high glucose DMEM supplemented with 10% heat- inactivated FBS, 2 mM L-glutamine, 100 units/mL, 100 μg/mL streptomycin (all from Invitrogen), and 10% conditioned media containing macrophage colony stimulating factor (M-CSF) produced by CMG 12-14 cells. After cultured for 7 days, BMDMs were dissociated using Cell Dissociation Buffer (Invitrogen) and seeded on experimental substrates.

Human peripheral blood monocytes were a kind gift from Dr. Melissa Lodoen's laboratory (Department of Molecular Biology and Biochemistry, University of California, Irvine). Human blood samples were collected as previously described (REF) within the guidelines and approval of the University of California, Irvine Institutional Review Board. Human peripheral blood mononuclear cells were processed to isolate human monocytes using countercurrent centrifugal elutriation. Human monocytes were cultured at 5×10^5 cells per ml for 7 days in RPMI1640, 10% FBS, 2 mM L-Glutamine and 1% penicillin/streptomycin, and 25 ng/mL recombinant human M-CSF (rhM-CSF) (PeproTech) (complete media) (All from Invitrogen). After 6-7 days of culture, human monocyte derived macrophages were dissociated using cell dissociation buffer and cultured on experimental substrates with complete media overnight prior to ultrapure LPS (Invivogen) stimulation.

THP-1 cell line was obtained from ATCC and cultured in RPMI1640 and 10% FBS as ATCC's instruction. At passage 4-9, THP-1 cells were used to culture on experimental substrates in addition to 20 nM phorbol 12-myristate 13-acetate (PMA) (Sigma Aldrich) for 48 h prior to ultrapure LPS stimulation.

ECM coating

All ECM proteins were prepared following the manufacturer's instructions. The concentrations of ECM proteins used for coating the wells were 100 μm/mL Collagen type I (CI, rat; Corning) in 0.02 N acetic acid, 100 μm/mL Collagen type IV (CIV, mouse; Corning) in 0.05 M HCl, 250 μm/mL fibrinogen (Fg, bovine; Sigma-Aldrich) in PBS, 20 μm/mL fibronectin (Fn, human; Corning) in H_2O, 20 μm/mL laminin (La, mouse; Corning) in high glucose DMEM, 150 μm/mL Matrigel GFR (Mg, mouse; Corning) in high glucose DMEM, and

10 μm/mL vitronectin (Vn, mouse; Abcam) in PBS. The ECM proteins were coated using a 1 mL solution per well of a 6-well plate overnight at 4°C. Coated wells were washed thoroughly with their corresponding diluents prior to cell seeding. After 4 h of seeding, cells were stimulated with a combination of E.coli LPS (Sigma-Aldrich), recombinant murine IFN-γ (R&D systems), IL-4 (Invitrogen) and IL-13 (Invitrogen) with concentrations as described in the figure legends.

Cell micropatterning

Micro-patterned substrates were prepared as previously described [2]. Polydimethylsiloxane (PDMS; Dow Corning) stamps were replica-molded from silicon wafers with 20 μm microgrooves, which were fabricated using standard photolithography to make patterned stamps, or from petri dishes to make flat stamps. The stamps were sonicated for 10 min in 70% ethanol, washed thoroughly with ethanol, and then dried using N_2 air stream. The sterile stamps were coated with ECM proteins at room temperature (RT) for 1 h. Then, the ECM coated stamps were washed thoroughly with their ECM corresponding diluent, and dried using N_2 air stream. ECM proteins were transferred from the stamps to PDMS-coated substrates, previously treated with UV ozone (Jelight) for 8 min. Then, the stamped substrates were blocked with a 0.2% Pluronic F-127 solution (Sigma-Aldrich) at RT for 1 h, and washed with sterile PBS prior to cell seeding. After 2 h of cell seeding, substrates were washed thoroughly with DMEM to remove non-adherent cells, and then transferred to new culture wells with fresh D10 media.

Gel fabrication

Collagen gels were fabricated at 2.0 mg/mL using rat tail Type I collagen (Corning) following the manufacturer's protocol. On ice, collagen was added into the mixture of 10X PBS (Lonza), 1 N NaOH, and Millipore water. Then, the gels were formed in 37°C incubator for 1 h, and then hydrated with complete media.

Matrigel gels were fabricated at 3.0 mg/mL following the manufacturer's protocol. On ice, Matrigel growth factor reduced basement membrane matrix (Corning) proteins were mixed in RPMI1640. Matrigel gels were formed in 37°C incubator for 1 h, and then hydrated with complete media.

Fibrin gels were fabricated at 2.0 mg/mL using human plasma fibrinogen (EMD Millipore). The lyophilized proteins were reconstituted in Millipore water to approximately 50 mg/mL as the manufacturer's suggestion. Fibrinogen solution diluted in RPMI1640 was added to human thrombin, 0.2 U/mg, to form gels on tissue culture plates or glasses in 37°C incubator for 3 h prior to being hydrated with complete media.

Cell shape and morphological analysis

For analysis of cell morphology, cell images were acquired with a 20x objective on an Olympus inverted microscope, or EVOS microscope. The long axis was defined as the longest length of the cell while the short axis was determined as the length across the nucleus and perpendicular to the long axis. The long axis and the short axis of each cell were manually traced and measured using ImageJ software (National Institutes of Health). Inverted aspect ratio was calculated as the ratio of the short axis to the long axis. The ratios close to 1 correspond to round cells and to 0 indicate highly elongated cells.

Immunofluorescence staining and imaging

BMDMs were cultured on flat and patterned substrates as described above for 40 h before immunofluorescence staining as previously described in Chapter 2. Cells were fixed with 100% cold methanol on ice for 15 min, and then incubated with primary antibody, goat anti-arginase-I (Santa Cruz Biotechnology Inc.), for 1 h at RT. After cells were washed thoroughly with 1% BSA, they were incubated with secondary antibody, Alexa Fluor-594 donkey anti-goat (Jackson ImmunoResearch) for 1 h at RT. All cells were counterstained with Hoechst 3342 dye (Invitrogen). Fluorescent images were acquired using an Olympus inverted microscope with a 20x objective. Arg1 integrated intensity was quantified using CellProfiler software (MIT Broad Institute) using methods previously described [62].

Cytokine secretion

BMDMs were cultured on ECM coated substrates as described above for 24 h before quantification of secreted cytokines. Human monocyte derived macrophages and THP-1 cells on substrates were stimulated with LPS for 6 h before quantifying cytokine secretion. Supernatants were collected and analyzed for TNF-α and IL-10 by enzyme-linked immunosorbent assay (ELISA) following the manufacturer's instructions (BioLegend, San Diego, CA).

TLR agonist assay

TLR ligands (human TLR1-9 agonist kit; Invivogen) were used to treat cells following the manufacturer's instructions. After 6 h of culture, supernatants were collected for ELISA to examine TNF-α concentration.

RNA isolation

For RNA isolation the cells were lysed directly on culture dish. For every 10 cm^2 of culture plate 1 ml of TRI Reagent was used (Sigma T9424). After adding the reagents, the lysate was passed several times through a pipette and left at room temperature (RT) for 5 minutes. Then, to the lysate, 0.2 ml of chloroform was added to every 1ml of TRI reagent used. To allow phase separation, the samples were vortexed vigorously for 15 sec and allowed to stand at RT for 10 min. Then, the mixture was centrifuged for 10 min at 12,000xg for 15 min at 4°C. The upper colorless aqueous phase that contains RNA was separated carefully to a new tube and 0.5 ml of 2-propanol per ml of TRI Reagent used was added. Then the samples were allowed to stand at RT for 10 min and further centrifuged at 12,000xg for 10 min at 4°C. This step precipitates RNA and forms a pellet on the bottom of the tube. The supernatant was removed and the pellet was washed with 1 ml of 75% ethanol per ml of TRI Reagent used in sample preparation. The pellet was briefly air-dried and the RNA was dissolved in DEPC treated water.

Quantitative Real-time PCR

For making cDNA High Capacity cDNA Reverse Transcription Kit from Applied Biosystems was used (4368814). 1 µg of total RNA was used to make cDNA using random primers provided in the kit and following the manufacturer's protocol. Once the cDNA was made, it was diluted 50 times with ultrapure water and used for qPCR. Bio-Rad's SsoFast EvaGreen supermix was used for real-time PCR. Briefly, for every 20ul reaction, 10 µl of the SsoFast Evagreen supermix, 2 µl of diluted cDNA and 1 µl (500 nM) of each forward and reverse primers and 6 µl of ultrapure water was used. A total of 40 cycles were performed

on Bio-Rad's CFX-96 real-time PCR system. Further the relative gene expression was analyzed by $2^{-\Delta\Delta CT}$ method.

Statistical analysis

All data were presented as the mean ± SEM across at least three independent experiments, unless otherwise specified in the figure legends. Statistical analysis was performed using two-tailed Student's t-test, or ANOVA, unpaired with Tukey's post hoc test as described in the figure legends. $p<0.05$ was considered statistically significant.

3.3 Results

The effect of ECM composition on macrophage cell shape response during polarization

To begin to examine the effect of the ECM on macrophages, we obtained commercially available ECM proteins that are found during wound healing and diseases, including fibronectin (Fn), fibrinogen (Fg), collagen type I (CI), collagen type IV (CIV), laminin (Ln), Matrigel (Mg), and vitronectin (Vn). BMDMs were cultured on ECM coated substrates with or without stimulation by LPS/IFN-γ, IL-4/IL-13, or IL-4/IL-13/LPS for 24 h. However, BMDMs cultured on most ECM coated substrates adhered and spread similarly within the same stimulation condition (Figure 12A). Compared to the control, unstimulated condition, macrophages treated with IL-4/IL-13 were typically more elongated, but more circular, although spread, when treated with LPS/IFN-γ. We observed that BMDMs on Ln coated substrates assumed round shapes regardless of stimulation condition (Figure 12A). To more quantitatively assess cell shape, the degree of elongation was determined by measuring the width across the cell nucleus and dividing by the length of the longest axis,

calculating an inverted aspect ratio. A small ratio value, close to 0, indicated a high degree of elongation, and a large ratio, close to 1, corresponded to a circular shape.

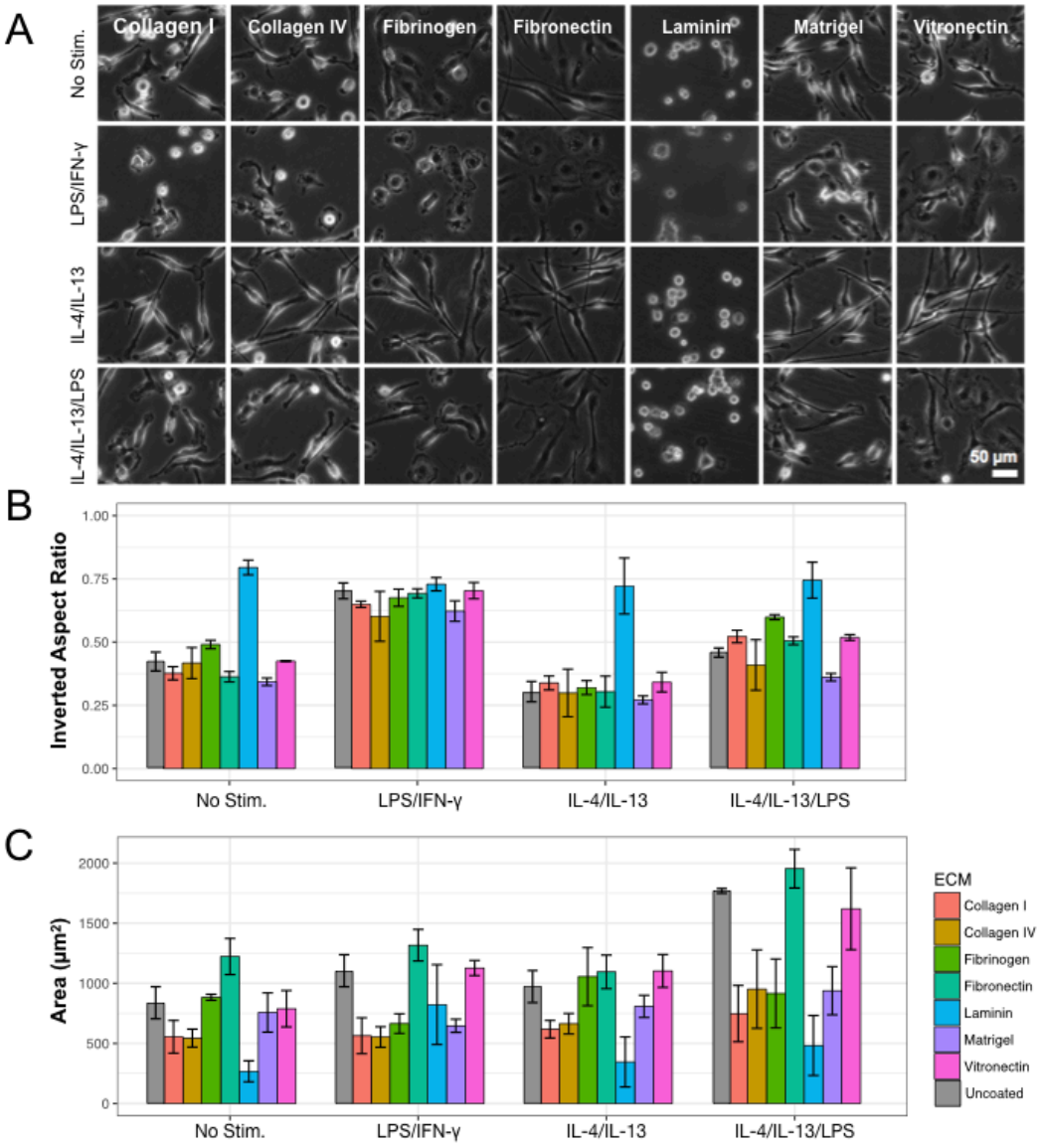

Figure 12. The effect of extracellular matrix ligands on macrophage morphology. (A) Representative phase contrast images of BMDM on different ECM coated substrates. Scale bar = 50 µm. **(B)** Quantified inverted aspect ratio, **(C)** quantified area of BMDM cultured on different ECM coated substrates. Mean ± SEM, *n = 3* (Collagen IV, Mean ± SD, *n = 2*). No Stim. denotes unstimulated, LPS/IFN-γ was stimulated with 1 ng/mL LPS and 10 ng/mL IFN-γ, IL-4/IL-13 was stimulated with 20 ng/mL IL-4 and 20 ng/mL IL-13, IL-4/IL-13/LPS was stimulated with 20 ng/mL IL-4, 20 ng/mL IL-13 and 1 ng/mL LPS.

We observed that across all stimulation, except LPS/IFN-γ condition, BMDM cultured on Ln substrates exhibited significant higher inverted aspect ratio, round shape, and significant smaller area, compared to other ECM substrates (Figure 12, Table 1 and 2). In addition, across all ECM conditions, except Ln, macrophages stimulated with LPS/IFN-γ assumed round shape and their inverted aspect ratios were in range of 0.7 to 0.8, and cells stimulated with IL-4/IL-13 adopted elongated shapes and their ratios were from 0.25 to 0.37 (Figure 12B and Table 1). Together, the data suggested that the effect of soluble factors on macrophage morphology was more potent than the ECM composition, which for the most part did not significantly influence changes in macrophage cell shape caused by soluble stimulation.

Inverted Aspect Ratio	alpha = 0.05			
Ordinary One-way ANOVA	Tukey's Multiple comparisons test			
Multiple comparisons	**Stimulation**	**Significant?**	**Summary**	**Adjusted P value**
Collagen I vs. Laminin	No Stim.	Yes	****	< 0.0001
Laminin vs. Fibrinogen	No Stim.	Yes	****	< 0.0001
Laminin vs. Fibronectin	No Stim.	Yes	****	< 0.0001
Laminin vs. Matrigel	No Stim.	Yes	****	< 0.0001
Laminin vs. Vitronectin	No Stim.	Yes	****	< 0.0001
Laminin vs. Uncoated	No Stim.	Yes	****	< 0.0001
Fibrinogen vs. Fibronectin	No Stim.	Yes	*	0.0314
Fibrinogen vs. Matrigel	No Stim.	Yes	*	0.011
Collagen I vs. Laminin	IL4/IL13	Yes	**	0.0032
Laminin vs. Fibrinogen	IL4/IL13	Yes	**	0.0021
Laminin vs. Fibronectin	IL4/IL13	Yes	**	0.0015
Laminin vs. Matrigel	IL4/IL13	Yes	***	0.0007
Laminin vs. Vitronectin	IL4/IL13	Yes	**	0.0035
Laminin vs. Uncoated	IL4/IL13	Yes	**	0.0012
Collagen I vs. Laminin	IL4/IL13/LPS	Yes	**	0.0024
Collagen I vs. Matrigel	IL4/IL13/LPS	Yes	*	0.0311
Laminin vs. Fibronectin	IL4/IL13/LPS	Yes	**	0.0012
Laminin vs. Matrigel	IL4/IL13/LPS	Yes	****	< 0.0001
Laminin vs. Vitronectin	IL4/IL13/LPS	Yes	**	0.0021
Laminin vs. Uncoated	IL4/IL13/LPS	Yes	***	0.0002
Fibrinogen vs. Matrigel	IL4/IL13/LPS	Yes	**	0.0013
Matrigel vs. Vitronectin	IL4/IL13/LPS	Yes	*	0.0366

Table 1. ANOVA of inverted aspect ratio of BMDM on different ECM coated substrates (Figure 12B) within the same stimulation.

Area	alpha = 0.05			
Ordinary One-way ANOVA	Tukey's Multiple comparisons test			
Multiple comparisons	**Stimulation**	**Significant?**	**Summary**	**Adjusted P value**
Collagen I vs. Fibronectin	No Stim.	Yes	***	0.0004
Laminin vs. Fibrinogen	No Stim.	Yes	***	0.0008
Laminin vs. Fibronectin	No Stim.	Yes	****	< 0.0001
Laminin vs. Matrigel	No Stim.	Yes	**	0.0064
Laminin vs. Vitronectin	No Stim.	Yes	**	0.0038
Laminin vs. Uncoated	No Stim.	Yes	**	0.0019
Fibronectin vs. Matrigel	No Stim.	Yes	**	0.0095
Fibronectin vs. Vitronectin	No Stim.	Yes	*	0.0162
Fibronectin vs. Uncoated	No Stim.	Yes	*	0.0332
Collagen I vs. Fibronectin	LPS/IFNγ	Yes	***	0.0009
Collagen I vs. Vitronectin	LPS/IFNγ	Yes	*	0.0109
Collagen I vs. Uncoated	LPS/IFNγ	Yes	*	0.0156
Laminin vs. Fibronectin	LPS/IFNγ	Yes	*	0.0283
Fibrinogen vs. Fibronectin	LPS/IFNγ	Yes	**	0.0033
Fibrinogen vs. Vitronectin	LPS/IFNγ	Yes	*	0.0436
Fibronectin vs. Matrigel	LPS/IFNγ	Yes	**	0.0025
Matrigel vs. Vitronectin	LPS/IFNγ	Yes	*	0.034
Matrigel vs. Uncoated	LPS/IFNγ	Yes	*	0.0483
Collagen I vs. Fibronectin	IL4/IL13	Yes	*	0.0307
Collagen I vs. Vitronectin	IL4/IL13	Yes	*	0.0275
Laminin vs. Fibrinogen	IL4/IL13	Yes	**	0.0012
Laminin vs. Fibronectin	IL4/IL13	Yes	***	0.0007
Laminin vs. Matrigel	IL4/IL13	Yes	*	0.0376
Laminin vs. Vitronectin	IL4/IL13	Yes	***	0.0006
Laminin vs. Uncoated	IL4/IL13	Yes	**	0.0034
Collagen I vs. Fibronectin	IL4/IL13/LPS	Yes	***	0.0003
Collagen I vs. Vitronectin	IL4/IL13/LPS	Yes	**	0.0061
Collagen I vs. Uncoated	IL4/IL13/LPS	Yes	**	0.0016
Laminin vs. Fibronectin	IL4/IL13/LPS	Yes	****	< 0.0001
Laminin vs. Vitronectin	IL4/IL13/LPS	Yes	***	0.0005
Laminin vs. Uncoated	IL4/IL13/LPS	Yes	***	0.0002
Fibrinogen vs. Fibronectin	IL4/IL13/LPS	Yes	**	0.0013
Fibrinogen vs. Vitronectin	IL4/IL13/LPS	Yes	*	0.0304
Fibrinogen vs. Uncoated	IL4/IL13/LPS	Yes	**	0.0076
Fibronectin vs. Matrigel	IL4/IL13/LPS	Yes	**	0.0016
Matrigel vs. Vitronectin	IL4/IL13/LPS	Yes	*	0.0376
Matrigel vs. Uncoated	IL4/IL13/LPS	Yes	**	0.0094

Table 2. ANOVA of area of BMDM on different ECM coated substrates (Figure 12C) within the same stimulation.

Role of ECM composition on macrophage polarization response

To examine the interactions between macrophages and ECM ligands on cell function, we characterized the secretion of TNF-α, an inflammatory marker that is known to express in response to stimulation with LPS or LPS/IFN-γ. Representation of the data in a heatmap showed that there was not significant difference in TNF-α concentration

secreted by macrophages among the various ECM coating conditions (Figure 13A). Moreover, we also examine secretion of IL-10, an anti- inflammatory cytokine mostly secreted in response to IL-4/IL-13/LPS stimulation. We observed that IL-10 secretion by macrophages was also similar across different ECM coating conditions (Figure 13A). To prove how these phenotypic markers, TNF-α and IL-10, might be correlated with cell shape, we plotted their average concentration against the average inverted aspect ratios for all matrix and stimulation conditions.

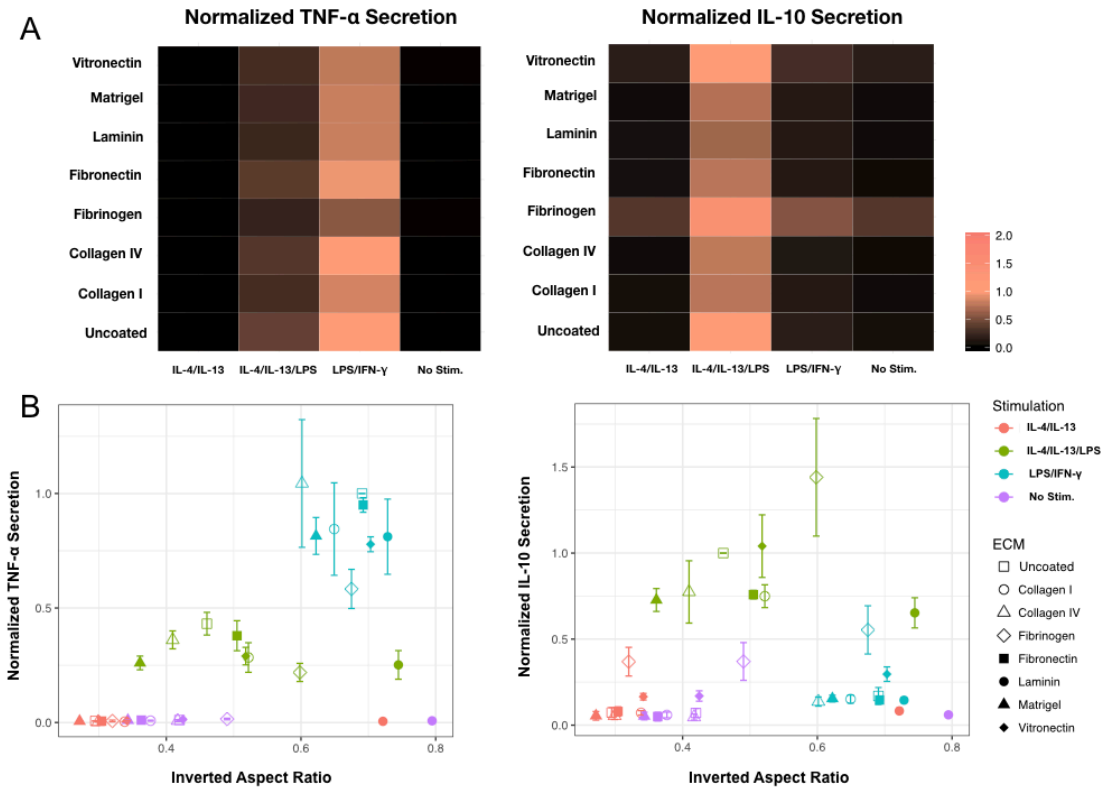

Figure 13. Cytokine secretion from macrophages on different ECM coated substrates. **(A)** Column-wise mean normalized heat map of cytokines secreted by macrophages after culture on different substrates. TNF-α, and IL-10 secretions by macrophages cultured on different substrates were sequentially normalized to uncoated substrates' LPS/IFN-γ, and IL-4/IL-13/LPS conditions. **(B)** Correlation of TNF-α and IL-10 cytokine secretions with macrophage cell shape. Uncoated was uncoated polystyrene substrate. No Stim. denotes unstimulated, LPS/IFN-γ was stimulated with 1 ng/mL LPS and 10 ng/mL IFN-γ, IL-4/IL-

13 was stimulated with 20 ng/mL IL-4 and 20 ng/mL IL-13, IL-4/IL-13/LPS was stimulated with 20 ng/mL IL-4, 20 ng/mL IL-13 and 1 ng/mL LPS. Mean ± SEM, *n = 3.*

Interestingly, the data suggest that TNF-α secretion was highly correlated to cell shape. More specifically, cells with high levels of TNF-α secretion, including those stimulated with LPS/IFN-γ (noted with blue symbols) exhibited inverted aspect ratios close to 1 (Figure 13B). Macrophages stimulated with IL-4/IL-13 (shown with red symbols) secreted undetectable TNF-α levels, and clustered close to 0 in inverted aspect ratios (Figure 13B). Thus, elongated cells exhibit a reduced inflammatory response compared to round cells. We did not observe any correlation between IL-10 secretion and cell shape (Figure 13B). Together, our data show that although cell shape and phenotype may be correlated in some cases, adhesion to different ECM ligands does not affect the secretion of TNF-α or IL-10 by macrophages in response to LPS, IFN-γ, IL-4 and IL-13, at least at the concentrations tested here.

ECM composition and adhesive geometry regulates on macrophages anti-inflammatory activation

Our previous work found that macrophage elongation on fibronectin lines leads to enhance Arg1 expression, a marker of pro-healing function in murine macrophages. To further examine the combined effect of ECM ligand and adhesion geometry on cell function, we micropatterned cells into 20-μm wide line patterns using different ECMs. BMDMs were cultured on ECM line or flat substrates for 40 h, and then cell shape and arginase1 expression were assessed. ECM proteins including Fn, Fg, CI, CIV, Ln, Mg, and Vn were microcontact-printed on PDMS coated substrates, as previously described [2]. We found that

on flat substrates, macrophages cultured on Ln and Mg substrates were rounded (Figure 14A and 14C), and the degree of cell elongation was higher when cells were cultured on other ECM substrates including Fn, Fg, CIV, and Vn (Figure 14A and 14C). Cells cultured on flat CI substrates displayed a mixture of round and elongated cells (Figure 14). We found that in ECM conditions, culturing macrophages on patterned substrates enhanced the degree of elongation when compared to their respective flat substrates (Figure 14C). To examine whether the changes in cell elongation induced changes in expression of macrophage phenotypic markers, cells were cultured on ECM flat or patterned substrates, and Arg1 expression was evaluated by immunofluorescence.

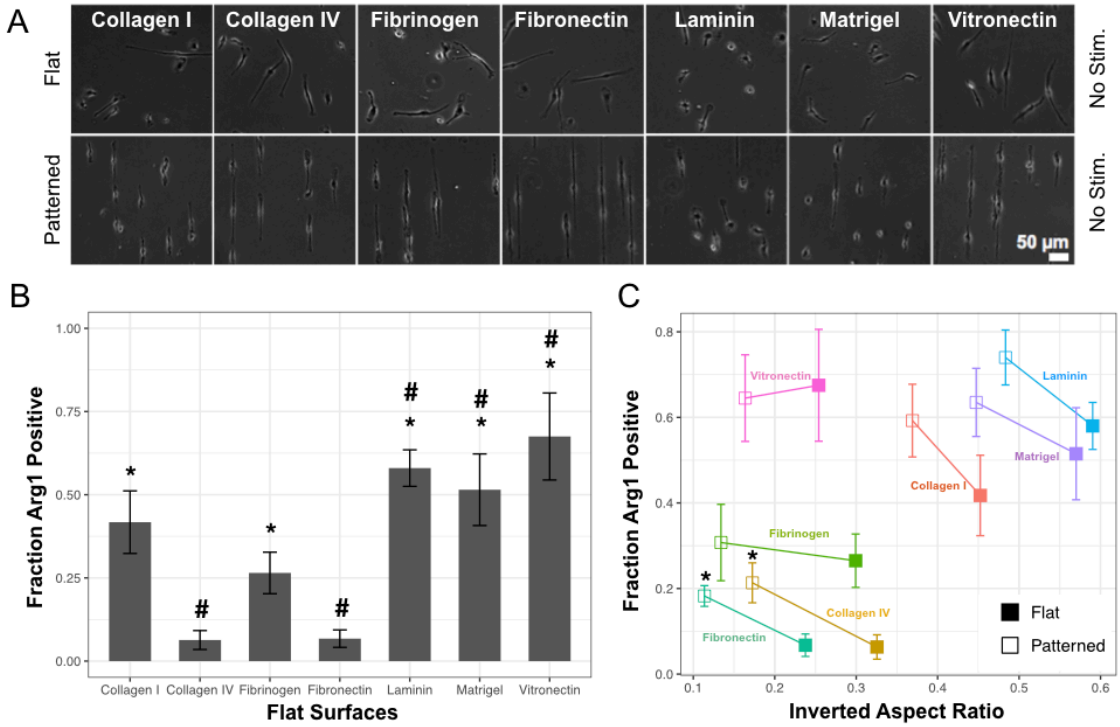

Figure 14. The effect of ECM composition and adhesive geometry on BMDM arginase-1 expression. (A) Representative phase contrast images of cells cultured on different ECM substrates unpatterned or micropatterned with 20 μm wide line. Scale bar = 50 μm. **(B)** Arg1 expression corresponding to the ECM on flat substrates. Mean ± SEM (*p < 0.05, compared to collagen IV or fibronectin coated substrates; #p< 0.05, compared to fibrinogen

coated substrates, a paired two-tailed students t-test, $n \geq 3$). **(C)** Correlation of Arg1 expression, corresponding to the ECM ligands, with macrophage cell shape. Mean ± SEM (*$p < 0.05$; an unpaired two-tailed students t-test, for each ECM ligand, patterned substrate compared to flat substrate, $n \geq 3$). No Stim. denotes unstimulated.

Interestingly, we found that in comparison of cells on CI or Fn flat surfaces, the expression of Arg1 was significantly higher when cells were cultured on other ECM flat surfaces and cells cultured on La, Mg, and Vn flat surfaces expressed significantly higher Arg1, compared to Fg flat surfaces (Figure 14B). Cells cultured on CI, Ln, Mg, and Vn substrates expressed high level of Arg1 regardless to cell shapes (Figure 14B). In comparison, macrophages cultured on Fn, Fg, and CIV flat substrates expressed lower level of Arg1. However, compared to their flat substrates, cells forced to elongate on Fn and CIV patterned substrates expressed significantly higher level of arginase1 (Figure 14C). Together, these data demonstrate that adhesion to different ECMs affects expression of Arg1, and adhesive geometries that elicit elongation enhance Arg1 expression across all ECMs.

3D ECM hydrogels inhibited inflammatory response of human macrophages to LPS

To understand the effect of 3D microenvironment on macrophages in comparison to 2D microenvironment, we seeded human primary macrophages on hydrogels as 3D culture and a polystyrene tissue culture plate as 2D culture, and examined the inflammatory response of macrophages to LPS. Human monocytes isolated from human blood peripheral mononuclear cells were cultured on petri dishes, in the supplement of human MCSF to differentiate to human macrophages. At day 6 of culture, cell culture supernatants were collected and examined for TNF-α secretion. We observed that in

response to different LPS concentrations, from 0 ng/mL to 50 ng/mL, human macrophages cultured on polystyrene substrates secreted the highest amount of TNF-α, compared to cells cultured on hydrogels, including fibrin, collagen I gels, and Matrigel (Figure 15). Human macrophages on collagen I gels and matrigels had similar TNF-α secretion, the smallest amount (Figure 15). Together, hydrogels including fibrin, collagen I gels, and matrigels inhibited TNF-α secretion by human primary macrophages in response to various LPS concentrations.

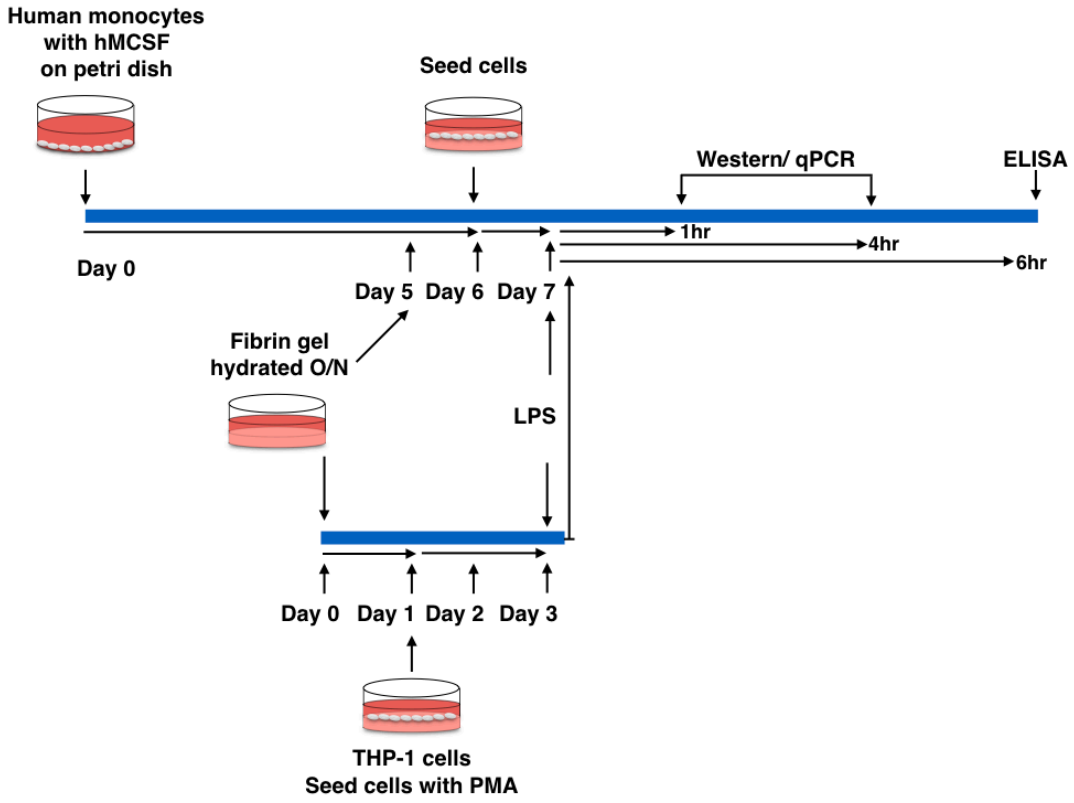

Scheme 1. Schematic diagram of experimental setup

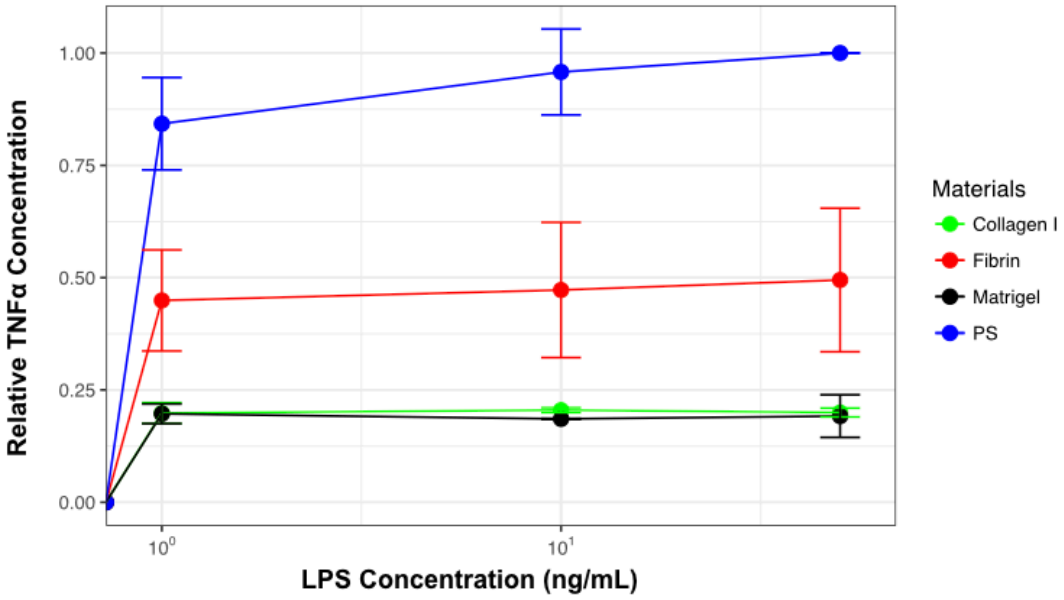

Figure 15. TNF-α secretion by human primary macrophages. Cells were cultured on different hydrogels (2 mg/mL fibrin in red, 2 mg/mL collagen 1 gel in green, and 3 mg/mL Matrigel in black) and tissue culture plates (PS in blue) in response to ultrapure LPS concentrations (0 ng/mL, 1 ng/mL, 10 ng/mL, and 50 ng/mL). Mean ± SD, *n = 2.*

Fibrin inhibited human macrophages' TNF-α secretion in response to various LPS concentrations

In order to further understand the inhibitory effect of 3D microenvironment on macrophage inflammatory response to LPS, we seeded human primary macrophages and THP-1 cells on fibrin or polystyrene tissue culture plate, as 2D culture control. In this study, we examined inflammatory response of macrophages to LPS, with and without fibrinogen stimulation, as illustrated in Scheme 1. We also examined the effects of a larger range of LPS doses. We observed that the anti-inflammatory effects of fibrin on human macrophages extended to high concentrations (up to 100 ng/mL) (Figure 16B and 16D). We also found that soluble fibrinogen significantly enhanced TNF-α secretion by THP-1

cells stimulated with LPS (Figure 16C), although this was not observed in primary human macrophages (Figure 16A). In addition, fibrin inhibited the expression of TNF-α gene after 4 h and protein secretion by human macrophages after 6 h of culture when cells were stimulated with LPS or fibrinogen (Figure 16C, 16E and 16F). Together, we observed that fibrin inhibited the inflammatory response of human macrophages to LPS and soluble fibrinogen.

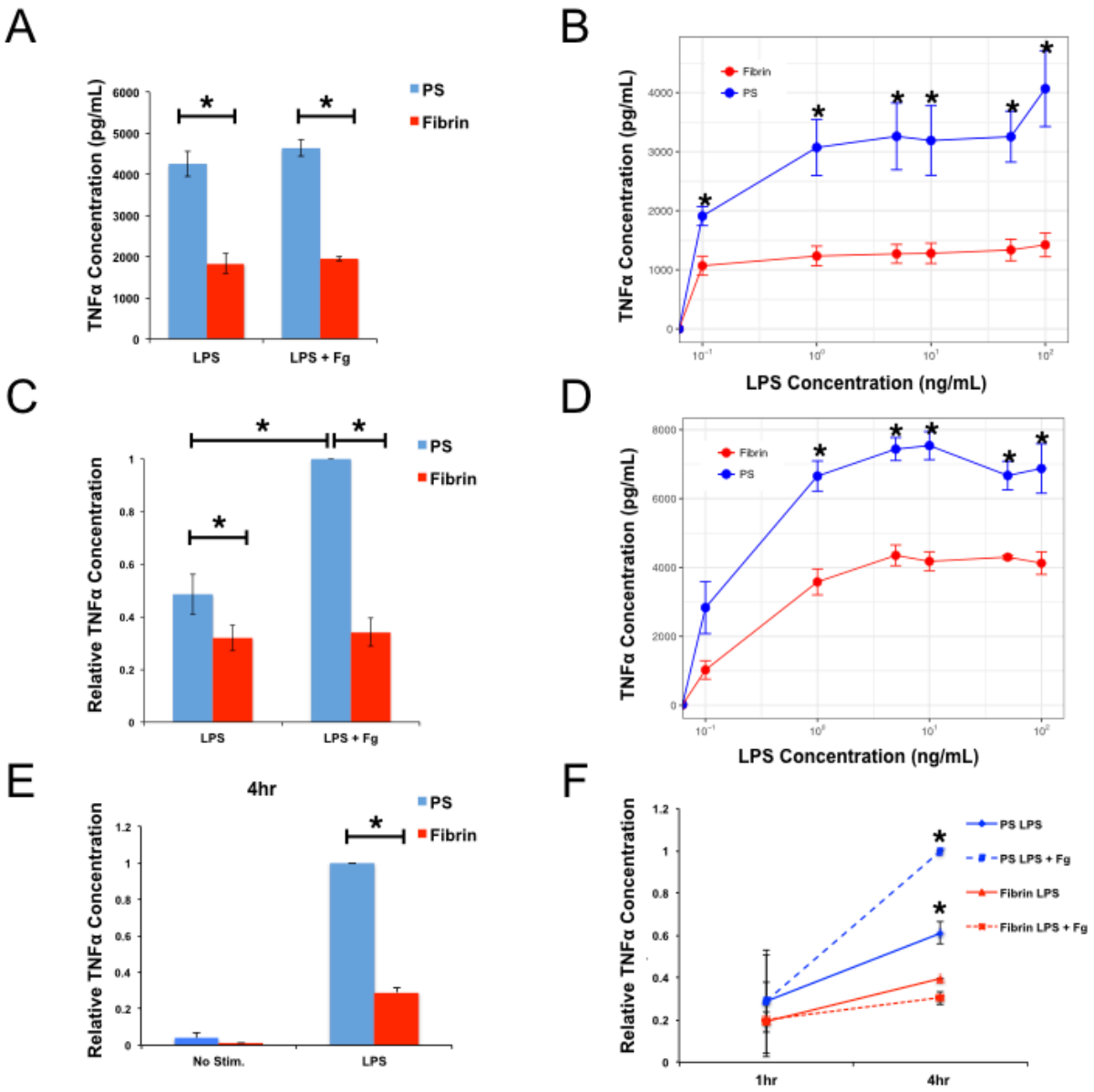

Figure 16. The effect of fibrin gels on inflammatory responses of human macrophages to LPS. TNF-α secretion by human primary macrophages **(A)** and THP-1 cells **(C)** on 2 mg/mL fibrin and PS, stimulated with 10 ng/mL LPS and (2 mg/ml fibrinogen + 10 ng/ml LPS). Mean ± SEM (*p < 0.05; an unpaired two-tailed students t-test, *n ≥ 3*). Human primary macrophages **(B)** and THP-1 cells **(D)** stimulated with different LPS concentrations (0 ng/mL, 0.1 ng/mL, 1 ng/mL, 5 ng/mL, 10 ng/mL, 50 ng/mL, and 100 ng/mL). Supernatants were collected after 6 h for ELISA. TNF-α gene expression, real-time RT-PCR at 4 h of culture **(E)** by THP-1 cells on fibrin and PS, stimulated with or without 10 ng/mL LPS. TNF-α gene expression at 1 h and 4 h of culture **(F)** by THP-1 cells stimulated with 10 ng/mL LPS and (2 mg/ml fibrinogen + 10 ng/ml LPS). Mean ± SEM (*p < 0.05; an unpaired two-tailed students t-test, fibrin condition compared to PS condition, *n ≥ 3*).

Fibrin inhibited human primary macrophages' TNF-α secretion in response to different TLR ligands

Up to this point, the results show that fibrin inhibits inflammatory activation by LPS, an agonist of TLR4, but there are many other TLRs presented on macrophage cells that bind to a variety of ligands [118]. To examine how the culture environment affects the macrophage response to other TLR ligands, we stimulated cells with a wide range of TLR ligands including synthetic triacylated lipoprotein (PamCK) for TLR1/2, heat killed listeria monocytogenes (HKLM) for TLR2, zymosan for TLR2, FSL for TLR6/2, flagellin for TLR5. Interestingly, we observed that fibrin moderately inhibited inflammatory effect on human primary macrophages in response to flagellin and zymosan, and completely suppressed the inflammatory response to PamCK and FSL in different concentrations (Figure 17). Together, these results demonstrated that hydrogels as 3D microenvironment inhibited inflammatory effect on human macrophages in comparison to polystyrene surfaces as 2D microenvironment.

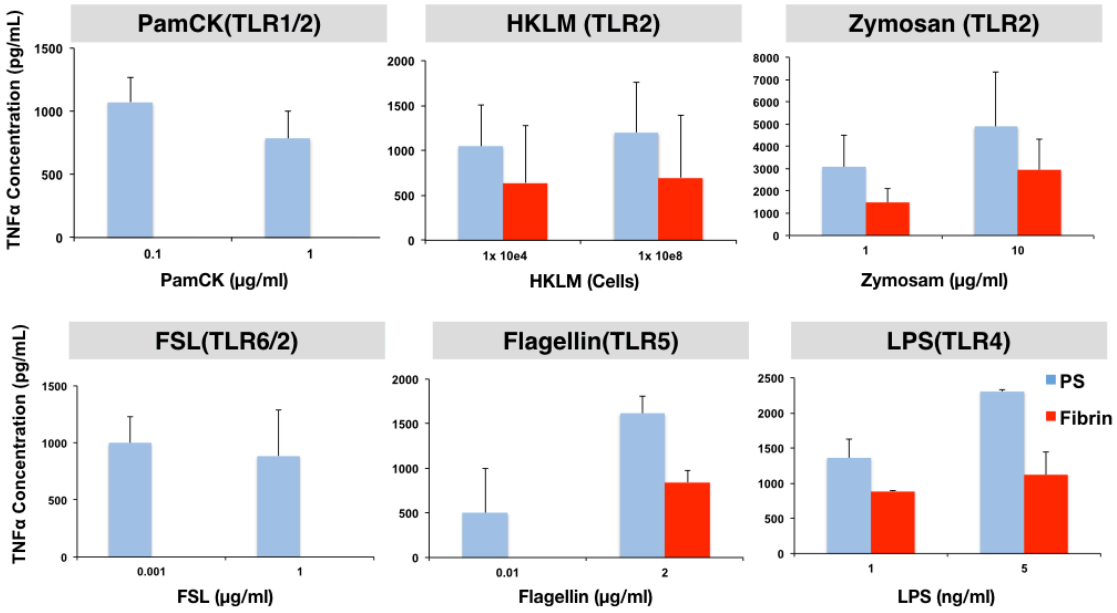

Figure 17. TNF-α secretion by human primary macrophages responded to different TLR ligands. Cells were cultured on 2 mg/mL fibrin and PS, stimulated with different concentrations of ligands including PamCK (TLR1/2), HKLM (TLR2), zymosan (TLR2), FSL (TLR6/2), flagellin (TLR5), and LPS (TLR4). Supernatants collected after 6 h for ELISA. Mean ± SD, *n = 2*.

3.4 Discussion

In this work, we screened the effects of different cell matrix proteins on macrophage function. Overall, our results showed that the effects of soluble factors on macrophage cell shape and function were more potent than adhesion ligands, although macrophage elongation and Arg1 expression depended on ECM composition and adhesive geometry presented by line patterns. We observed that cell shape was more modulated by the soluble factors, as has been reported in many studies, but these cell shape changes were largely independent on adhesive ligands (Figure 12 and 13) [2,76,119]. We observed that regardless of ECM proteins, except Ln, macrophages stimulated with LPS/IFN-γ adopt

round shape, but cells stimulated with IL-4/IL-13 spread and elongated on substrates, consistent with our previous works and other groups on macrophages (Figure 12) [2,119]. The change in cell shape was not observed for macrophages seeded on Ln substrates, where cells remained round across all stimulation conditions (Figure 12). We previously reported that cells forced to elongate on micro-patterned lines enhanced the expression of phenotypic markers associated with the pro-healing phenotype [2]. Studies on topographical substrates, which included wrinkled materials and titanium substrates with multiple different groove sizes, also demonstrated that macrophages with more elongated cell shape expressed high level of phenotypic markers associated to anti-inflammatory phenotypes [62,93]. In this work, we found that cells were forced to elongate along adhesive patterns of ECM generally increased Arg1 expression, with statistically significant differences observed on Fn or CIV. We also demonstrated that Arg1 expression of BMDMs cultured on Ln, Mg, Vn, and CI substrates was higher than cells on Fn, Fg, and CIV substrates (Figure 14). Together, the data suggest that ECM composition and adhesion geometry both regulate macrophage behavior.

Our studies may provide insight to the effect of ECM ligands on macrophage function during wound healing and disease. Specifically, we observed significantly different levels of Arg1 expression in cells cultured on different adhesive ligands, some of which play a major role in disease. Laminin, vitronectin, and Matrigel are all associated with pathological conditions in which macrophages adopt a pro-healing phenotype including, for example, cancer [120-122]. Since we observed that macrophages enhance their expression of Arg1 when cultured on these ECMs, our data suggest that the ECM itself may be playing a role in regulating the function of TAMs. On the other hand, collagen type IV, a principal

component of the basement membrane, increases in content with atherosclerotic lesion progression [123], and surrounding smooth muscle cells increases from a relatively thin layer to a thick, multi-layered structure [124]. Meanwhile, fibronectin, is also prominent along with collagen type IV around cells that are localized in the deeper layers of an advanced human atherosclerotic lesion [125]. Our study suggests that ECM ligands, that have the homologous functions in wound healing and disease, exert similar effect on macrophages' Arg1 expression.

Proper expression of Arg1 by macrophages is thought to facilitate collagen remodeling [126], and dysregulation can lead to excessive deposition of collagen and scar formation during wound healing [9,14]. Both collagen amount and type are altered in keloids and hypertrophic scar – it has been reported that there is 20 times collagen in keloids and three times more in hypertrophic scars than in normal skin. The ratio of collagen I/III is 6:1 in normal scars, but 17:1 in keloids [127]. Together, these data suggest that our understanding the role of ECM protein composition and geometric micropatterning for Arg1 expression of macrophages is needed to modulate wound healing response to achieve minimal fibrosis or scar formation.

Our studies investigating the effect of ECM-based hydrogels including collagen 1, fibrin, and Matrigel showed a similar suppression of TNF-α secretion in response to LPS, across all hydrogels (Figure 15). Recently, other studies from our laboratory have shown that fibrin matrices are protective and inhibit macrophage inflammatory activation, whereas its soluble precursor fibrinogen potentiates inflammation [117]. Thus, we confirmed the inhibitory effect of fibrin on inflammatory response of human macrophages to LPS (Figure 16), as well as in response to other TLR ligands. Together, the results demonstrated

that across all conditions, hydrogels as 3D microenvironment, specifically fibrin, inhibited inflammatory effect on human macrophages, compared to polystyrene surfaces as 2D microenvironment. These results may be caused by changes in adhesive ligand presentation or physical cues such as substrate stiffness or fibrillar architecture. Most recently, using collagen-coated polyacrylamide gels, Alvey *et al.* synthesized soft 0.3 kPa gels (like marrow) and stiff 40 kPa gels (like solid tumors) to examine the effect of stiffness on human macrophages' anti-tumor properties [128]. Compared to stiff gels, macrophages cultured on soft gels expressed significantly lower levels of SIRPα and lamin-A, which favored tumor regression and phagocytosis of tumors [128]. Moreover, stiff ECMs stimulated tumor metastasis while softening matrix prevented tumor metastasis [19]. Future work is focused on understanding the signaling pathway downstream of adhesion regulating macrophage activation, which can be used to design new materials to encourage macrophage-mediated wound healing.

In conclusion, we demonstrate that ECM composition and adhesion geometry independently regulate the shape and function of macrophages. When macrophages cultured on ECM ligands coated substrates including Fn, Fg, CI, CIV, Ln, Mg, and Vn were stimulated with soluble factors, the effect of soluble factors on macrophage behavior was more potent than physical cues represented by ECM ligands. Furthermore, when macrophages cultured on ECM flat printed on PDMS coated substrates, cells adhered to Ln, Mg and Vn ligands expressed higher levels of Arg1 expression than Fn, CIV ligands. In addition, compared to flat substrates, ECM patterned substrates enhance cell elongation level, and the expression of Arg1 was increased when macrophages were cultured Fn, CIV patterned substrates. Moreover, 2D and 3D cultures differently regulated macrophage

inflammatory responses. Together, these results show the regulation of macrophage morphology and function by ECM ligands, and may suggest potential influences on tissue regeneration. Further studies will be necessary to determine new material structures to encourage macrophage wound healing polarization during tissue injury.

CHAPTER 4- Investigation of Signaling Pathways Downstream of Adhesion In Regulating Macrophage Inflammatory Responses

4.1 Introduction

Integrins are receptors that primarily mediate cellular adhesive interactions with ECM proteins and other cells. Integrins facilitate the transduction of signals from the extracellular matrices into the cell, and can lead to changes in macrophage activation and the production of inflammatory cytokines and chemoattractants [129]. Integrin α_M, CD11b, is not only a myeloid lineage marker, but also a receptor of fibrinogen [130], a major component of fibrin matrix. Several studies have implicated CD11b in regulating TLR-triggered inflammatory response, but it is controversial whether the effect is negative or positive on the TLR4-induced signaling pathway. A study on peritoneal macrophages by Han *et al.* showed that CD11b activation negatively regulated a TLR4-triggered inflammatory response [131]. Compared to wild type mice, macrophages isolated from CD11b knockout mice had significantly increased secretion of pro-inflammatory cytokines TNF-α and IL-6 when cells were stimulated with TLR ligands such as LPS, Poly(I:C), and CpG [131]. However, a study by Ling *et al.* demonstrated that CD11b can positively regulate the response [132]. Compared to cells from wild type mice, dendritic cells of CD11b knockout mice showed significantly enhanced secretion of pro-inflammatory cytokines, but no difference in TNF-α and IL6 secretion was observed between bone-marrow-derived macrophages from $CD11b^{-/-}$ and wild type mice [132]. Together, the observations from both studies indicate that the effect of CD11b on regulating TLR-triggered inflammatory response may depend on cell sources and cell types.

Integrin binding has been shown to lead to remodeling of cytoskeletal structures and activation of small RhoGTPase signaling pathways. Following integrin activation or adhesion to materials, integrins facilitate changes in cytoskeletal structures and leads to changes in gene expression, cell proliferation, and cell function [133]. Small RhoGTPase proteins RhoA, Rac1, and Cdc42 regulate cell morphology and functions through the rearrangement of the actin cytoskeleton and microtubule network [133-135]. This rearrangement drives changes in macrophage morphology, which facilitates cell migration to injured sites and enhances cell functions [135]. Thus, to understand how the signaling pathways responsive to adhesion environment regulate macrophage function, it is important to understand how cytoskeletal structures and small RhoGTPase proteins influence the anti-inflammatory effect of fibrin on human macrophages.

Toll-like receptors (TLR) play critical roles in innate immunity, and recognize a wide variety of ligands in order to promote host defense. For instance, LPS triggers TLR4, flagellin activates TLR5, and triacylated lipopeptides are involved in TLR2-TLR1 activation [118]. Signaling downstream of TLRs occurs through the recruitment of adaptors including MyD88 or TRIF, and leads to the activation of IKKα/β, MAPK, and NF-κB pathways via phosphorylation [136]. The translocation of phosphorylated NF-κB to the nucleus leads to enhanced pro-inflammatory cytokine expression. TLR-triggered signaling pathways may crosstalk with integrin-mediated signaling downstream of adhesion in the inflammatory response to LPS.

In this study, we explored the signaling downstream of adhesion on the inflammatory response to LPS. We examined the expression of CD11b, of which fibrin is a ligand, and TLR4, triggered by LPS. We used pharmacological inhibitors of actin

polymerization, microtubule polymerization, cytoskeletal contractility, small RhoGTPase proteins, and RhoA effector ROCK to study the role of cytoskeletal structure and contractility in adhesive regulation of macrophage activity. Furthermore, we characterized how fibrin regulated the signaling through MAPK and NF-κB, which are downstream of TLR activation. We observed that human macrophages cultured on polystyrene had higher TLR4 and CD11b expression compared to cells in a 3D fibrin microenvironment. From the drug studies, we found that cytoskeletal contractility may be involved in the anti-inflammatory property of fibrin while small RhoGTPase proteins were not. Finally, fibrin suppressed phosphorylation of NF-κB and MAPK in human macrophages. These findings suggest a promising strategy for regulating macrophage function in wound healing by using fibril immune-mediated biomaterials.

4.2 Materials and Methods

Cell isolation and culture

Human primary macrophages were cultured using cell isolation and culture methods previously described in Chapter 3

Gel fabrication

Fibrin gel were formed followed the gel fabrication method previously described in Chapter 3

RNA isolation

RNA isolation was performed using the RNA isolation method previously described in Chapter 3.

Quantitative Real-time PCR

Real-time PCR was conducted using the quantitative real-time PCR method previously described in Chapter 3.

Cytokine secretion

Human monocyte derived macrophages and THP-1 cells on substrates were stimulated with LPS for 6 h before cytokine secretion quantification. Enzyme-linked immunosorbent assay (ELISA) was used to determine TNF-α secretion according to the manufacturer's instructions (BioLegend, San Diego, CA).

Immunofluorescence

Immunofluorescence was performed following the method previously described in Chapter 2.1. Primary antibodies were mouse monoclonal anti-TLR4 (25) (1:500) (Santa Cruz Biotechnology) and mouse monoclonal anti-CD11b Primary-H5A4 (2 μg/mL) (Developmental Studies Hybridoma Bank). The secondary antibody was anti-mouse IgG Alexa Fluor 594 (1:200) (Biolegend).

Western blotting

Cells on tissue culture plates were washed and protein lysates were collected as previously described in the Chapter 2. To isolate cells on gels, after supernatants were removed, and gels were gently ground using a Biomasher (Kimble). Cell pellets were rinsed

with PBS and lysed in RIPA buffer supplemented with 1% protease and phosphatase inhibitor cocktails (Thermo Scientific Halt). Western blotting of samples was done following the protocol described in the Chapter 2. The antibodies used were mouse anti-GAPDH (Biolegend), HRP goat anti-mouse IgM (Jackson ImmunoResearch), mouse monoclonal anti-TLR4 HRP (25) (Santa Cruz Biotechnology), rabbit anti-CD11b (Abcam), rabbit anti-myD88, HRP goat anti-rabbit, antibodies from MAPK family antibody sampler Kit, phospho-MAPK family antibody sampler kit, and NF-κB pathway sampler kit (all from Cell Signaling). Antibody concentrations followed the manufacturer's suggestions.

Drug inhibition study

For the drug inhibition study, cells were treated with inhibitor drugs 15-20 min prior to LPS stimulation. Drug inhibitors include Y-27632 30 μM (Sigma Aldrich), RKI-1447 10 μM, cytochalasin D 10 μM, nocodazole 30μM, ML9 50 μM, blebbistatin 30 μM, Rho II (Y16) 15 μM, Rac1 100 μM, Cdc42 III (ZCL278) 50 μM (all from Calbiochem). Cells were cultured for 6h before cytokine secretion assays.

NanoString

Gene expression analysis was performed using the nanoString human immunology panel according to the manufacturer's standard protocol. Data were normalized to endogenous housekeeper controls, and transcript counts were log transformed for statistical analyses.

Statistical analysis

All data were presented as the mean ± SEM across at least three independent experiments, unless otherwise specified in the figure legends. Statistical analysis was performed using two-tailed Student's t-test, or ANOVA, unpaired with Tukey's post hoc test as described in the figure legends. $p<0.05$ was considered statistically significant.

4.3 Results

Fibrin downregulates the expression of TLR4 and Cd11b in macrophages

To understand the role of the signaling pathway downstream of adhesion in regulating macrophage inflammatory responses, we seeded human macrophages on fibrin and polystyrene surfaces, and subjected cells to LPS or control stimulation. Then, we examined the expression of TLR4 and CD11b by macrophages using immunofluorescence and Western blotting. The results showed that compared to unstimulated condition, human primary macrophages and THP-1 cells on glass or fibrin expressed higher TLR4 (Figure 18A) when cells were stimulated with LPS. 3D fibrin culture suppressed TLR4 and CD11b expression of human macrophages stimulated with or without LPS compared to cells on glass (Figure 18). The anti-inflammatory effect of fibrin indicated in immunofluorescent images was also confirmed in Western blot data. In Figure 19, the Western blots showed that both human primary macrophages and THP-1 cells on fibrin expressed less TLR4 and CD11b with or without LPS treatment. Moreover, soluble fibrinogen did not enhance the expression of these proteins (Figure 19). Together, these results demonstrate that a fibrin microenvironment inhibits the inflammatory effect of human macrophages in response to

LPS and downregulated the expression of TLR4 and CD11b, compared to a 2D polystyrene microenvironment.

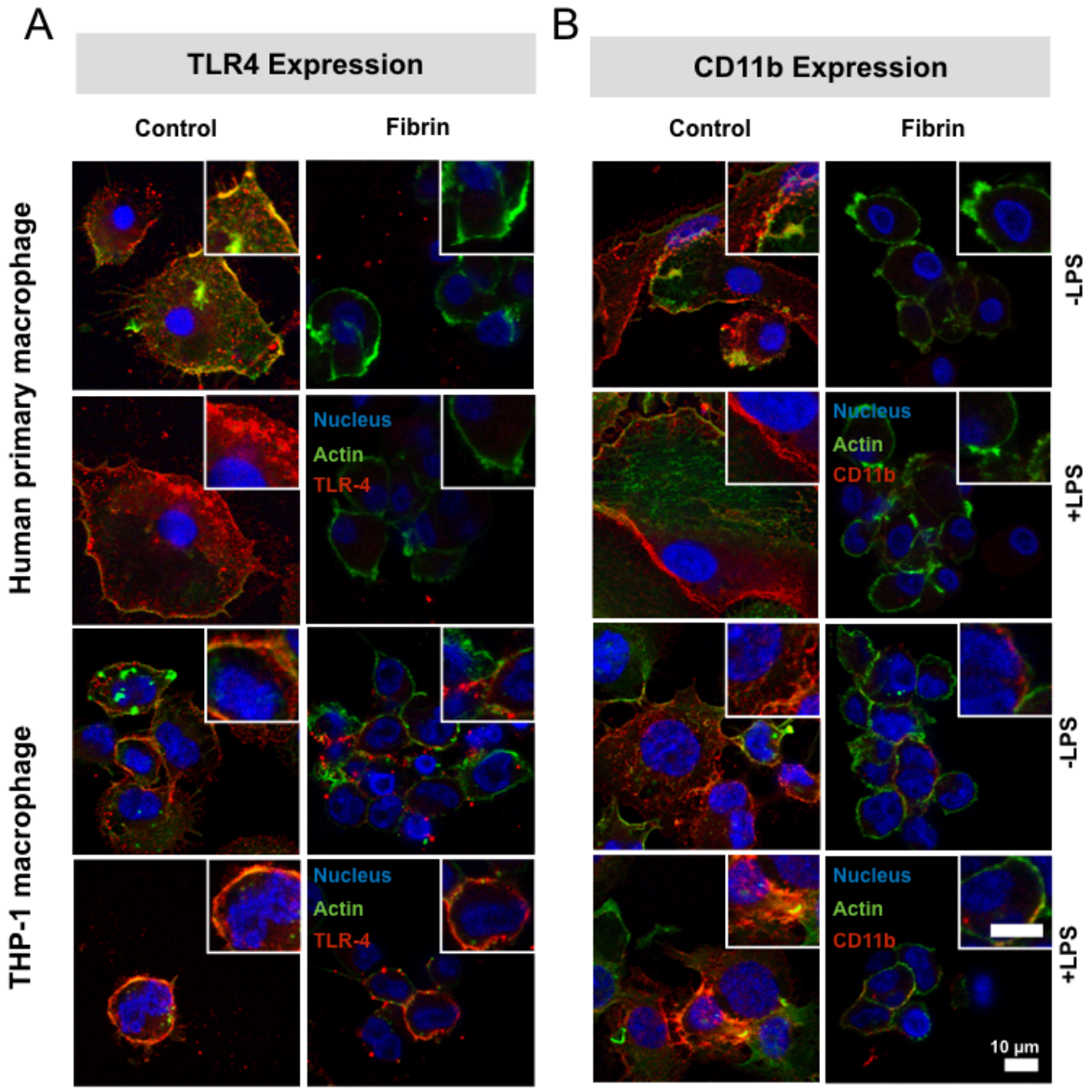

Figure 18. TLR4 and CD11b expression of human primary macrophages and THP-1 cells. Cells were cultured on 2 mg/mL fibrin and glass (control), stimulated with or without ultrapure LPS. Representative immunofluorescent images of TLR4 expression **(A)**, and CD11b expression **(B)**

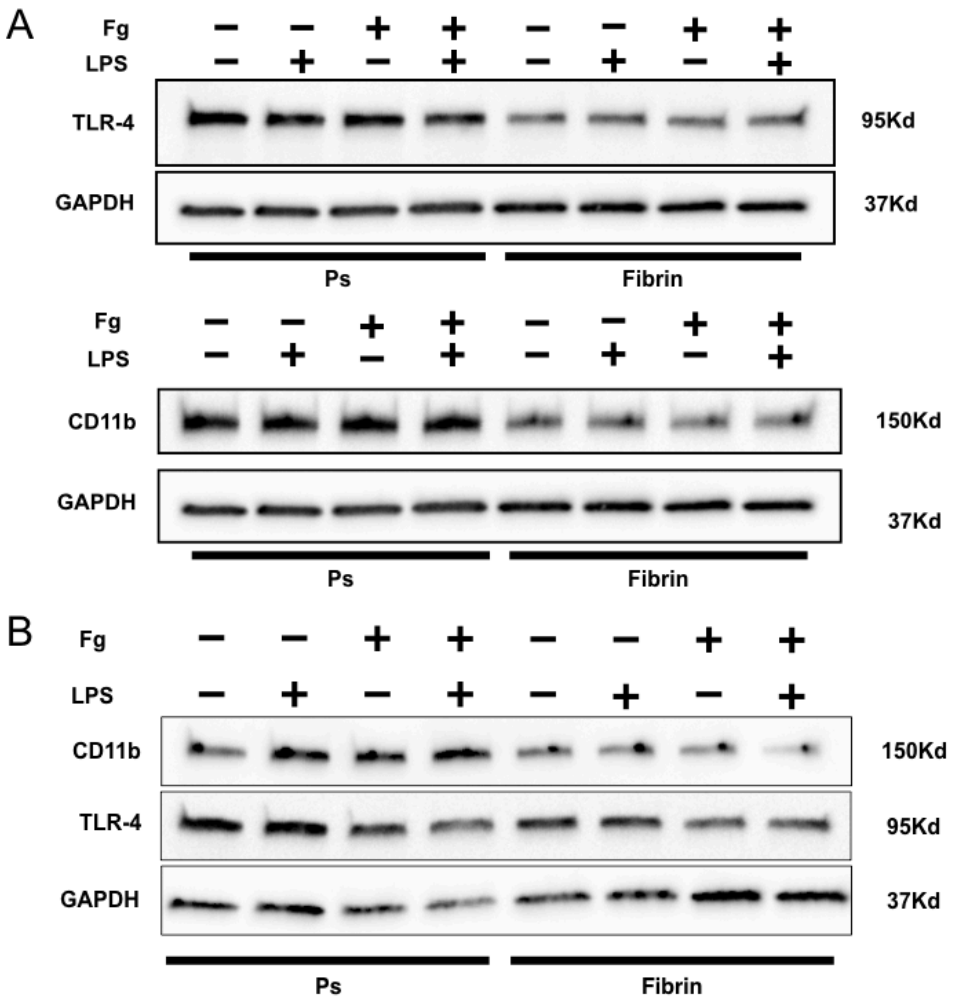

Figure 19. Western blotting for TLR4 and CD11b expression of human primary macrophages and THP-1 cells. Cells were cultured on 2 mg/mL fibrin or tissue culture plates (Ps - control), stimulated with or without stimulation with ultrapure LPS or 2 mg/mL fibrinogen (Fg). Qualification of CD11b and TLR4 expression by human primary macrophages **(A)**, and THP-1 cells **(B)**

Cytoskeletal contractility is involved in the anti-inflammatory activity of fibrin

To examine the effect of cytoskeletal structure and mechanotransduction on the anti-inflammatory properties of fibrin, we treated human macrophages with cytoskeletal and RhoGTPase inhibitor drugs or DMSO vehicle control. Cytoskeletal inhibitor drugs

included cytochalasin D to inhibit actin polymerization, nocodazole to inhibit microtubule polymerization, blebbistatin to inhibit myosin phosphorylation, and ML9 to inhibit myosin light chain kinase. RhoGTPase inhibitors included Rac1, RhoY16, Cdc42 inhibitors, and Y27632 and RKI 1447 to inhibit Rho/ROCK. Between Y27632 and RKI1447, the latter is more potent. Drug inhibitors for RhoGTPase and Rho/ROCK did not affect TNF-α secretion in primary human macrophages (Figure 20). For THP-1 cells, RhoGTPase inhibitors did not change the anti-inflammatory effect of fibrin, and inhibitors for Rho/ROCK including Y27632 and RKI1447 inhibited TNF-α secretion independently of the fibrin or polystyrene culture condition (Figure 21). Moreover, we did not observe any difference in TNF-α secretion by human macrophages when cells were treated with and without drugs including cytochalasin D and nocodazole, in regardless of 2D and 3D microenvironments (Figure 20 and 21). Interestingly, when human primary macrophages were cultured on fibrin, blebbistatin increased TNF-α secretion, and ML9 inhibited cytokine secretion when compared to control (Figure 20). However, we did not observe the effect of blebbistatin and ML9 on THP-1 cells (Figure 21). Together, the data indicated that cytoskeletal contractility might be involved in the anti-inflammatory property of fibrin.

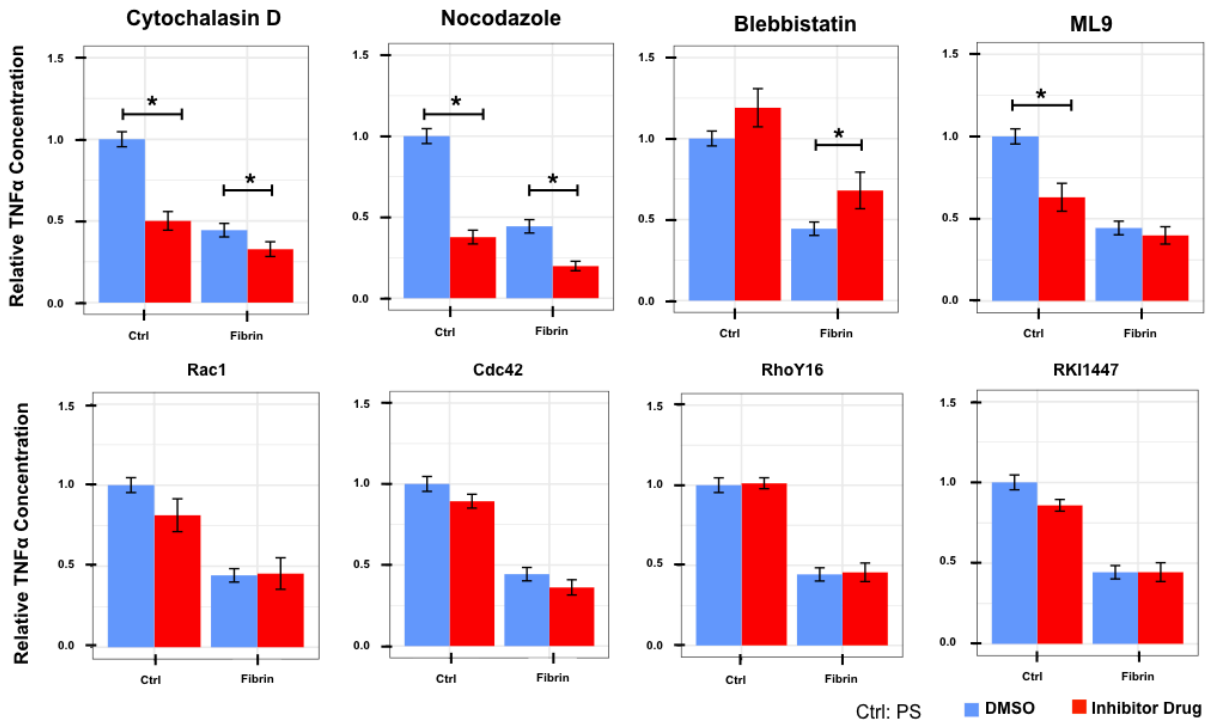

Figure 20. Secretion of TNF-α by human primary macrophages on polystyrene (Ctrl) or fibrin, stimulated with LPS, and treated with inhibitor drugs. Mean ± SEM, * $p < 0.05$, drug treated condition compared to DMSO control, $n \geq 3$.

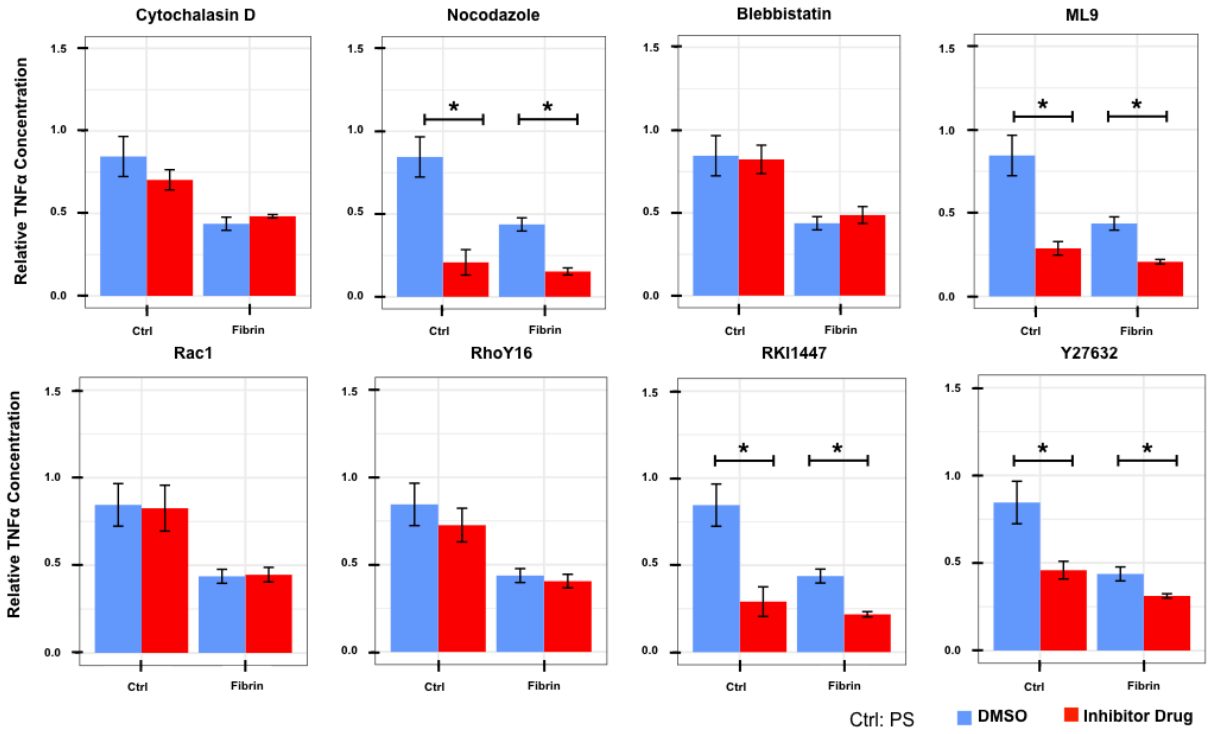

Figure 21. Secretion of TNF-α by THP-1 cells on polystyrene (Ctrl) or fibrin, stimulated with LPS, and treated with inhibitor drugs. Mean ± SEM, * $p < 0.05$, drug treated condition compared to DMSO control, $n \geq 3$.

Fibrin downtregulates NF-κB signaling

In immune cells, signaling downstream of TLRs activated by LPS can be involved in the recruitment of myeloid differentiation primary-response protein 88 (MyD88) and the activation of MAPK and NF-κB pathways. In this study, we analyzed the involvement of MyD88 and the phosphorylation of IKKα/β, ERK1/2 (MAPK) and NF-κB p65 (NF-κB) to understand the signaling downstream of adhesion in regulating macrophage inflammatory response. Human macrophages cultured on PS and fibrin expressed similar amounts of MyD88, regardless of LPS stimulation (Figure 22A). Moreover, the expression of IKKα/β, a precursor to NF-κB phosphorylation, was high when cells were stimulated with LPS, as others have observed [137-140]. IKKα/β expression was inhibited when cells were cultured on fibrin, compared to PS. Moreover, we also observed that both at 1 h and 4 h after cells were stimulated with LPS, the expression of ERK1/2 and NF-κB was highly increased, but the expression almost disappeared when cells were cultured on fibrin (Figure 22). Together, our results suggest that culturing cells in a 3D fibrin microenvironment inhibits the activation of MAPK and NF-κB in macrophages when compared to cells on a 2D PS microenvironment. The protective effect of fibrin was independent of MyD88, the canonical adaptor in innate immune signaling.

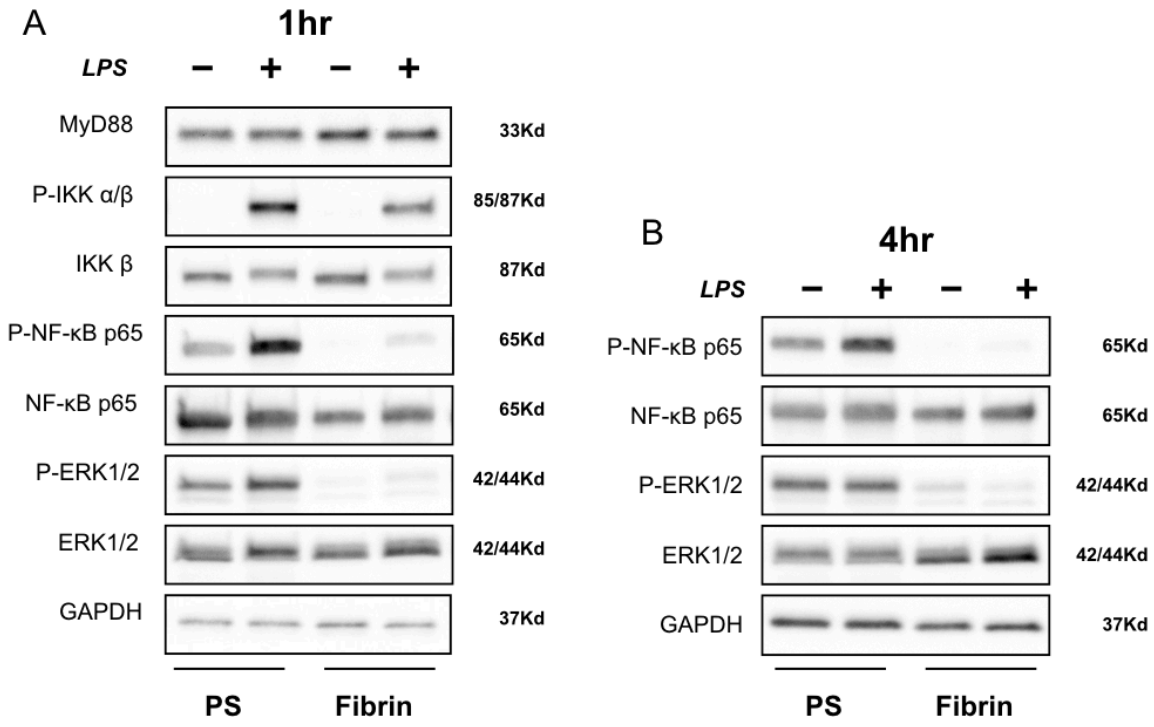

Figure 22. The intracellular signaling pathways of human primary macrophages on fibrin and PS, regulated by LPS. Western blot depicting activation of MyD88, MAPK, and NF-κB at 1 h **(A)** and 4 h **(B)** after stimulation with LPS

Gene expression of human macrophages regulated by fibrin

We examined the expression of inflammatory genes when human primary macrophages were cultured on PS and fibrin, with or without LPS treatment. The genes were grouped to specific functions using the differential expression list provided by nSolver software including cell-cell signaling, inflammatory response, signal transduction, and cell development and proliferation. Examination of genes that were up-regulated and down-regulated when cells were cultured on fibrin (Figure 23), and also stimulated with LPS (Figure 24) in comparison to polystyrene revealed that fibrin highly up-regulated the expression of TLR7, C1QA, and C1QB with or without LPS stimulation and strongly down-

regulated the expression of CFS1 and FLT1 when human macrophages were cultured on fibrin. Confirmation of gene expression RT-qPCR is ongoing. Together, these results demonstrated that compared to polystyrene, fibrin regulates the expression of many different genes that were involved in cell-cell signaling, signal transduction, cell development and proliferation, and inflammatory response.

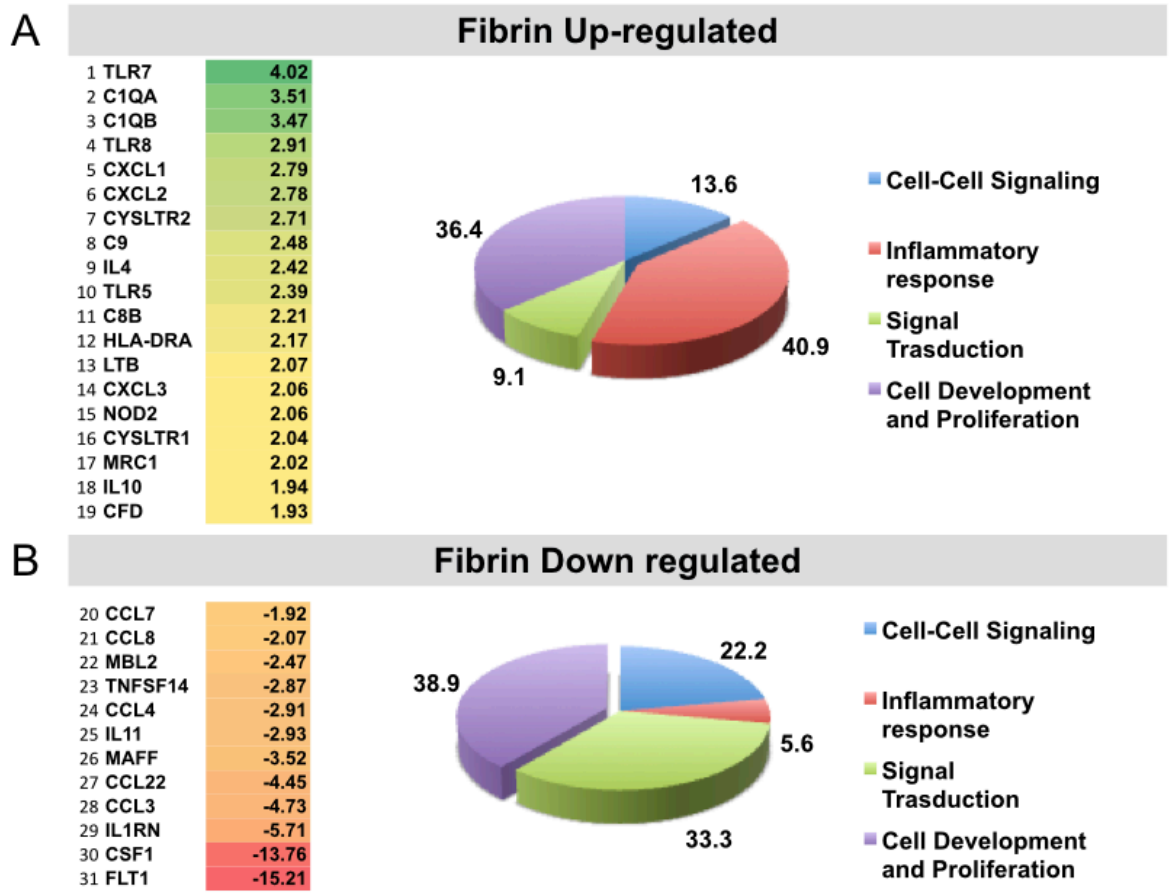

Figure 23. Gene expression of human primary macrophages, quantified by NanoString human inflammation panel and analyzed by nSolver analysis software 4.0. Genes up-regulated **(A)** and genes down-regulated **(B)** by cells on fibrin, compared to PS. Genes were grouped using DE list provided by NanoString.

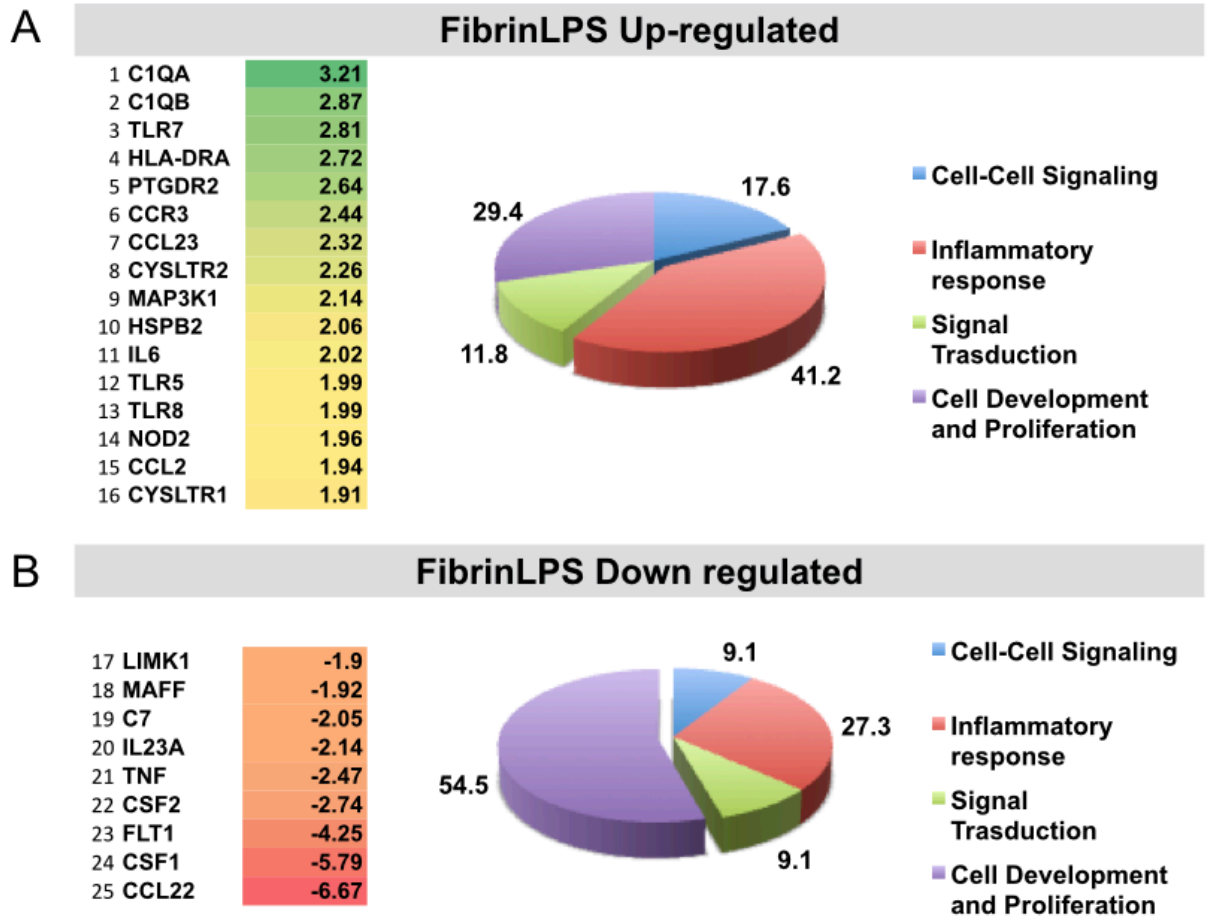

Figure 24. Gene expression of human primary macrophages stimulated with ultrapure LPS, quantified by NanoString human inflammation panel and analyzed by nSolver analysis software 4.0. Genes up-regulated **(A)** and genes down-regulated **(B)** by cells on fibrin, compared to PS. Genes were grouped using DE list provided by NanoString.

4.4 Discussion

Previous studies investigating crosstalk between CD11b and TLR4 demonstrated that CD11b negatively regulated TLR-triggered inflammatory responses of peritoneal macrophages [131] but upregulated inflammatory responses in dendritic cells, and had no influence on BMDMs [132]. The regulation of CD11b on TLR-triggered TNF-α secretion therefore appears to depend on cell types and sources. In this work, we observed that not

only the expression of total CD11b but also TLR4 and TNF-α (Chapter 3) of human macrophages on fibrin were lower than cells on polystyrene, suggesting TLR-triggered inflammatory response might be modulated by the expression of CD11b. To understand the engagement of fibrin matrix to CD11b, future work will examine activated CD11b using an activation-specific CBRM1/5 antibody [131]. Moreover, the actin structure of macrophages on fibrin appeared around the periphery of the cell, while on glass, the actin formed stress fibers and bundles (Figure 18). Additionally, it is conventionally thought that signaling downstream of integrins includes regulation of cytoskeletal structures and small RhoGTPase proteins. We examined the regulation of macrophage function by adhesion environment using cytoskeletal and small RhoGTPase inhibitor drugs. Our results suggest that small RhoGTPase proteins are not involved in regulating human macrophages' inflammatory responses. Consistent with the observations from other groups on macrophages, we also observed that cytochalasin D and nocodazole inhibited LPS-induced TNF-α secretion by macrophages [141,142]. Interestingly, blebbistatin and ML9 regulated TNF-α production in human macrophages cultured on fibrin. The results suggest that cytoskeletal contractility might be involved in the anti-inflammatory properties of fibrin. Moreover, our results suggest that, compared to 2D microenvironments, 3D microenvironments inhibited the activation of the MAPK and NF-κB pathways, independent of MyD88. In addition, the NanoString data demonstrated that 2D and 3D microenvironments regulated the expression of many different genes related to cell-cell signaling, inflammatory response, signal transduction, and cell development and proliferation. We proposed a potential model for the signaling pathway downstream of adhesion in regulating macrophage inflammatory responses in 2D and 3D cultures (Figure

25). Specifically, we demonstrated that human macrophages cultured on polystyrene in a 2D microenvironment expressed higher amounts of TLR4, CD11b, and enhanced actin polymerization, compared to cells in 3D fibrin microenvironments, which inhibited the inflammatory response of human macrophages to LPS. Moreover, the anti-inflammatory effects of fibrin likely involve signaling downstream of adhesion including reduced activation of MAPK and NF-κB.

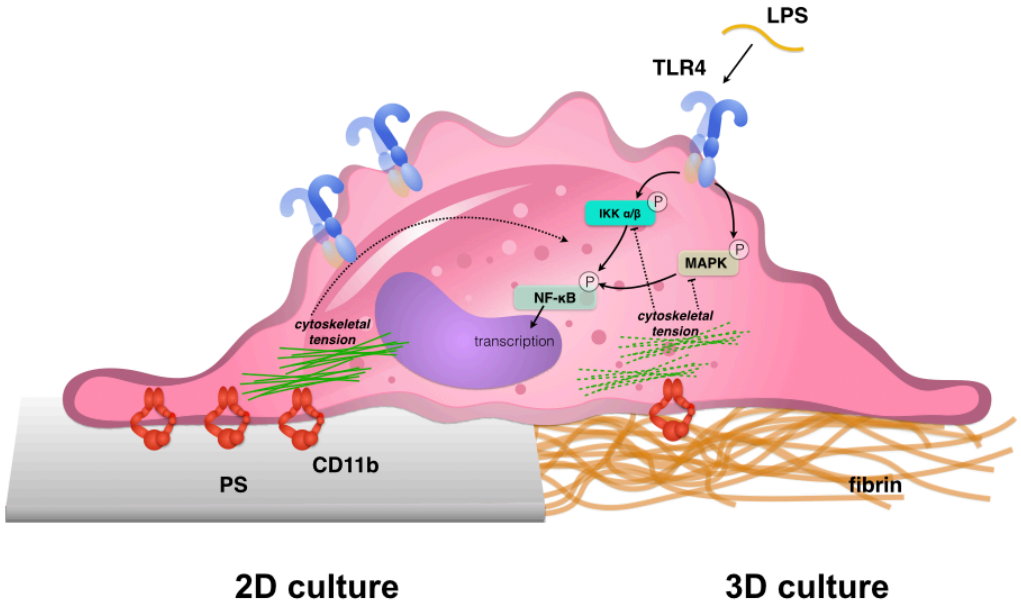

Figure 25. Potential model for the signaling pathway downstream of adhesion in regulating macrophage inflammatory responses, 2D and 3D cultures

Future work is focused on how the phosphorylation of MAPK and NF- κB changes when human macrophages are treated by contractility inhibitor drugs, blebbistatin and ML9. Recent studies have begun to elucidate the role of Yes-associated protein (YAP) and transcriptional coactivator with PDZ-binding motif (TAZ) in mechanotransduction. Most strikingly, changes in cell morphology induced by matrix stiffness regulated YAP/TAZ activation and actin-myosin contractility was required for the regulation of YAP/TAZ [143,144].

Recently, Liu *et al.* found that MAPK signaling regulates mechanical-tension induced YAP activation [145]. Further work will explore the role of YAP/TAZ on the regulation of macrophage functions by the adhesion microenvironment. Ultimately, understanding how the adhesion microenvironment regulates macrophage function may be useful for developing fibril immune-mediated biomaterials in tissue engineering and regenerative medicine.

CHAPTER 5 - Conclusions and Future Directions

Together, the studies described in this work elucidate how the adhesive microenvironment contributes to macrophage morphology and function. Chapter 2 presented the role of topographical cues on macrophage behaviors *in vitro* and *in vivo,* demonstrating that topographical cues can regulate macrophage morphology, which leads to alteration of cell phenotype. Using deep-etched titanium surfaces with a wide range of groove sizes (150 nm to 50 μm), we demonstrate that intermediate groove sizes ranging from 400 nm to 5 μm in width induced the highest degree of elongation, and the macrophages on these surfaces expressed the highest level of phenotypic markers associated with a pro-healing M2 phenotype. The study highlights the potential utility of groove-patterned materials to promote wound healing process by controlling macrophage behavior. The advantage of the grooved titanium materials was that we were able to efficiently investigate the effect of many topographical features on macrophage behaviors because we can fabricate many different groove sizes on single piece of titanium. However, it is difficult and costly to fabricate grooved titanium materials, so we continued to examine the potential functions of groove-patterned materials using shrink-film multi-scale wrinkled materials, which were cheap to make and easy to use in implants. We demonstrated that wrinkled materials regulate macrophage form and function. Wrinkled materials induced macrophage elongation aligned along 1D wrinkles and led to alterations in cell function. Macrophages that elongated on the wrinkled materials displayed increased expression of anti-inflammatory biomarkers and reduced expression of inflammatory biomarkers both *in vitro* and *in vivo*. Together, the studies highlight the potential use of material topography to regulate macrophage activities in response to biomaterial implants.

However, without a clear understanding of the signaling pathway downstream of macrophage regulation by topographical cues, it is difficult to translate these findings into clinical applications.

Epigenetic regulation of macrophage morphology and function

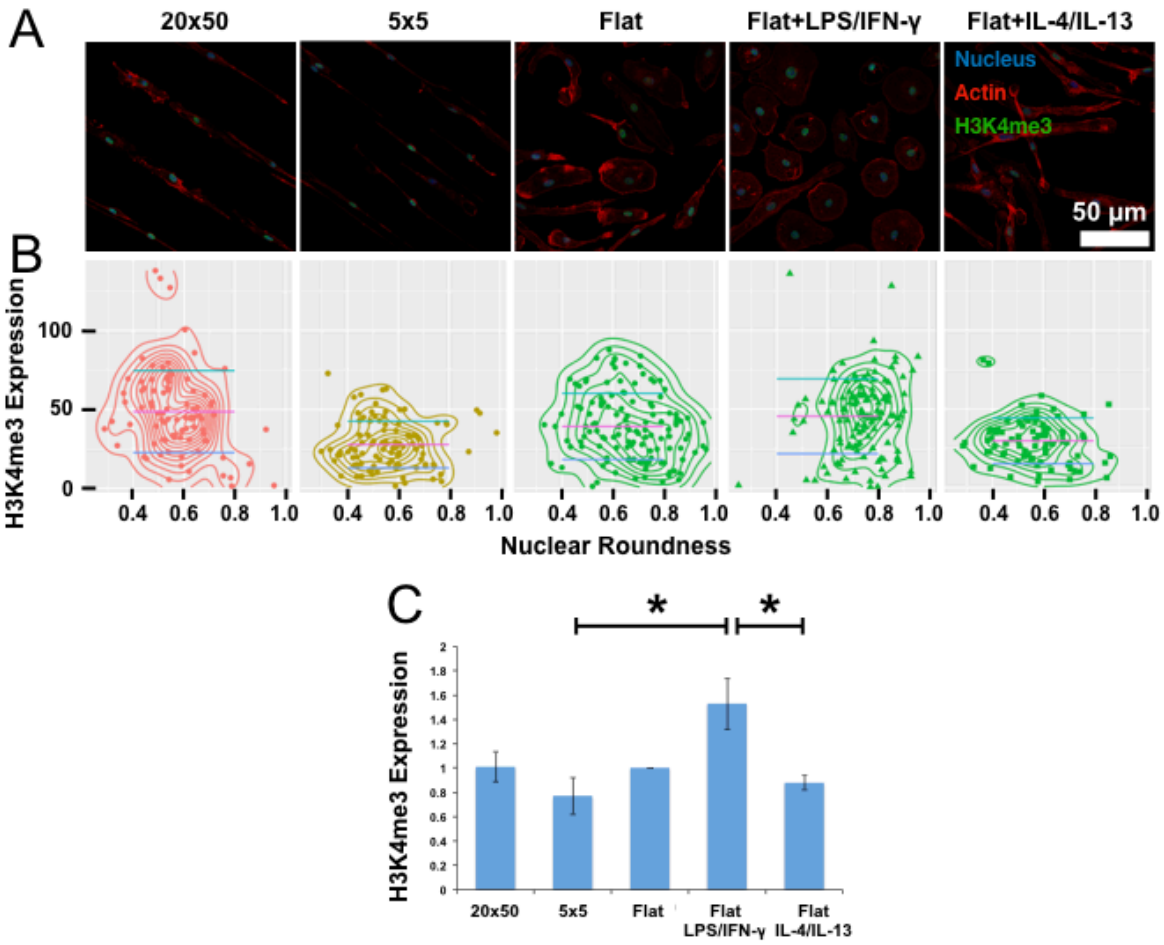

Figure 26. Histone tri-methylation lysine 4 (H3K4me3) expression. (A) Representative immunofluorescent images of BMDM on different substrates. **(B)** H3K4me3 expression versus nuclear roundness on different substrates. **(C)** Quantification of H3K4me3 expression. Mean ± SEM, * $p < 0.05$, *n = 3*

Recent work has highlighted the modulation of macrophage function and polarization by epigenetic state [146,147]. Our preliminary data on the effect of soluble cues on modulating macrophage epigenetic state suggested that histone tri-methylation lysine 4 (H3K4me3) expression was regulated by adhesion geometry and macrophage phenotypes (Figure 26). Particularly, the H3K4me3 expression of cells cultured on 5 μm line substrates was comparable to expression in macrophages on flat substrates stimulated with IL-4 and IL-13, and significantly less than in cells on flat substrates stimulated with LPS and IFN-γ. Interestingly, the underlying mechanism of regulation by adhesive cells' physical cues that were induced by surface topographies and 2D versus 3D microenvironments relied on the cells' epigenetic state [148]. Specifically, Downing T.L. *et al.* demonstrated that nuclei of murine fibroblasts cultured on 10 μm grooved surfaces adopted an elongated shape and expressed significantly levels of higher histone modifications including histone acetylation (AcH3), histone di-methylation lysine 4 (H3K4me2), and H3K4m3 than cells on flat surfaces [149]. The study also suggested that changes in cell shape could lead to the modulation of the epigenetic state. Our preliminary understanding of epigenetic modification in macrophages and its regulation by topographical cues describes an underlying intracellular signaling pathway responsive to mechanobiological differences. To examine the effect of histone modification on macrophage function induced by adhesion geometry, we cultured BMDMs on flat or 5 μm line substrates and treated cells with histone modification inhibitors iBet 762 and sodium butyrate prior to LPS stimulation. Without inhibitor treatment, macrophages cultured on 5 μm line substrates and stimulated with LPS and IFN-γ expressed significantly lower levels of inflammatory biomarkers iNOS and MCP-1 than cells cultured on flat substrates (Figure 27A). Relative to cells on flat

substrates, the macrophages on 5 μm line substrates treated with iBet 762, which down-regulates histone acetylation, suppressed the expression of inflammatory biomarkers, while cells treated with sodium butyrate, which up-regulated histone acetylation, enhanced the expression of inflammatory biomarkers iNOS and MCP-1 (Figure 27B). Together, the data suggest that histone acetylation potentially regulates immunomodulation by adhesion geometry. To further elucidate the underlying molecular mechanism of physical regulation of macrophage activation, future work is focused on the role of the epigenetic state in this molecular mechanism.

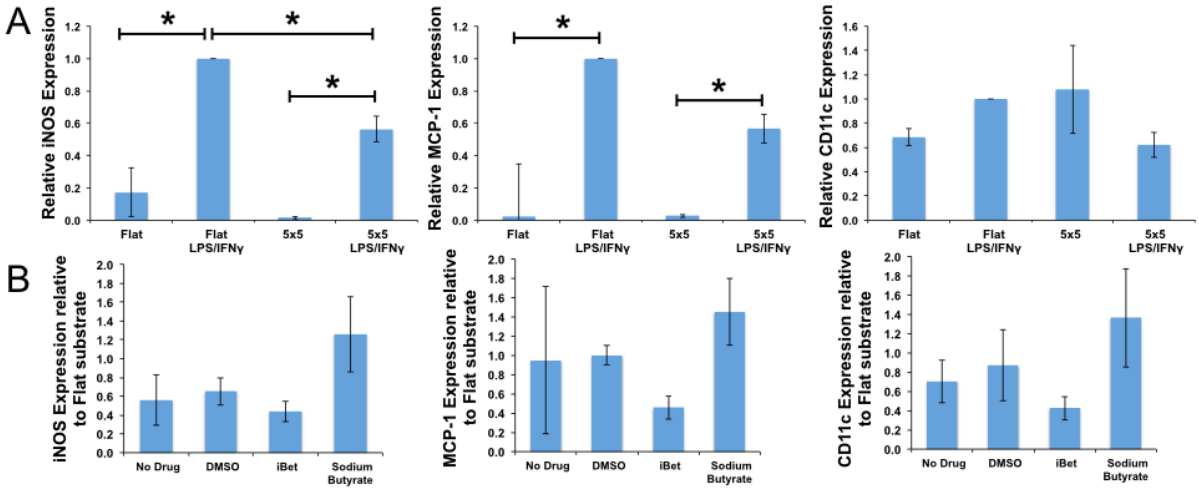

Figure 27. The inflammatory response of BMDM to different substrates. After 2 hours of LPS/IFN-γ stimulation, cell lysates were collected and used for qPCR to examine gene expression of inflammatory markers. (A) Quantification of inflammatory markers (iNOS, MCP-1, CD11c) expression. Mean ± SEM, * $p < 0.05$, $n \geq 3$. (B) Expression of inflammatory markers by BMDM on 5 μm line substrates (5x5) relative to flat substrates (Flat), corresponding to histone modification inhibitors iBet 762 and sodium butyrate. Mean ± SD, $n = 1$.

The studies described in Chapter 3 demonstrated that polarization by soluble factors on 2D surfaces is independent of ECM ligands, and 3D ECM hydrogels exert protective effects on macrophages against LPS. The studies in Chapter 4 further described signaling pathways downstream of adhesion in regulating macrophage inflammatory responses in 2D and 3D microenvironments. Interestingly, the data suggested that cytoskeletal contractility might be responsible for the anti-inflammatory properties of 3D fibrin hydrogels. Therefore, to further understand the underlying molecular mechanism, it is important to investigate how cytoskeletal contractility regulates fibrin's inhibitory effect on human macrophages. Blebbistatin and ML9 can be used to treat macrophages seeded in 2D and 3D cultures, and the activity of CD11b, TLR-4, MAPK and the NF-κB pathway will be examined as described in Chapter 4.

Non-ligand effects contributing to the anti-inflammatory property of hydrogels

The stiffness of surrounding tissues helps define a cell's mechanical environment. Human tissues have a large range of stiffness, from blood to collagenous bone. Engler *et al*. showed in a landmark study that matrix elasticity induced cell function [54]. Moreover, Chapter 1.3.3 showed recent evidence of the significance of stiffness in regulating macrophage morphology and function. Thus factors beside the identity of the ECM protein, such as stiffness, could contribute to the anti-inflammatory properties of ECM hydrogels. Elaborating the function of stiffness in protecting macrophages from an inflammatory response to LPS could complete the underlying mechanism.

In addition, investigating how engineered fibrillar hydrogels with more physiological architectures and fibril stiffness affect macrophage activation could

contribute to determining new material structures to encourage macrophages' wound healing polarization during tissue injury. We have developed a matrix with physiological architecture and fibril stiffness in order to study its effect on macrophage morphology and activation. We generated micro-patterned substrates as previously described [2]. Polydimethylsiloxane (PDMS; Dow Corning) stamps were replica-molded from grooved titanium with 5x5 μm microgrooves, or from petri dishes to make flat stamps. The sterile stamps were coated with 20 μg/mL fibronectin protein at room temperature (RT) for 1 h. Fibronectin proteins were transferred from the stamps to glass substrates previously treated with UV ozone (Jelight) for 8 min. NIH 3T3 fibroblasts were seeded on the FN micro-printed substrates. After 2 h, substrates were washed thoroughly with DMEM to remove non-adherent cells, and then cultured for 7 days in fresh DMEM supplemented with 10% FBS and 1% penicillin/streptomycin. Murine BMDMs differentiated for 7 days were stained with cell tracker green CMFDA as previously described [62] and then added to the fibroblast cultures. Our preliminary results demonstrated BMDM, green cells, elongated along aligned fibroblast cell culture, but randomly spreading on unaligned cell culture (Figure 28). Although replication is necessary and better methods are required to grow aligned fibroblasts on 5 μm line fibronectin patterned substrates, the preliminary data suggest the potential of using this fibroblast culture approach to develop physiological 3D biomaterials.

To examine if topographical materials can be used to generate aligned cell cultures, we used 5 μm grooved PDMS pre-coated with fibronectin as a fibroblast substrate to create a cell-derived matrix. Fibroblasts were seeded at a low density, 5,000 cells/cm^2, or a higher density, 10,000 cells/cm^2, on the FN coated grooved substrates and then phase contrast

images were taken at day 3 and day 6 of culture to examine cell shape. The results showed that although at day 3 of culture, fibroblasts were not well aligned on the grooved substrates, at day 6 of culture well-aligned sheets of fibroblasts were generated, both from low and high density seeding conditions (Figure 28). This result suggests that growing fibroblasts on grooved PDMS materials can generate aligned cell-derived materials. This work follows in a tradition of using fibroblasts to assemble fibronectin matrices, which may be decellularized for later work [150]. In one work, fibroblast cell culture was decellularized to obtain fibronectin ECM and the effect of the matrix, cell-mediated fibronectin fibril matrix, on cell morphology was examined [151,152]. Using decellularized fibroblast fibril matrix, Harris G.M. *et al.* demonstrated that the micropatterned physiological ECM architecture governed neural cells outgrown along the aligned patterned ECM [152]. Investigating the regulation of macrophage morphology and activation by the cell-derived matrix will offer the promise of being able to develop engineered fibril hydrogels with more physiological architecture and fibril stiffness.

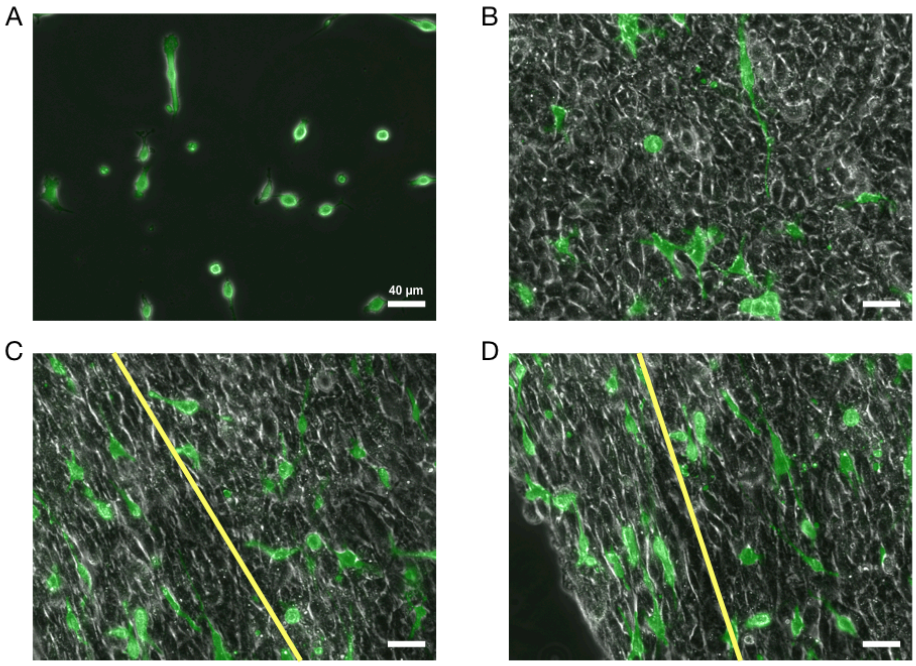

Figure 28. **Representative images of murine bone marrow derived macrophages (stained with cell tracker green CMFDA dye)** seeded on flat glass substrates **(A)**, sheet of NIH 3T3 fibroblasts (phase contrast images) cultured on flat FN stamped glass substrates **(B)**, sheet of NIH 3T3 fibroblasts (phase contrast images) cultured on 5 μm line fibronectin stamped glass substrates **(C)(D)**, aligned fibroblasts on the left of the yellow line and unaligned cells on the right

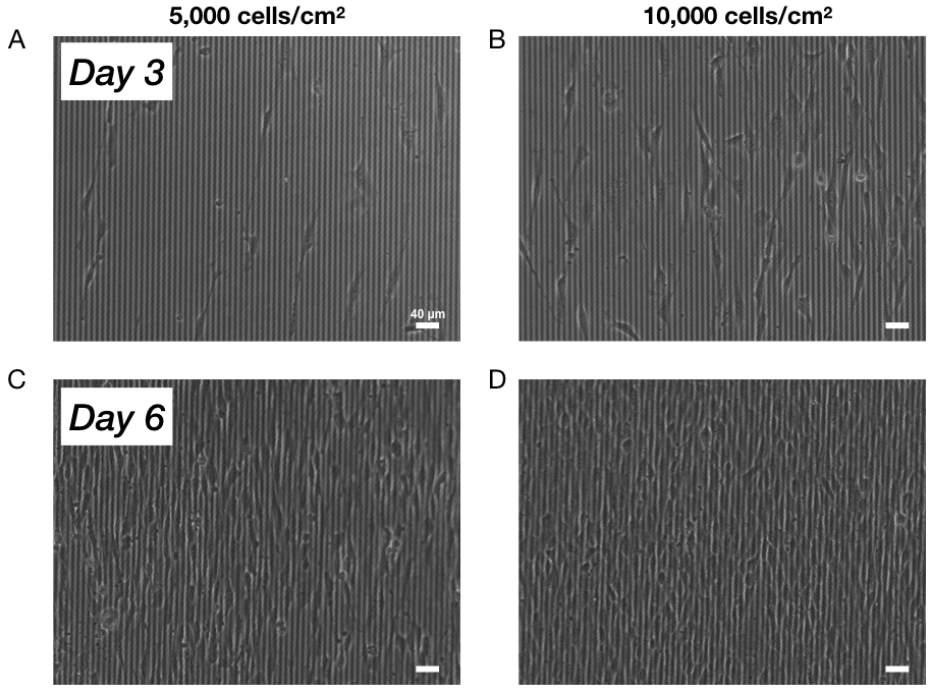

Figure 29. Representative phase contrast images of NIH 3T3 fibroblasts cultured on FN coated 5x5 μm grooved PDMS substrates. 5,000 cells/cm^2 cells **(A)(C)**, or 10,000 cells/cm^2 cells **(B)(D)** were seeded on the PDMS substrates. Samples were imaged after 3 days of culture **(A)(B)**, and after 6 days of culture **(B)(D)**

In conclusion, this work elucidates the regulation of macrophage morphology and activation by the adhesive microenvironment. We characterized the effects of micro- and nano-scale topographies on macrophages *in vitro* and *in vivo*. We also demonstrated the regulation of macrophage function by ECM in 2D and 3D microenvironments. Finally, the work identifies signaling pathways downstream of adhesive microenvironment, which

modulate the macrophage inflammatory response. With further study, deeper understanding of these mechanisms should lead to the ability to develop biomaterials capable of controlling macrophage polarization in order to improve the wound healing process after material implantation.

REFERENCES

1 Hughes, D. F. a. J. Macrophages and dendritic cells: what is the difference? *Kidney International* **74**, 5-7, doi:10.1038/ki/2008.189 (2008).

2 McWhorter, F. Y., Wang, T., Nguyen, P., Chung, T. & Liu, W. F. Modulation of macrophage phenotype by cell shape. *Proc Natl Acad Sci U S A* **110**, 17253-17258, doi:10.1073/pnas.1308887110 (2013).

3 Wynn, T. A., Chawla, A. & Pollard, J. W. Macrophage biology in development, homeostasis and disease. *Nature* **496**, 445-455, doi:10.1038/nature12034 (2013).

4 Vanessa Byles, A. J. C., Issam Ben-Sahra, Dudley W. Lamming, David M. Sabatini, Brendan D. Manning, and Tiffany Horng. The TSC-mTOR pathway regulates macrophage polarization. *Nature communications* **4**, 2834-2845, doi:10.1038/ncomms3834 (2013).

5 Anderson, J. M., Rodriguez, A. & Chang, D. T. Foreign body reaction to biomaterials. *Semin Immunol* **20**, 86-100, doi:10.1016/j.smim.2007.11.004 (2007).

6 James D. Bryers, C. M. G., Buddy D. Ratner. Engineering Biomaterials to Integrate and Heal: The Biocompatibility Paradigm Shifts. *Biotechnology and Bioengineering* **109**, 1898-1911, doi:10.1002/bit.24559 (2012).

7 Tang L, J. T., Eaton JW. Mass cells mediate acute imflammatory responses to implanted biomaterials. *PNAS* **95**, 8841-8846 (1998).

8 Broughton II G, J. J., Attinger CE. The basic science of wound healing. *Plast Reconstr Surg* **117**, 12S-34S (2006).

9 Xue, M. & Jackson, C. J. Extracellular Matrix Reorganization During Wound Healing and Its Impact on Abnormal Scarring. *Adv Wound Care (New Rochelle)* **4**, 119-136, doi:10.1089/wound.2013.0485 (2015).

10 O'Toole, E. A. Extracellular matrix and keratinocyte migration. *Clin. Exp. Dermatol.* **26**, 525-530, doi:10.1046/j.1365-2230.2001.00891.x (2001).

11 Clark, R. A. F. *et al.* Blood Vessel Fibronectin Increases in Conjunction with Endothelial Cell Proliferation and Capillary Ingrowth During Wound Healing. *Journal of Investigative Dermatology* **79**, 269-276, doi:10.1111/1523-1747.ep12500076 (1982).

12 Jennewein, C. *et al.* Novel aspects of fibrin(ogen) fragments during inflammation. *Mol Med* **17**, 568-573, doi:10.2119/molmed.2010.00146 (2011).

13 Chow, S. & Di Girolamo, N. Vitronectin: a migration and wound healing factor for human corneal epithelial cells. *Invest Ophthalmol Vis Sci* **55**, 6590-6600, doi:10.1167/iovs.14-15054 (2014).

14 Barker, T. H. & Engler, A. J. The provisional matrix: setting the stage for tissue repair outcomes. *Matrix Biol* **60-61**, 1-4, doi:10.1016/j.matbio.2017.04.003 (2017).

15 Hinz, B. The extracellular matrix and transforming growth factor-beta1: Tale of a strained relationship. *Matrix Biol* **47**, 54-65, doi:10.1016/j.matbio.2015.05.006 (2015).

16 Brancato, S. K. & Albina, J. E. Wound macrophages as key regulators of repair: origin, phenotype, and function. *Am J Pathol* **178**, 19-25, doi:10.1016/j.ajpath.2010.08.003 (2011).

17 Paszek, M. J. *et al.* Tensional homeostasis and the malignant phenotype. *Cancer Cell* **8**, 241-254, doi:10.1016/j.ccr.2005.08.010 (2005).
18 Mouw, J. K. *et al.* Tissue mechanics modulate microRNA-dependent PTEN expression to regulate malignant progression. *Nat Med* **20**, 360-367, doi:10.1038/nm.3497 (2014).
19 Leight, J. L., Wozniak, M. A., Chen, S., Lynch, M. L. & Chen, C. S. Matrix rigidity regulates a switch between TGF-β1-induced apoptosis and epithelial-mesenchymal transition. *Mol. Biol. Cell* **23**, 781-791, doi:10.1091/mbc.E11-06-0537 (2012).
20 Yang, L. & Zhang, Y. Tumor-associated macrophages: from basic research to clinical application. *J Hematol Oncol* **10**, 58, doi:10.1186/s13045-017-0430-2 (2017).
21 Katsuda, S. *et al.* Collagens in human atherosclerosis. Immunohistochemical analysis using collagen type-specific antibodies. *Arterioscler Thromb* **12**, 494-502, doi:10.1161/01.ATV.12.4.494 (1992).
22 Megens, R. T. A. *et al.* Imaging Collagen in Intact Viable Healthy and Atherosclerotic Arteries Using Fluorescently Labeled CNA35 and Two-Photon Laser Scanning Microscopy. *Mol. Imaging* **6**, 247-260, doi:10.2310/7290.2007.00021 (2007).
23 Wesley II, R. B., Meng, X., Godin, D. & Galis, Z. S. Extracellular matrix modulates macrophage functions characteristic to atheroma: collagen type I enhances acquisition of resident macrophage traits by human peripheral blood monocytes in vitro. *Arterioscler Thromb Vasc Biol.* **18**, 432-440 (1998).
24 Hansson, G. K. & Libby, P. The immune response in atherosclerosis: a double-edged sword. *Nature reviews. Immunology* **6**, 508-519, doi:10.1038/nri1882 (2006).
25 Greaves, D. R. & Gordon, S. Recent insights into the biology of macrophage scavenger receptors. *Journal of Lipid Research* **46**, 11-20 (2005).
26 Jonasson, L., Holm, J., Skalli, O., Bondjers, G. & Hansson, G. K. Regional accumulations of T cells, macrophages, and smooth muscle cells in the human atherosclerotic plaque. *Arteriosclerosis, Thrombosis, and Vascular Biology* **6**, 131-138, doi:10.1161/01.ATV.6.2.131 (1986).
27 HoJun Jeon, C. G. S., Jr, GeunHyung Kim. A mini-review: Cell response to microscale, nanoscale, and hierarchical patterning of surface structure. *Journal of Biomedical Material Research* **Part B**, 000-000, doi:10.1002/jbm.b.33158 (2014).
28 Sridharan, R., Cameron, A. R., Kelly, D. J., Kearney, C. J. & O'Brien, F. J. Biomaterial based modulation of macrophage polarization: a review and suggested design principles. *Materials Today* **18**, 313-325, doi:10.1016/j.mattod.2015.01.019 (2015).
29 Kim DH, K. P., Song I, Cha JM, Lee SH, Kim B, Suh KY. Guided three-dimensional growth of functional cardiomyocytes on polyethylene glycol nanostructures. *Langmuir* **22**, 5419-5426 (2006).
30 Choi CH, H. S., Wu BM, Dunn JCY, Beygui RE, Kim CJ. Cell interaction with three-dimensional sharp-tip nanotopography. *Biomaterials* **28**, 1672-1679 (2007).
31 Sharma, V. P. *et al.* Reconstitution of in vivo macrophage-tumor cell pairing and streaming motility on one-dimensional micro-patterned substrates. *Intravital* **1**, 77-85, doi:10.4161/intv.22054 (2012).
32 Van Goethem, E. *et al.* Macrophage podosomes go 3D. *Eur J Cell Biol* **90**, 224-236, doi:10.1016/j.ejcb.2010.07.011 (2011).

33 Isaac A. Janson, A. J. P. Extracellular matrix elasticity and topography: Material-based cues that affect cell function via conserved mechanisms. *Journal of Biomedical Material Research* **Part A**, 000-000, doi:10.1002/jbm.a.35254 (2014).
34 Dalby MJ, G. N., Tare R, Andar A, Riehle MO, Herzyk P, Wilkinson CDW, Oreffo ROC. The control of human mesenchymal stem cell differentiation using nanoscale symmetry and disorder. *Nature Materials* **6**, 1672-1679 (2007).
35 Bota, P. C. *et al.* Biomaterial topography alters healing in vivo and monocyte/macrophage activation in vitro. *J Biomed Mater Res A* **95**, 649-657, doi:10.1002/jbm.a.32893 (2010).
36 Kulangara, K. *et al.* The effect of substrate topography on direct reprogramming of fibroblasts to induced neurons. *Biomaterials* **35**, 5327-5336, doi:10.1016/j.biomaterials.2014.03.034 (2014).
37 Yim E, R. R., Pang S, Yee A, Chen C, Leong K. Nanopattern-induced changes in morphology and motility of smooth muscle cells. *Biomaterials* **26**, 5405-5413 (2005).
38 Cha HD, H. J., Kang T-Y, Jung JW, Ha D-H, Cho D-W. Effects of micro-patterns in three-dimensional scaffold for tissue engineering applications. *Journal of Micromechanical Microenginneering* **22**, doi:10.1088/0960-1317/22/12/125002 (2012).
39 Vogt AK, B. G., Offenhausser A. Connectivity patterns in neuronal networks of experimentally defined geometry. *Tissue Eng Part A* **11** (2005).
40 Bartneck, M. *et al.* Induction of specific macrophage subtypes by defined micro-patterned structures. *Acta Biomater* **6**, 3864-3872, doi:10.1016/j.actbio.2010.04.025 (2010).
41 Chen, S. *et al.* Characterization of topographical effects on macrophage behavior in a foreign body response model. *Biomaterials* **31**, 3479-3491, doi:10.1016/j.biomaterials.2010.01.074 (2010).
42 Lund, A. W., Yener, B., Stegermann, J. P. & Plopper, G. E. The natural and engineering 3D microenvironment as a regulatory cue during stem cell fate determination. *Tissue Eng Part B* **15**, 371-380 (2009).
43 Edmondson, R., Broglie, J. J., Adcock, A. F. & Yang, L. Three-dimensional cell culture systems and their applications in drug discovery and cell-based biosensors. *Assay Drug Dev Technol* **12**, 207-218, doi:10.1089/adt.2014.573 (2014).
44 Cuklerman, E., Pankov, R., Stevens, D. R. & Yamanda, K. M. Taking cell-matrix adhesions to the third dimension. *Science* **294**, 1708-1712 (2001).
45 Li, Y. *et al.* Tissue-engineered 3-dimensional (3D) microenvironment enhances the direct reprogramming of fibroblasts into cardiomyocytes by microRNAs. *Sci Rep* **6**, 38815, doi:10.1038/srep38815 (2016).
46 Otani, T., Marchetto, M. C., Gage, F. H., Simons, B. D. & Livesey, F. J. 2D and 3D Stem Cell Models of Primate Cortical Development Identify Species-Specific Differences in Progenitor Behavior Contributing to Brain Size. *Cell Stem Cell* **18**, 467-480, doi:10.1016/j.stem.2016.03.003 (2016).
47 Linde, N., Gutschalk, C. M., Hoffmann, C., Yilmaz, D. & Mueller, M. M. Integrating macrophages into organotypic co-cultures: a 3D in vitro model to study tumor-associated macrophages. *PLoS One* **7**, e40058, doi:10.1371/journal.pone.0040058 (2012).

48 Van Goethem, E., Poincloux, R., Gauffre, F., Maridonneau-Parini, I. & Le Cabec, V. Matrix architecture dictates three-dimensional migration modes of human macrophages: differential involvement of proteases and podosome-like structures. *J Immunol* **184**, 1049-1061, doi:10.4049/jimmunol.0902223 (2010).
49 Cougoule, C. *et al.* Blood leukocytes and macrophages of various phenotypes have distinct abilities to form podosomes and to migrate in 3D environments. *Eur J Cell Biol* **91**, 938-949, doi:10.1016/j.ejcb.2012.07.002 (2012).
50 Jacob, S. S. & Sudhararan, P. R. Monocyte-macrophage differentiation in three dimentional collagen lattice. *Biochimica et Biophysica Acta* **1540**, 50-58 (2001).
51 Discher, D. E., Janmey, P. & Wang, Y. Tissue cells feel and respond to the stiffness of their substrate. *Science* **310**, 1139-1143 (2005).
52 Pelham, R. J. & Wang, Y. Cell locomotion and focal adhesions are regulated by substrate flexibility. *Proc Natl Acad Sci U S A* **94**, 13661-13665 (1997).
53 Yeung, T. *et al.* Effects of substrate stiffness on cell morphology, cytoskeletal structure, and adhesion. *Cell Motil Cytoskeleton* **60**, 24-34, doi:10.1002/cm.20041 (2005).
54 Engler, A. J., Sen, S., Sweeney, H. L. & Discher, D. E. Matrix elasticity directs stem cell lineage specification. *Cell* **126**, 677-689, doi:10.1016/j.cell.2006.06.044 (2006).
55 Irwin, E. F. *et al.* Modulus-dependent macrophage adhesion and behavior. *J Biomater Sci Polym Ed* **19**, 1363-1382, doi:10.1163/156856208786052407 (2008).
56 Blakney, A. K., Swartzlander, M. D. & Bryant, S. J. The effects of substrate stiffness on the in vitro activation of macrophages and in vivo host response to poly(ethylene glycol)-based hydrogels. *J Biomed Mater Res A* **100**, 1375-1386, doi:10.1002/jbm.a.34104 (2012).
57 Previtera, M. L. & Sengupta, A. Substrate Stiffness Regulates Proinflammatory Mediator Production through TLR4 Activity in Macrophages. *PLoS One* **10**, e0145813, doi:10.1371/journal.pone.0145813 (2015).
58 Adlerz, K. M., Aranda-Espinoza, H. & Hayenga, H. N. Substrate elasticity regulates the behavior of human monocyte-derived macrophages. *Eur Biophys J.* **45**, doi:10.1007/s00249-015-1096-8 (2016).
59 Mantovani, A. S. a. A. Macrophage plasticity and polarization: in vivo veritas. *The Journal of Clinical Investigation* **122**, 787-795, doi:10.1172/JCI59643 (2012).
60 Beata Wojciak-Stothard, A. C., William Monaghan, Karen Macdonald, and Chris Wilkinson. Guidance and Activation of Murine Macrophages by Nanometric Scale Topography. *Experimental Cell Research* **223**, 426-435 (1996).
61 Aaron F. Cipriano, N. D. H., Shannon C. Gott, Christopher Miller, Masaru P. Rao, and Huinan Liu. Bone Marrow Stromal Cell Adhesion and Morphology on Micro- and Sub-Micropatterned Titanium. *Journal of Biomedical Nanotechnology* **9**, 1-9, doi:10.1166/jbn.2013.1760 (2013).
62 Luu, T. U., Gott, S. C., Woo, B. W. K., Rao, M. P. & Liu, W. F. Micro- and Nanopatterned Topographical Cues for Regulating Macrophage Cell Shape and Phenotype. *ACS Appl. Mater. Interfaces*, doi:10.1021/acsami.5b10589 (2015).
63 Hubbell, J. A. & Langer, R. Translating materials design to the clinic. *Nat Mater* **12**, 963-966, doi:10.1038/nmat3788 (2013).
64 Martinez, F. O. & Gordon, S. The M1 and M2 paradigm of macrophage activation: time for reassessment. *F1000Prime Rep* **6**, 13, doi:10.12703/P6-13 (2014).

65 Ma, Q. L. *et al.* Improved implant osseointegration of a nanostructured titanium surface via mediation of macrophage polarization. *Biomaterials* **35**, 9853-9867, doi:10.1016/j.biomaterials.2014.08.025 (2014).
66 Veiseh, O. *et al.* Size- and shape-dependent foreign body immune response to materials implanted in rodents and non-human primates. *Nat Mater* **14**, 643-651, doi:10.1038/nmat4290 (2015).
67 Tan, K. S., Qian, L., Rosado, R., Flood, P. M. & Cooper, L. F. The role of titanium surface topography on J774A.1 macrophage inflammatory cytokines and nitric oxide production. *Biomaterials* **27**, 5170-5177, doi:10.1016/j.biomaterials.2006.05.002 (2006).
68 Refai, A. K., Textor, M., Brunette, D. M. & Waterfield, J. D. Effect of titanium surface topography on macrophage activation and secretion of proinflammatory cytokines and chemokines. *J Biomed Mater Res A* **70**, 194-205, doi:10.1002/jbm.a.30075 (2004).
69 Moura, C. C. G., Zanetta-Barbosa, D., Dechichi, P., Carvalho, V. F. & Soares, P. B. F. Effects of Titanium Surfaces on the Developmental Profile of Monocytes/Macrophages. *Brazilian Dental Journal* **25**, 96-103, doi:10.1590/0103-6440201302260 (2014).
70 Cao, H., McHugh, K., Chew, S. Y. & Anderson, J. M. The topographical effect of electrospun nanofibrous scaffolds on the in vivo and in vitro foreign body reaction. *J Biomed Mater Res A* **93**, 1151-1159, doi:10.1002/jbm.a.32609 (2010).
71 Saino, E. *et al.* Effect of electrospun fiber diameter and alignment on macrophage activation and secretion of proinflammatory cytokines and chemokines. *Biomacromolecules* **12**, 1900-1911, doi:10.1021/bm200248h (2011).
72 Garg, K., Pullen, N. A., Oskeritzian, C. A., Ryan, J. J. & Bowlin, G. L. Macrophage functional polarization (M1/M2) in response to varying fiber and pore dimensions of electrospun scaffolds. *Biomaterials* **34**, 4439-4451, doi:10.1016/j.biomaterials.2013.02.065 (2013).
73 Alford, P. W., Nesmith, A. P., Seywerd, J. N., Grosberg, A. & Parker, K. K. Vascular smooth muscle contractility depends on cell shape. *Integr Biol (Camb)* **3**, 1063-1070, doi:10.1039/c1ib00061f (2011).
74 Ryall, K. A., Bezzerides, V. J., Rosenzweig, A. & Saucerman, J. J. Phenotypic screen quantifying differential regulation of cardiac myocyte hypertrophy identifies CITED4 regulation of myocyte elongation. *J Mol Cell Cardiol* **72**, 74-84, doi:10.1016/j.yjmcc.2014.02.013 (2014).
75 Ye, G. J. *et al.* The contractile strength of vascular smooth muscle myocytes is shape dependent. *Integr Biol (Camb)* **6**, 152-163, doi:10.1039/c3ib40230d (2014).
76 Waldo, S. W. *et al.* Heterogeneity of human macrophages in culture and in atherosclerotic plaques. *Am J Pathol* **172**, 1112-1126, doi:10.2353/ajpath.2008.070513 (2008).
77 Chinetti-Gbaguidi, G. *et al.* Human atherosclerotic plaque alternative macrophages display low cholesterol handling but high phagocytosis because of distinct activities of the PPARgamma and LXRalpha pathways. *Circ Res* **108**, 985-995, doi:10.1161/CIRCRESAHA.110.233775 (2011).
78 Dalby, M. J., Riehle, M. O., Yarwood, S. J., Wilkinson, C. D. W. & Curtis, A. S. G. Nucleus alignment and cell signaling in fibroblasts: response to a micro-grooved topography.

Experimental Cell Research **284**, 272-280, doi:10.1016/s0014-4827(02)00053-8 (2003).
79 Teixeira, A. I., Abrams, G. A., Bertics, P. J., Murphy, C. J. & Nealey, P. F. Epithelial contact guidance on well-defined micro- and nanostructured substrates. *J Cell Sci* **116**, 1881-1892, doi:10.1242/jcs.00383 (2003).
80 Yim, E. K., Pang, S. W. & Leong, K. W. Synthetic nanostructures inducing differentiation of human mesenchymal stem cells into neuronal lineage. *Exp Cell Res* **313**, 1820-1829, doi:10.1016/j.yexcr.2007.02.031 (2007).
81 George Kirmizidis, M. R., and Mark A. Birch. Microfabricated Grooved Substrates Influence Cell-Cell Communication and Osteoblast Differentiation In Vitro *Tissue Eng Part A* **15**, 1427-1436, doi:10.1089/ten.tea.2008.0137 (2009).
82 Yim, E. K., Darling, E. M., Kulangara, K., Guilak, F. & Leong, K. W. Nanotopography-induced changes in focal adhesions, cytoskeletal organization, and mechanical properties of human mesenchymal stem cells. *Biomaterials* **31**, 1299-1306, doi:10.1016/j.biomaterials.2009.10.037 (2010).
83 Lee, J., Abdeen, A. A., Zhang, D. & Kilian, K. A. Directing stem cell fate on hydrogel substrates by controlling cell geometry, matrix mechanics and adhesion ligand composition. *Biomaterials* **34**, 8140-8148, doi:10.1016/j.biomaterials.2013.07.074 (2013).
84 Kilian, K. A., Bugarija, B., Lahn, B. T. & Mrksich, M. Geometric cues for directing the differentiation of mesenchymal stem cells. *Proc Natl Acad Sci U S A* **107**, 4872-4877, doi:10.1073/pnas.0903269107 (2010).
85 Vandrangi, P., Gott, S. C., Kozaka, R., Rodgers, V. G. & Rao, M. P. Comparative endothelial cell response on topographically patterned titanium and silicon substrates with micrometer to sub-micrometer feature sizes. *PLoS One* **9**, e111465, doi:10.1371/journal.pone.0111465 (2014).
86 Aimi, M. F., Rao, M. P., MacDonald, N. C., Zuruzi, A. S. & Bothman, D. P. High-aspect-ratio bulk micromachining of titanium. *Nat Mater* **3**, 103-105, doi:10.1038/nmat1058 (2004).
87 Parker, E. R., Thibeault, B. J., Aimi, M. F., Rao, M. P. & MacDonald, N. C. Inductively Coupled Plasma Etching of Bulk Titanium for MEMS Applications. *Journal of The Electrochemical Society* **152**, C675, doi:10.1149/1.2006647 (2005).
88 Morgado, P., Ong, Y. C., Boothroyd, J. C. & Lodoen, M. B. Toxoplasma gondii induces B7-2 expression through activation of JNK signal transduction. *Infect Immun* **79**, 4401-4412, doi:10.1128/IAI.05562-11 (2011).
89 Pelegrin, P. & Surprenant, A. Dynamics of macrophage polarization reveal new mechanism to inhibit IL-1beta release through pyrophosphates. *EMBO J* **28**, 2114-2127, doi:10.1038/emboj.2009.163 (2009).
90 Calle, Y., Burns, S., Thrasher, A. J. & Jones, G. E. The leukocyte podosome. *Eur J Cell Biol* **85**, 151-157, doi:10.1016/j.ejcb.2005.09.003 (2006).
91 Linder, S. Invadosomes at a glance. *J Cell Sci* **122**, 3009-3013, doi:10.1242/jcs.032631 (2009).
92 Gott, S. C., Jabola, B. A. & Rao, M. P. Vascular stents with submicrometer-scale surface patterning realized via titanium deep reactive ion etching. *Journal of Micromechanics and Microengineering* **25**, 085016, doi:10.1088/0960-1317/25/8/085016 (2015).

93 Wang, T., Luu, T. U., Chen, A., Khine, M. & Liu, W. F. Topographical modulation of macrophage phenotype by shrink-film multi-scale wrinkles. *Biomater Sci* **4**, 948-952, doi:10.1039/c6bm00224b (2016).
94 Kou, P. M. & Babensee, J. E. Macrophage and dendritic cell phenotypic diversity in the context of biomaterials. *J Biomed Mater Res A* **96**, 239-260, doi:10.1002/jbm.a.32971 (2011).
95 Kim, Y. S. *et al.* Extracellular vesicles derived from Gram-negative bacteria, such as Escherichia coli, induce emphysema mainly via IL-17A-mediated neutrophilic inflammation. *J Immunol* **194**, 3361-3368, doi:10.4049/jimmunol.1402268 (2015).
96 Kzhyshkowska, J. *et al.* Macrophage responses to implants: prospects for personalized medicine. *J Leukoc Biol* **98**, 953-962, doi:10.1189/jlb.5VMR0415-166R (2015).
97 Mosser, D. M. & Edwards, J. P. Exploring the full spectrum of macrophage activation. *Nat Rev Immunol* **8**, 958-969, doi:10.1038/nri2448 (2008).
98 Mantovani, A. & Garlanda, C. Platelet-macrophage partnership in innate immunity and inflammation. *Nat Immunol* **14**, 768-770, doi:10.1038/ni.2666 (2013).
99 Madden, L. R. *et al.* Proangiogenic scaffolds as functional templates for cardiac tissue engineering. *Proc Natl Acad Sci U S A* **107**, 15211-15216, doi:10.1073/pnas.1006442107 (2010).
100 Chen, A. *et al.* Shrink-film configurable multiscale wrinkles for functional alignment of human embryonic stem cells and their cardiac derivatives. *Adv Mater* **23**, 5785-5791, doi:10.1002/adma.201103463 (2011).
101 Luna, J. I. *et al.* Multiscale biomimetic topography for the alignment of neonatal and embryonic stem cell-derived heart cells. *Tissue Eng Part C Methods* **17**, 579-588, doi:10.1089/ten.TEC.2010.0410 (2011).
102 Wojciak-Stothard, B., Denyer, M., Mishra, M. & Brown, R. A. Adhesion, Orientation, and Movement of Cells Cultured on Ultrathink Fibronectin Fibers. *In Vitro Cell. Dev. Biol.* **33**, 110-117 (1997).
103 Hesse, M. *et al.* Differential Regulation of Nitric Oxide Synthase-2 and Arginase-1 by Type 1/Type 2 Cytokines In Vivo: Granulomatous Pathology Is Shaped by the Pattern of L-Arginine Metabolism. *The Journal of Immunology* **167**, 6533-6544, doi:10.4049/jimmunol.167.11.6533 (2001).
104 Knipper, J. A. *et al.* Interleukin-4 Receptor alpha Signaling in Myeloid Cells Controls Collagen Fibril Assembly in Skin Repair. *Immunity* **43**, 803-816, doi:10.1016/j.immuni.2015.09.005 (2015).
105 Hakelius, L. & Ohlsén, L. A clinical comparison of the tendency to capsular contracture betweem smooth and textured gel-filled silicone mammary implants. *Plast Reconstr Surg* **90**, 247-254 (1992).
106 Duffy, R. M., Sun, Y. & Feinberg, A. W. Understanding the role of ECM protein composition and geometric micropatterning for engineering human skeletal muscle. *Annals of Biomedical Engineering* **44**, 2076-2089, doi:10.1007/s10439-016-1592-8 (2016).
107 Frangogiannis, N. G. The extracellular matrix in myocardial injury, repair, and remodeling. *J Clin Invest* **127**, 1600-1612, doi:10.1172/JCI87491 (2017).
108 Giussani, M., Merlino, G., Cappelletti, V., Tagliabue, E. & Daidone, M. G. Tumor-extracellular matrix interactions: Identification of tools associated with breast

cancer progression. *Semin Cancer Biol* **35**, 3-10, doi:10.1016/j.semcancer.2015.09.012 (2015).
109 Pickup, M. W., Mouw, J. K. & Weaver, V. M. The extracellular matrix modulates the hallmarks of cancer. *EMBO reports* **15**, 1243-1253, doi:10.15252/embr.201439246 (2014).
110 Slattery, M. L. *et al.* Matrix metalloproteinase genes are associated with breast cancer risk and survival: the Breast Cancer Health Disparities Study. *PLoS One* **8**, e63165, doi:10.1371/journal.pone.0063165 (2013).
111 Sorensen, H. T. *et al.* Risk of liver and other types of cancer in patients with cirrhosis: a nationwide cohort study in Denmark. *Hepatology* **28**, 921-925 (1998).
112 Neglia, J. P. *et al.* The risk of cancer among patients with cystic fibrosis. *NEJM* **332**, 494-499 (1995).
113 Du, J., Wang, Y. & Jia, L. in *Atherosclerosis: Risks, Mechanisms, and Therapies* (eds H. Wang & C. Patterson) 343-351 (John Wiley & Sons, Inc., 2015).
114 Armstrong, J. W. & Chapes, S. K. Effects of extracellular matrix proteins on macrophage differentiation, growth, and function: Comparison of liquid and agar culture systems. *J. Exp. Zool.* **269**, 178-187, doi:10.1002/jez.1402690303 (1994).
115 Toral D. Zaveri, J. S. L., Natalia V. Dolgova, Michael J. Clare-Salzler, Benjamin G. Keselowsky. Integrin-directed modulation of macrophage responses to biomaterials. *Biomaterials* **35**, 3504-3515, doi:10.1016/j.biomaterials.2014.01.007 (2014).
116 Bjorklund, M. & Koivunen, E. Gelatinase-mediated migration and invasion of cancer cells. *Biochim Biophys Acta* **1755**, 37-69, doi:10.1016/j.bbcan.2005.03.001 (2005).
117 Hsieh, J. Y. *et al.* Differential regulation of macrophage inflammatory activation by fibrin and fibrinogen. *Acta Biomater* **47**, 14-24, doi:10.1016/j.actbio.2016.09.024 (2017).
118 Takeda, K. & Akira, S. Toll-like receptors in innate immunity. *Int Immunol* **17**, 1-14, doi:10.1093/intimm/dxh186 (2005).
119 Neubrand, V. E. *et al.* Mesenchymal stem cells induce the ramification of microglia via the small RhoGTPases Cdc42 and Rac1. *Glia* **62**, 1932-1942, doi:10.1002/glia.22714 (2014).
120 Biswas, S., Bachay, G., Chu, J., Hunter, D. D. & Brunken, W. J. Laminin-Dependent Interaction between Astrocytes and Microglia: A Role in Retinal Angiogenesis. *Am J Pathol* **187**, 2112-2127, doi:10.1016/j.ajpath.2017.05.016 (2017).
121 Fridman, R. *et al.* Reconstituted basement membrane (matrigel) and laminin can enhance the tumorgenicity and the drug resistance of small cell lung cancer cell lines. *Proc Natl Acad Sci U S A* **87**, 6698-6702 (1990).
122 Hao, W. *et al.* Vitronectin: a promising breast cancer serum biomarker for early diagnosis of breast cancer in patients. *Tumour Biol* **37**, 8909-8916, doi:10.1007/s13277-015-4750-y (2016).
123 Murata, K., Motayama, T. & Kotake, C. Collagen types in various layers of the human aorta and their changes with the atherosclerotic process. *Atherosclerosis* **60**, 251-262, doi:10.1016/0021-9150(86)90172-3 (1986).
124 Stary, H. C. *et al.* A definition of advanced types of atherosclerotic lesions and a histological classification of atherosclerosis. *Arteriosclerosis, thrombosis, and vascular biology* **15**, 1512-1531, doi:10.1161/01.CIR.92.5.1355 (1995).

125 Shekhonin, B. V., Domogatsky, S. P., Idelson, G. L., Koteliansky, V. E. & Rukosuev, V. S. Relative distribution of fibronectin and type I, III, IV, V collagens in normal and atherosclerotic intima of human arteries. *Atherosclerosis* **67**, 9-16, doi:10.1016/0021-9150(87)90259-0 (1987).
126 Mirza, R., DiPietro, L. A. & Koh, T. J. Selective and specific macrophage ablation is detrimental to wound healing in mice. *Am J Pathol* **175**, 2454-2462, doi:10.2353/ajpath.2009.090248 (2009).
127 Gauglitz, G. G., Korting, H. C., Pavicic, T., Ruzicka, T. & Jeschke, M. G. Hypertrophic scarring and keloids: pathomechanisms and current and emerging treatment strategies. *Mol Med* **17**, 113-125, doi:10.2119/molmed.2009.00153 (2011).
128 Alvey, C. M. *et al.* SIRPA-Inhibited, Marrow-Derived Macrophages Engorge, Accumulate, and Differentiate in Antibody-Targeted Regression of Solid Tumors. *Curr Biol* **27**, 2065-2077 e2066, doi:10.1016/j.cub.2017.06.005 (2017).
129 Lowell, G. B. a. C. A. Integrin Signalling in Neutrophils and Macrophages. *Cellular Signalling* **11**, 621-635 (1999).
130 Yokoyama, K., Zhang, X., Medved, L. & Takada, Y. Specific binding of integrin αvβ3 to the fibrinogen γ and α(E) chain C-terminal domains. *Biochem.* **38**, 5872-5877, doi:10.1021/bi9827619 (1999).
131 Chaofeng Han, J. J., Sheng Xu, Haibo Liu, Nan Li, Xuetao Cao. Integrin CD11b negatively regulates TLR-triggered inflammatory responses by activating Syk and promoting degradation of MyD88 and TRIF via Cbl-b. *Nature Immunology* **11**, 734-743, doi:10.1038/ni/1908 (2010).
132 Ling, G. S. *et al.* Integrin CD11b positively regulates TLR4-induced signalling pathways in dendritic cells but not in macrophages. *Nat Commun* **5**, 3039, doi:10.1038/ncomms4039 (2014).
133 Liu, W. F. Mechanical regulation of cellular phenotype: implications for vascular tissue regeneration. *Cardiovascular Research* **95**, 215-222, doi:10.1093/cvr/cvs168 (2012).
134 Ridley, K. R. a. A. J. ROCK: Multifunctional Kinases in Cell Behaviour. *Nature Reviews* **4**, 446-456, doi:10.1038/nrm1128 (2003).
135 Veronika E. Neubrand, M. P., Marta Caro, Irene Forte-Lago, Mario Delgada, and Elena Gonzalez-Rey. Mesenchymal Stem Cells Induce the Ramification of Microglia Via the Small RhoGTPases Cdc42 and Rac1. *GLIA* **00**, 000-000, doi:10.1002/glia.22714 (2014).
136 O'Neill, L. A., Golenbock, D. & Bowie, A. G. The history of Toll-like receptors - redefining innate immunity. *Nat Rev Immunol* **13**, 453-460, doi:10.1038/nri3446 (2013).
137 Viatour, P., Merville, M. P., Bours, V. & Chariot, A. Phosphorylation of NF-kappaB and IkappaB proteins: implications in cancer and inflammation. *Trends Biochem Sci* **30**, 43-52, doi:10.1016/j.tibs.2004.11.009 (2005).
138 Adli, M., Merkhofer, E., Cogswell, P. & Baldwin, A. S. IKKalpha and IKKbeta each function to regulate NF-kappaB activation in the TNF-induced/canonical pathway. *PLoS One* **5**, e9428, doi:10.1371/journal.pone.0009428 (2010).
139 Gao, Y. *et al.* Differential IKK/NF-kappaB Activity Is Mediated by TSC2 through mTORC1 in PTEN-Null Prostate Cancer and Tuberous Sclerosis Complex Tumor Cells. *Mol Cancer Res* **13**, 1602-1614, doi:10.1158/1541-7786.MCR-15-0213 (2015).

140 Kondylis, V., Kumari, S., Vlantis, K. & Pasparakis, M. The interplay of IKK, NF-kappaB and RIPK1 signaling in the regulation of cell death, tissue homeostasis and inflammation. *Immunol Rev* **277**, 113-127, doi:10.1111/imr.12550 (2017).
141 Shinji, H., Akagawa, K. S. & Yoshida, T. Cytochalasin D inhibits lipopolysaccharide-induced tumor necrosis factor production in macrophages. *J Leukoc Biol* **54**, 336-342 (1993).
142 Li, Z., Davis, G. S., Mohr, C., Nain, M. & Gemsa, D. Inhibition of LPS-Induced Tumor Necrosis Factor-α Production by Colchicine and Other Microtubule Disrupting Drugs. *Immunobiology* **195**, 624-639, doi:10.1016/s0171-2985(96)80027-1 (1996).
143 Dupont, S. *et al.* Role of YAP/TAZ in mechanotransduction. *Nature* **474**, 179-183, doi:10.1038/nature10137 (2011).
144 Wada, K., Itoga, K., Okano, T., Yonemura, S. & Sasaki, H. Hippo pathway regulation by cell morphology and stress fibers. *Development* **138**, 3907-3914, doi:10.1242/dev.070987 (2011).
145 Liu, Z. *et al.* MAPK-Mediated YAP Activation Controls Mechanical-Tension-Induced Pulmonary Alveolar Regeneration. *Cell Rep* **16**, 1810-1819, doi:10.1016/j.celrep.2016.07.020 (2016).
146 Wang, X. *et al.* Epigenetic regulation of macrophage polarization and inflammation by DNA methylation in obesity. *JCI Insight* **1**, e87748, doi:10.1172/jci.insight.87748 (2016).
147 Hoeksema, M. A. & de Winther, M. P. Epigenetic Regulation of Monocyte and Macrophage Function. *Antioxid Redox Signal* **25**, 758-774, doi:10.1089/ars.2016.6695 (2016).
148 Crowder, S. W., Leonardo, V., Whittaker, T., Papathanasiou, P. & Stevens, M. M. Material Cues as Potent Regulators of Epigenetics and Stem Cell Function. *Cell Stem Cell* **18**, 39-52, doi:10.1016/j.stem.2015.12.012 (2016).
149 Downing, T. L. *et al.* Biophysical regulation of epigenetic state and cell reprogramming. *Nat Mater* **12**, 1154-1162, doi:10.1038/nmat3777 (2013).
150 Singh, P., Carraher, C. & Schwarzbauer, J. E. Assembly of fibronectin extracellular matrix. *Annu Rev Cell Dev Biol* **26**, 397-419, doi:10.1146/annurev-cellbio-100109-104020 (2010).
151 Mao, Y. & Schwarzbauer, J. E. Stimulatory effects of a three-dimensional microenvironment on cell-mediated fibronectin fibrillogenesis. *J Cell Sci* **118**, 4427-4436, doi:10.1242/jcs.02566 (2005).
152 Harris, G. M. *et al.* Nerve Guidance by a Decellularized Fibroblast Extracellular Matrix. *Matrix Biol* **60-61**, 176-189, doi:10.1016/j.matbio.2016.08.011 (2017).